2009-08-07

Characterization of the Nef-TCR Zeta Interaction and Its Role in Modulation of Src Family Kinase Activity: A Dissertation

Walter Minsub Kim
University of Massachusetts Medical School

CHARACTERIZATION OF THE NEF-TCR ZETA INTERACTION AND ITS ROLE IN MODULATION OF SRC FAMILY KINASE ACTIVITY

A Dissertation Presented

By

WALTER MINSUB KIM

A.B. Biochemical Sciences
Harvard College 2000

Submitted to the Faculty of the
University of Massachusetts Graduate School of Biomedical Sciences, Worcester
In partial fulfillment of the requirements for the degree of

DOCTOR OF PHILOSOPHY

AUGUST 7, 2009

CHARACTERIZATION OF THE NEF-TCR ZETA INTERACTION AND ITS ROLE IN MODULATION OF SRC FAMILY KINASE ACTIVITY

A Dissertation Presented

By

Walter Minsub Kim

The signatures of the Dissertation Defense Committee signifies completion and approval as to style and content of the Dissertation

Lawrence J. Stern, Ph.D., Thesis Advisor

Leslie J. Berg, Ph.D., Member of Committee

Ronald C. Desrosiers, Ph.D., External Member of Committee

Thomas Greenough, M.D., Member of Committee

Kendall Knight, Ph.D., Member of Committee

The signature of the Chair of the Committee signifies that the written dissertation meets the requirements of the Dissertation Committee

Celia Schiffer, Ph.D., Chair of Committee

The signature of the Dean of the Graduate School of Biomedical Sciences signifies that the student has met all graduation requirements of the school

Anthony Carruthers, Ph.D.
Dean of the Graduate School of Biomedical Sciences

MD/PhD Program in Biomedical Sciences
August 7, 2009

DEDICATION

I dedicate this thesis to those who dare to extend their limits
and expand their goals in order to benefit their community.

ACKNOWLEDGEMENTS

I feel that I am a true product of my environment and for that reason, I am grateful to everybody who has played a role in shaping me into the person I am today. I would like to especially thank the following individuals for their assistance and care during my scientific endeavors.

Larry Stern, my thesis advisor and mentor, has been an incredible resource as a scientist, educator and renaissance man. He showed immense patience while challenging me to develop as a thinker, explore my scientific curiosities and perform experiments without fear or limitation.

Alexander Sigalov has been an invaluable guide in my scientific and personal growth. He pushed me to think logically, act fairly and to be true to myself and my peers.

Elliot Androphy, MD/PhD Program Director, has been instrumental in providing an identity for MD/PhD Program. He also pushed me to think globally, focus on defined goals and to keep perspective on my endeavors.

Zu Ting Shen and Zarixia Zavala-Ruiz have been incredible bay mates who provided amazing support, friendship and scientific insight. It's been a true honor to have worked beside you.

I would like to thank the members of my thesis committee who challenged me to focus on pursuing viable experiments while asking relevant questions. I also thank you for showing immense care in my personal and career development. Thank you Celia Schiffer, Leslie Berg, Tom Greenough and Ken Knight.

I would also like to thank the members of the Stern group old and new: Sriram Chitta, Tina Nguyen, Kathy Bateman, Aniuska Beccerra, Mauricio Calvo-Calle, Loretta Lee, Guoqi Li, Liying Lu, Sarah Mortimer, Dorthea Maria Nastke, Corrie Painter, Peter Trenh, Liusong Liu, Ben Roscoe, Prasanna Venkatramen, Eftratios Stratikos, Jennifer Stone, Greg Carven, Christian Parry and Sabrina Vollers for being great friends, offering scientific insight and for enduring my antics.

I also need to thank my former mentors who encouraged me to pursue science and discovery as part of my career. From my undergraduate years, Thilo Stehle and Mykol Larvie showed me that scientific research could be challenging and fun. From my years at Vertex Pharmaceuticals, Steve Chambers and John Fulghum encouraged me to find a balance in my scientific curiosities and my hobbies.

Finally, I would like to thank my family. My parents, Young and Eun Kim, always encouraged me to take every opportunity presented to me and to strive for excellence. Those are two principles I live by every day. My sisters, Anna, Lisa and Linda, my brother-in-law, Dwight and my nephew, Ethan, have been my biggest supporters and encouraged me to succeed in everything that I do. Lastly, I would like to thank my dear wife Adonia who has shown me patience that I never imagined could be possible and incredible encouragement to pursue all of my goals and dreams. She has been an amazing co-pilot on this scientific journey.

ABSTRACT

One of the hallmarks of an infection with pathogenic HIV-1 is the elevated level of immune activation that leads to rapid progression to AIDS. Surprisingly, nonhuman primates naturally infected with SIV do not exhibit an augmented activation phenotype nor severe immunodeficiency. One of the viral components implicated in determining the state of immune activation is the accessory protein Nef which has been demonstrated to affect T cell signaling pathways from within the intracellular compartment and for Nef from SIV, to downregulate TCR surface expression. Recently, Nef from HIV-1 and SIV have been demonstrated to bind the ζ chain of the TCR which functions as the primary signaling subunit of the receptor. However, the molecular details of the Nef-TCRζ interaction as well as the role of complex formation in modulation of immune activation remain largely unknown.

This thesis describes work directed at elucidating the biochemical and structural features of the Nef-TCRζ interaction and the functional consequences of complex formation relevant to T cell activation. Chapter I provides a brief introduction on HIV/SIV classification and pathogenesis with an emphasis on Nef and its pleiotropic function in T cells.

Chapter II describes the biochemical characterization of the interaction of the conserved core domain of Nef proteins from HIV-1, HIV-2 and SIV with the cytoplasmic domain of TCRζ. The core domains of HIV-2 ST and SIVmac239 are demonstrated to bind the cytoplasmic domain of TCRζ at two distinct regions and with different affinities. In contrast, the core domain of HIV-1 isolate ELI Nef only binds to one region and with

the weakest calculated affinity among the HIV-1, HIV-2 and SIV Nef proteins studied. In addition, both the N-terminal domain and the strong TCRζ-binding core domain of SIVmac239 Nef each are demonstrated to be necessary but not sufficient for downregulation of TCR surface expression.

Chapter III describes the crystallization and structure determination methods used to solve the crystal structures of the core domain of SIVmac239 Nef in complex with two overlapping TCRζ polypeptides. Crystals of Nef in complex with the longer $TCR\zeta_{DP1}$ (L51-D93) polypeptide grew in a tetragonal space group but only diffracted to low resolution. In contrast, crystals of the Nef_{core}-$TCR\zeta_{A63\text{-}R80}$ complex grew in an orthorhombic space group and diffracted to high resolution but were nearly perfectly pseudo-merohedrally twinned thus complicating structure determination. Following identification of the twin law relating the twin domains, the structure of the Nef_{core}-$TCR\zeta_{A63\text{-}R80}$ complex was determined using refinement procedures that accounted for crystal twinning to 2.05 Å. The structure of the Nef_{core}-$TCR\zeta_{DP1}$ complex was solved to 3.7 Å from a single non-twinned crystal. The altered crystal packing induced by the shorter $TCR\zeta_{A63\text{-}R80}$ polypeptide is postulated to have led to a reduction in crystal symmetry and increase in proneness to crystal twinning.

Chapter IV provides a detailed analysis of the structure of the Nef_{core}-$TCR\zeta_{A63\text{-}R80}$ complex and demonstrates its effect on modulation of Src family kinase activity. The TCRζ polypeptide adopts an alpha helical conformation and occupies a hydrophobic crevice on Nef not shared by any of Nef's reported interaction partners. The interaction of Nef_{core} with TCRζ is mediated primarily by the burial of hydrophobic residues on

TCRζ (L75, L77) in a hydrophobic pocket on Nef and a salt bridge between a glutamic acid (E74) on TCRζ and a basic patch on Nef consisting of two conserved arginines (R105, R106). The TCRζ polypeptide additionally orders the N-terminus of Nef_{core} into a polyproline type II helix that has been described to bind the SH3 domain of Src family kinases. We demonstrate that *in vitro* phosphorylation of $TCR\zeta_{cyt}$ by Fyn and Src is specifically augmented by HIV-1 and SIV Nef_{core} and suggest that Nef-TCRζ complex formation cooperatively enhances kinase activity.

Chapter V contains overall conclusions, future directions and a model illustrating the proposed role of the Nef-TCRζ interaction in immune activation modulation. The Appendices contain sequences of the proteins, gene constructs and primers used in this work.

TABLE OF CONTENTS

LIST OF TABLES

LIST OF FIGURES

LIST OF SYMBOLS AND ABBREVIATIONS

AIDS	Acquired immunodeficiency syndrome
CD	Circular dichroism
DTT	1,4-Dithiothreitol
E.coli	Escherichia coli
ELISA	Enzyme-linked immunosorbent assay
GFP	Green fluorescence protein
HIV	Human immunodeficiency virus
IS	Immunological synapse
ITAM	Immunoreceptor tyrosine activation motif
MHC	Major histocompatibility complex
MW	Molecular weight
Nef_{core}	Nef core domain
PBS	Phosphate buffered saline
PE	R-Phycoerythrin
PMSF	Phenylmethylsulphonyl fluoride
PPII	Polyproline type II (helix)
PTK	Protein tyrosine kinase
RU	Resonance unit
SDS-PAGE	Sodium dodecyl sulfate-polyacrylamide gel electrophoresis
SH3	Src homology 3 (domain)
SIV	Simian immunodeficiency virus
SNID	SIV Nef interaction domain
SPR	Surface plasmon resonance
TCRζ	T cell receptor zeta chain
$TCR\zeta_{cyt}$	T cell receptor zeta chain cytoplasmic domain (L51-R164)
$TCR\zeta_{DP1}$	T cell receptor zeta chain fragment DP1 (L51-D93)
$TCR\zeta_{DP2}$	T cell receptor zeta chain fragment DP2 (P94-R164)

PREFACE

References to publications that represent the work contained within this thesis:

Kim WM, Sigalov AB and Stern LJ. (2009) Crystal structure of the SIV Nef-TCRζ polypeptide complex and its role in modulation of kinase activity. *In preparation*.

Kim WM, Sigalov AB and Stern LJ. (2009) Pseudo-merohedral twinning and non-crystallographic symmetry in orthorhombic crystals of SIVmac239 Nef core domain bound to different length TCR zeta fragments. *Submitted.*

Sigalov, A. B., Kim, W. M., Saline, M., and Stern, L. J. (2008). The intrinsically disordered cytoplasmic domain of the T cell receptor zeta chain binds to the nef protein of simian immunodeficiency virus without a disorder-to-order transition. *Biochemistry*, 47, 12942-12944.

Structures deposited in the Protein Data Bank (PDB) from work contained within this thesis:

3IOZ Structure of the SIVmac239 Nef_{core}-$TCR\zeta_{DP1}$ complex
3IK5 Structure of the SIVmac239 Nef_{core}-$TCR\zeta_{A63\text{-}R80}$ complex

Alexander Sigalov expressed and purified the $TCR\zeta_{cyt}$, $TCR\zeta_{DP1}$ and $TCR\zeta_{DP2}$ proteins used in this work

CHAPTER I: Introduction

The causative agent of acquired immunodeficiency syndrome (AIDS) in humans was first identified in 1983 by two groups who named the retrovirus lymphadenopathy-associated virus (LAV) (Barre-Sinoussi et al., 1983) and human T-cell leukemia virus III (HTLV-III) (Gallo et al., 1983). A simian virus that exhibited similar growth characteristics and antigenic properties to LAV and HTLV-III was described two years later in rhesus macaques (Daniel et al., 1985) and was aptly named simian T- cell leukemia virus III (STLV-III). The identification of an additional AIDS-associated retrovirus (ARV) prompted the classification of LAV, HTLV-III and ARV as human immunodeficiency viruses (Coffin et al., 1986), thus burgeoning an expansive research effort targeted at understanding the mechanism of HIV disease and developing anti-viral therapeutics and vaccines. STLV-III, later referred to as simian immunodeficiency virus (SIV), provided a unique opportunity to study HIV pathogenesis in an animal model [reviewed in (Desrosiers et al., 1989)].

Despite significant advances in the investigation of HIV pathogenesis, the development of curative therapies and vaccines has remained elusive. This is in large part due to the immense sequence variability found among different clinical HIV isolates as well as a lack of detailed understanding of the numerous HIV-host interactions that contribute to disease progression. In addition, the viral components of HIV perform a multitude of functions that collectively determine the pathogenicity of the infecting virus. Therefore, detailed investigation of HIV-host interactions as well as the correlative analysis of viral function and disease outcome will need to be performed to further

advance our knowledge of HIV disease and to develop novel strategies of therapeutic intervention.

I.A. Human immunodeficiency virus and simian immunodeficiency virus

I.A.1. Classification

HIV and its orthologous simian SIV partner comprise the primate lentiviral group of viruses in the *Retroviridae* family. HIV is divided into two types, HIV-1 and HIV-2, based on differences in viral genome architecture and serological properties of infected individuals. HIV-1 is further divided into three groups: the "main" group M, the "outlier" group O and the extremely rare "non-M, non-O" group N. Over 90% of the sequenced HIV-1 isolates belong to M group and are classified into eleven subtypes or clades (A1, A2, B, C, D, F1, F2, G, H, J, K) based on their *env* and *gag* gene sequences. Each clade differs by over 20% and 15% in their *env* and *gag* sequences, respectively, and some clades are reclassified subtypes of precursor clades such as clades A1 and A2 from clade A. Hybrid HIV-1 viruses that develop during co-infection with HIV from different clades form a separate subtype designated as the circulating recombinant form (CRF). To date, 43 CRF subtypes have been classified and are deposited in the HIV sequence compendium (HIV Sequence Compendium 2009). The less investigated HIV-2 viruses are organized into eight distinct sequence clusters and form groups A-H, with group A being the most prevalent HIV-2 group (>10%).

According to the 2009 edition of the HIV Sequence Compendium, over 25 unique nonhuman primate lentiviruses have been classified. SIV classification is species-based

and categorizes genetically distinct viral isolates according to their infected hosts. For example, SIV isolates found in sooty mangabeys and chimpanzees are designated as SIV_{SMM} and SIV_{CPZ} viruses, respectively. Analysis of genomic architecture and sequence homology reveals that SIV_{CPZ} is closely related to HIV-1 whereas SIV_{SMM} is more closely linked to HIV-2 (Hahn et al., 2000). SIV_{MAC} presents an interesting classification dilemma as the highly pathogenic virus found in macaques is highly homologous to SIV_{SMM} and has been suggested to have been acquired during captivity from infected sooty mangabey monkeys (Desrosiers et al., 1989; Hirsch et al., 1989) . Therefore, SIV_{MAC} may not be a naturally infecting virus but an experimental cross-species virus that is not native to its host species [reviewed in (Desrosiers, 1990)].

In total, 229,451 sequences of HIV-1, HIV-2 and SIV isolates have been deposited in the HIV sequence database and continuous re-evaluation of the classification methods is ongoing. Owing to the high sequence variability nature of primate lentiviruses, classification of the numerous viral isolates based on sequence homology is a difficult challenge that complicates HIV research, predictions of disease outcome as well as the development of subtype or clade-specific antiviral therapies or vaccines.

I.A.2. Genome architecture

The HIV and SIV genomes are compact (~9.2-9.7kb) and exist either as single stranded RNA or double stranded DNA depending on their location (Muesing et al., 1985). In mature viral particles, the viral genome exists as single stranded RNA and in the intracellular compartment it is found in proviral double-stranded DNA form. Two

similar but distinct genomic organizations are found among the primate lentiviruses for HIV-1 and HIV-2 with the heavily investigated SIV_{MAC} strains corresponding to the HIV-2 genomic architecture (Figure I-1). The genome is flanked at both ends by a repeat sequence known as the long terminal repeat (LTR). Between the 5' and 3' LTRs are overlapping open reading frames that encode one enzymatic (Pol) and two structural (Gag, Env) precursor polypeptides as well several essential (Tat, Rev) and non-essential (Vpu, Vpr, Vpx, Vif, Nef) viral accessory proteins. HIV-1 differs from HIV-2/SIV_{MAC} in its expression of the viral accessory protein Vpu which is substituted with Vpx in HIV-2/SIV_{MAC}. The open reading frame for the *nef* gene is also variable among the two viral types. In HIV-2/SIV_{MAC}, the *nef* gene overlaps with the 3' end of the *env* open reading frame where in HIV-1 it is distal to the *env* 3' termination site. Consequently, the N-terminus of the expressed Nef protein is highly variable among HIV-1 and HIV-2/SIV_{MAC} isolates.

I.A.4. Viral pathogenesis and disease outcome

Pathogenic HIV-1 infection results in the development of HIV disease that is characterized by profound viremia, chronic elevation in immune activation and depletion of $CD4^+$ T cells. As the disease progresses, the infected individual develops acquired immunodeficiency syndrome (AIDS), resulting in increased susceptibility to opportunistic infection, neoplastic growth and fatal disease. Current Center for Disease Control guidelines consider CD4+ T lymphocyte counts below 200 cells/μl to be the diagnostic threshold for AIDS. In contrast, HIV-2 is far less aggressive and

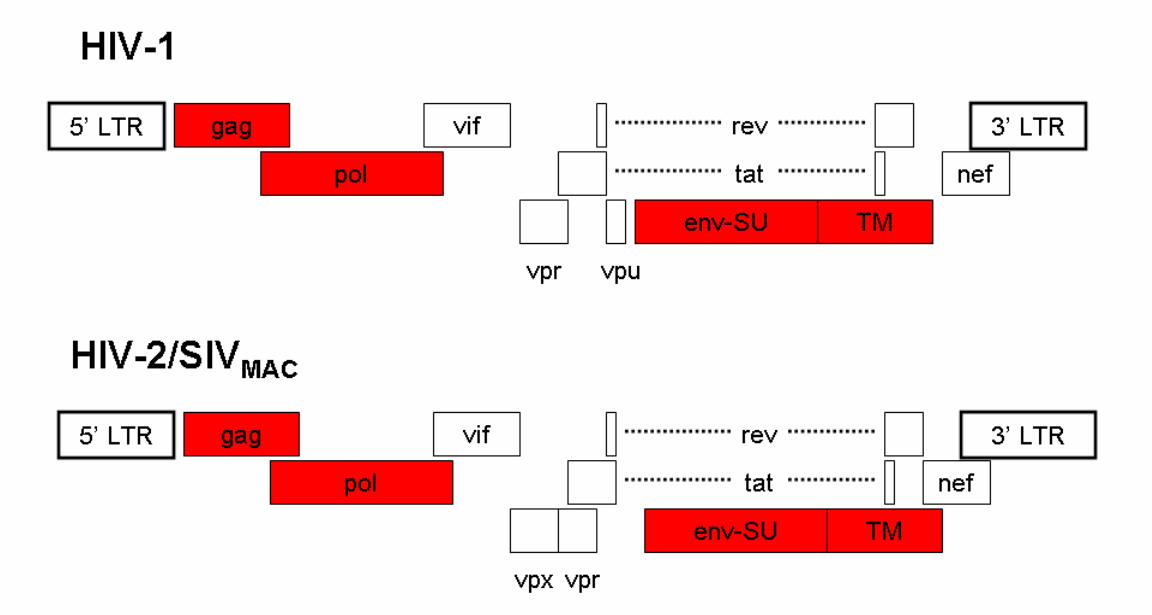

Figure I-1. Lentiviral genome structure. The genome organization of HIV-1 and HIV-2/SIV_{MAC} proviral DNA is shown. The structural genes (*gag*, *pol and env*) are shaded in red. The essential regulatory genes (tat, rev) and non-essential accessory genes (vif, vpr, vpx, vpu, nef) are boxed. (Adapted from (Fields et al, ed))

is out-replicated in the presence of HIV-1 (Koblavi-Deme et al., 2004; Sousa et al., 2002). Although capable of progressing to AIDS, HIV-2 infection more closely resembles the features of a natural infection of nonhuman primates with simian immunodeficiency virus (SIV) which is largely non-pathogenic. With the exception of experimentally-inoculated macaques with SIV_{MAC} strains, infected nonhuman primates predominately exhibit suppressive activation phenotypes despite high viremia throughout the course of infection without developing extensive symptoms of AIDS (Rey-Cuille et al., 1998; Silvestri et al., 2003).

The majority of HIV-1 transmission occurs through the anorectal and vaginal mucosa where $CCR5^{+}CD4^{+}$ T lymphocytes prone to HIV infection reside in the lamina propria (Royce et al., 1997; Schacker et al., 1996). Transmission of HIV into the blood circulation (i.e. blood transfusion, sharing of contaminated needles, trauma during sexual intercourse) requires clearance to regional lymph nodes and the spleen for viral propagation; circulating T lymphocytes only comprise ~2-5% of the total T cell population. Dendritic cells, through their surface lectin DC-SIGN, have been suggested to serve as critical viral transporters by binding surface gp120 molecules on circulating HIV particles and delivering them to $CD4^{+}$ T cells present in lymph nodes (Granelli-Piperno et al., 1999). Propagated virus then disseminates from the primary site of infection to other regions of the body, including the mucosa-associated lymphoid tissue (MALT) and gut-associated lymphoid tissue (GALT), and develops into a persistent and chronic infection that can lead to the development of AIDS.

The MALT and GALT represent the largest pools of lymphocytes in the body (Guy-Grand and Vassalli, 1993) and have therefore been widely considered as major targets of HIV during infection (Brenchley et al., 2004; Veazey et al., 1998). Destruction of the mucosal immune system has been postulated extensively to result in the development of AIDS (Grossman et al., 2006; Haase, 2005; Picker and Watkins, 2005; Veazey and Lackner, 2005). However, depletion of the mucosal and intestinal $CCR5^{+}CD4^{+}$ T cell population is only a precursor in the development of AIDS and is not a valid predictor of pathogenicity. In HIV-1 infected individuals (Brenchley et al., 2004; Guadalupe et al., 2003; Mehandru et al., 2004) and SIV-infected macaques (Li et al., 2005b; Mattapallil et al., 2005; Picker et al., 2004; Veazey et al., 2000a; Veazey et al., 2000b), extensive depletion of the MALT and GALT-associated $CD4^{+}$ T cells occurs within weeks of infection whereas progression to AIDS can take several years. Recent studies in rhesus macaques with pathogenic SIV strains demonstrated that infection of intestinal $CD4^{+}$ T cells occurred within days of infection with > 60% of $CD4^{+}$ T cells depleted by day 14 (Mattapallil et al., 2005). This was suggested to occur in part due to virus-triggered, Fas-Fas ligand–mediated apoptosis (Li et al., 2008) in addition to the host's cytotoxic T lymphocyte (CTL) and natural killer (NK) cell response. In follow-up studies of nonhuman primates infected with pathogenic (SIV_{SMM} in rhesus macaques), non-pathogenic (SIV_{AGM} in African green monkeys) and controlled (SIV_{AGM} infection in rhesus macaques) SIV, all of the infected hosts exhibited similar extensive and rapid GALT destruction and mucosal damage despite presenting with varying levels of disease,

suggesting that viral pathogenicity could not be forecast by the time course nor the extent of $CD4^+$ T cell depletion (Pandrea et al., 2007)

In both humans and rhesus macaques, pathogenic HIV and SIV-induced destruction of the mucosal architecture is followed by elevated chronic immune activation that continues to increase during progression to AIDS (Deeks et al., 2004; Giorgi et al., 1999; Grossman et al., 2006). The augmented immune activation profile includes several components of the immune system, including both the humoral and adaptive immune system where B cell, $CD4^+$ T cell and $CD8^+$ T cell proliferation is observed [reviewed in (Lawn et al., 2001)]. Prominent among HIV's effects on immune activation is the augmentation of T cell activation that promotes active viral replication [reviewed in (Jerome, 2008)]. Additional features, including increased activation of TNF-α signaling pathways and increased cytokine release also have been demonstrated to contribute to disease progression [reviewed in (Lawn et al., 2001; Matsuyama et al., 1991)]. However, due to the generalized nature of the immune activation, detailed investigation of the mechanisms by which HIV modulated immune function has proven to be difficult [reviewed in (Douek et al., 2009)] and will require careful dissection of HIV-1 numerous effects on the immune system.

I.B. Nef

Expressed in abundance during the early stages of HIV/SIV replication, the viral accessory protein negative factor (Nef) has been demonstrated to enhance viral infectivity, downregulate surface receptor molecules and importantly, modulate immune

activation in infected $CD4^+$ T cells. Nef has therefore been suggested to play a vital role in HIV pathogenesis and progression to AIDS (Kestler et al., 1991). In both rhesus monkeys (Kestler et al., 1991) and isolated human cases (Kirchhoff et al., 1995), *nef*-deleted variants of SIV and HIV-1 respectively failed to exhibit disease progression and instead displayed low viral loads and stable $CD4^+$ lymphocyte counts in the affected individual, similar to HIV-2 infected patients. Furthermore, *nef*-transgenic mice have been observed to display AIDS-like phenotypes (Hanna et al., 1998a; Hanna et al., 1998b; Hanna et al., 2006), further highlighting the importance of Nef in determining viral pathogenicity.

I.B.1 Structure

Nef is the largest of the non-essential viral accessory proteins encoded by HIV-1 (206 residues, ~27kDa) and HIV-2/SIV (250-263 residues, ~35kDa). The full length protein consists of a highly variable N-terminal anchor domain and a structured C-terminal core domain that is well-conserved among HIV-1 and HIV-2/SIV strains (Figure I-2). In HIV-1 Nef, the N-terminal domain and core domain are separated by a cleavage sequence (ACAW $^{\downarrow}$ LEAQ) that is sensitive to proteolysis by HIV-1 protease during viral assembly. As a result, the Nef protein present in the mature viral particle is comprised only of the core domain whereas the Nef protein that is found in the intracellular cytoplasmic space of the host cell exists in its full length form. HIV-2 and SIV Nef do not contain a cleavage sequence and are thus resistant to post-translation proteolysis by their respective proteases.

The N-terminal domain (HIV-1: M1-W57; SIV: M1-S95) contains a consensus myristylation sequence (MGxxxS/T) that results in the covalent linkage of a myristate to residue G2 by N-myristyl transferase (Resh, 1994; Resh, 1999). The myristyl modification directs Nef to the inner leaflet of the plasma membrane where it performs the majority of its functions [reviewed in (Kirchhoff et al., 2008)]. In the NMR solution structure (pdb code IQA4) of its unmyristylated form, the N-terminal domain of HIV-1 clone 12 Nef (G2-W57) is largely disordered with the exception of a short alpha helix (A33-G41) near the C-terminus. In its myristylated form (pdb code 1QA5) (Figure I-2A), the N-terminal domain contains a well-defined second alpha helix (P14-R22) that is stabilized by the myristyl modification (Geyer et al., 1999). Overall, the N-terminal domain is largely flexible and devoid of compact globular structure allowing it to adopt multiple conformations (Barnham et al., 1997; Geyer et al., 1999). The N-terminal domain of HIV-2/SIV Nef is significantly longer in sequence and no structural information for that region has been reported.

In contrast to the N-terminal domain, the core domain of Nef (Nef_{core}) represents the structured globular domain of the protein (Figure I-2B) that is responsible for the majority of its interactions with host proteins (reviewed in (Geyer et al., 2001). As observed in the crystal structure of HIV-1 isolate LAI Nef_{core} (pdb code 1AVV) (Arold et al., 1997) and the NMR solution structure of HIV-1 isolate BH10 Nef_{core} (pdb code 2NEF) (Grzesiek et al., 1997), Nef_{core} contains two pairs of alpha helices (α1- α2, α3- α4) that flank a four stranded anti-parallel β-sheet. The longer alpha helices α1 and α2

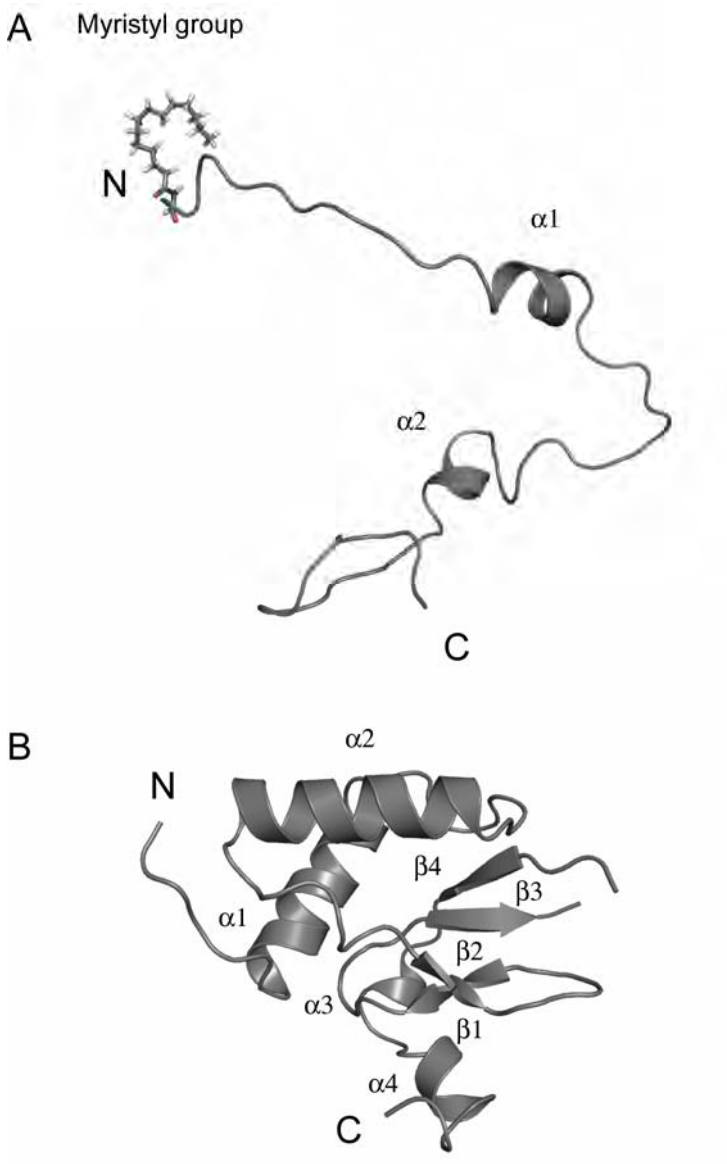

Figure I-2. Nef structure. A. The NMR solution structure of the myristylated N-terminal domain (G2-W57) of HIV-1 clone 12 Nef (pdb code 1QA5) is shown in ribbon diagram. Secondary structure elements are labeled and the myristyl group is depicted in stick model. B. The crystal structure of the core domain (L58-C206) of HIV-1 isolate LAI Nef is shown in ribbon diagram with secondary structure elements labeled.

along with the α1-α2 connecting loop form a solvent-accessible crevice thought to potentially serve as a binding site for a binding partner (Lee et al., 1996), however none has been identified. The structure of the four stranded β-sheet is irregular due to the presence of conserved proline residues (P136, P147) that introduce kinks into the β-sheet structure. This results in the presence of two distinct pairs of anti-parallel β-strands that contain elements of the hydrophobic core of the protein. Between β-strands β3 and β4 is a long disordered loop (E159-E173) that is not visualized in the crystal structure of HIV-1 Nef_{core} and had to be removed from the protein in order to determine the NMR solution structure.

In the crystal structures of HIV-1 Nef_{core} in complex with the SH3 domain of wildtype Fyn (pdb code 1AVZ) (Arold et al., 1997) and mutant (F96I) Fyn (pdb code 1EFN) (Lee et al., 1996), an N-terminal region of the Nef core domain (70-77) is ordered in a polyproline type II helix at the Nef-Fyn interface. The PxxP structural motif responsible for binding the SH3 domain is conserved among HIV-1, HIV-2 and SIV Nef variants and has been suggested to modulate activity of Src family kinases including Lck, Fyn and Hck *in vitro* (Arold et al., 1997; Lee et al., 1996)

I.B.2. Function

Although Nef's influence on HIV/SIV pathogenesis is well-documented, the precise mechanisms by which Nef acts and more importantly, how they collectively affect disease progression are not well understood. Nef does not possess any enzymatic activity and therefore exerts its function through protein-protein interactions. Recent

studies have identified a series of host cellular binding partners including type I membrane proteins, cellular kinases involved in T-cell signaling pathways and members of the endocytotic machinery (reviewed in (Baur, 2004; Greenway et al., 1996; Piguet and Trono, 1999); summarized in Table I-1). The majority of the binding motifs and the structural features required for Nef function localize to the core domain (Figure I-2) that is well conserved among HIV-1, HIV-2 and SIV. Nef's activities in the intracellular compartment can be reduced to two major activities that collectively enhance viral fitness: downregulation of surface receptors and modulation of T cell activation.

I.B.2.a. Downregulation of surface receptors

HIV-1 and SIV Nef downregulate a number of cell surface receptors that participate in the immunological synapse, including MHC Class I molecules (Collins et al., 1998; Le Gall et al., 1997; Schindler et al., 2006; Schwartz et al., 1996), CD4 (Aiken et al., 1994; Anderson et al., 1993; Benson et al., 1993; Garcia and Miller, 1991; Mariani and Skowronski, 1993; Schindler et al., 2006) and CD28 (Bell et al., 2001; Schindler et al., 2006; Swigut et al., 2001). Nef also downregulates surface TCR expression but only in the context of HIV-2 and SIV and not HIV-1 (Schindler et al., 2006).

Downregulation of MHC Class I molecules by Nef is a conserved function among HIV-1 and SIV strains (DeGottardi et al., 2008; Specht et al., 2008). Interestingly, Nef-mediated MHC downregulation is restricted to HLA-A and -B alleles and is not observed for HLA-C and -E. The selective allelic downregulation results in the clever protection of the infected cell from lysis by cytotoxic T lymphocytes (CTL) and killing by surveilling

Table I-1. Interaction of Nef with cellular proteins

Region on Nef important for binding and/or function[1]	Interaction partner	Region on partner important for binding and/or function	Requirement for pathogenicity[2]
Protein modification			
$MGxxS_1$	N-myristoyl transferase	n.d.[3]	+
$CAW^{\downarrow}LEA_{55}$	HIV-1 protease	n.d.	-[4]
Cell surface receptors			
$MGxxS_1$, WL_{57},L_{110}, FPD_{121}, $D/ExxLL_{160}$, EE_{154}, DD_{174}	CD4	407-418	+
$MGxxS_1$	CD28	cytoplasmic tail	+
$MGxxS_1$, M_{20}, $EEEE_{62}$, $PxxPxR_{72}$, FPD_{121}, EE_{154}	MHC class I	cytoplasmic tail	+ (EEE_{62})
$MGxxS_1$, $D/ExxLL_{160}$, $EEEE_{62}$, $PxxPxR_{72}$	MHC class II	cytoplasmic tail	+ (EEE_{62})
Signalling			
$PxxPxR_{72}$	Fyn	SH3 domain	+/-
	Hck	SH3 domain	
	Lck	SH3 domain	
	Lyn	SH3 domain	
	MAPK	SH3 domain	
	Src	SH3 domain	
	Vav	SH3 domain	
	TCRζ[5]	n.d.	
n.d.[6]	TCRζ[7]	YENLNL(x), YSEIMGRR(x)	n.d.
$MGxxS_1$, $PxxPxR_{72}$, RR_{105}	PAK1/2 (NAK)	n.d.	+
$DDPxxE_{174}$	c-Raf1 kinase	n.d.	n.d.
N-, C-terminus	PI-3 kinase	p85 subunit	n.d.
n.d.	Ask1	n.d.	n.d.
M_1-W_{57}	p53	n.d.	+
Trafficking			
$EEEE_{62}$	PACS-1	n.d.	+
FPD_{121}	Human thioesterase (p35)	n.d.	n.d.
EE_{154}	β-COP	n.d.	n.d.
$D/ExxLL_{160}$	Adaptor proteins AP-1/2/3	μ subunit of AP-1/2/3	n.d.
	β1 of AP-1	β1 of AP-1	
DD_{174}	V1H	n.d.	+

[1] Residue numbering is shown for HIV-1 laboratory strain NL4-3 Nef
[2] Requirement of the binding motif on Nef for pathogenicity
[3] Intact full length protein is required for pathogenicity
[4] n.d., not determined
[5] As described for HIV-1 Nef (Fackler et al., 2001; Xu et al., 1999)
[6] To be described in this thesis
[7] As described for HIV-2 and SIVmac239 Nef (Schaefer et al., 2000)

Modified from (Das and Jameel, 2005; Geyer et al., 2001; Kirchhoff et al., 2008)

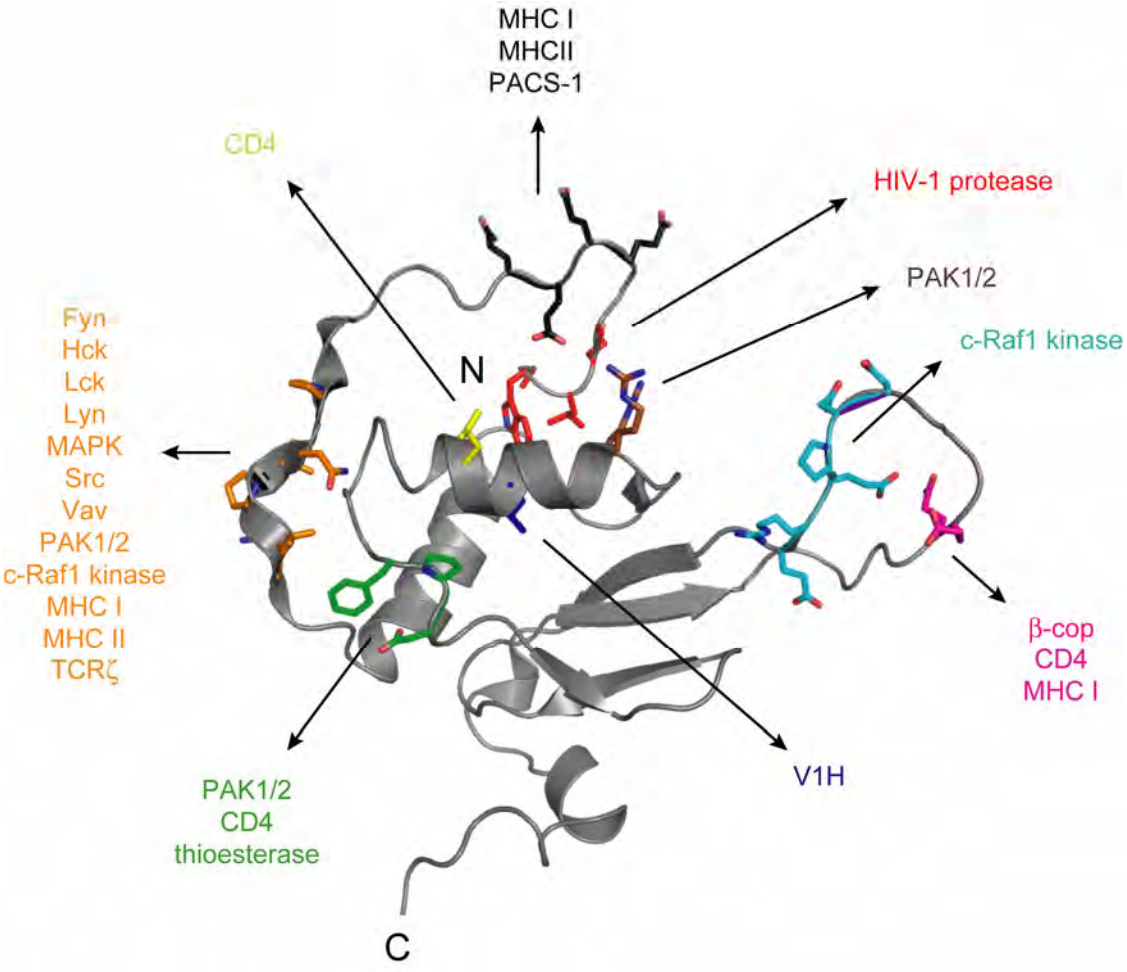

Figure I-3. Structural motifs on Nef important for binding and function. The NMR solution structure of HIV-1 isolate BRU Nef (H40-A206, Δ159-173, C206A; pdb code 2NEF) is shown in ribbon diagram The residues involved in the interaction of Nef with its host cellular partners or are important for functional activity are depicted in stick models.

natural killer (NK) cells (Collins et al., 1998; Specht et al., 2008). Nef mediates the downregulation of surface MHC expression through two unique sorting pathways. The first reported mechanism described Nef linking phosphofurin acidic cluster sorting protein-1 (PACS-1) with the short MHC cytoplasmic tail and directing the complex to the *trans*-Golgi network (TGN) (Crump et al., 2001; Piguet et al., 2000; Wan et al., 1998). Although the binding site on Nef specific for MHC is unknown, a highly acidic cluster of residues near the N-terminus of Nef (E62, E63, E64, E65) was found to be crucial in binding PACS-1 (Crump et al., 2001; Piguet et al., 2000). Subsequent studies demonstrated that Nef is also capable of downregulating surface MHC HLA-A2 expression in a PACS-1-independent manner that instead uses AP-1 and clathrin to direct MHC molecules to endosomes and lysosomes (Lubben et al., 2007).

The interaction of Nef with CD4 and its subsequent downregulation are among the most heavily investigated functions of Nef. Nef reduces surface expression of CD4 by directly coupling the cytoplasmic tail of CD4 to components of the endocytotic machinery, including clathrin, dynamin and the clathrin adaptor proteins AP-1 and AP-2; complex formation results in the direction of CD4 to the lysosomal compartment for eventual degredation. The interaction of HIV-1 Nef with CD4 is determined by the presence of an alpha helix in the cytoplasmic tail of CD4 (403-433) that allows for high affinity binding (K_D = 0.5 – 1.4 μM) of Nef (Grzesiek et al., 1996b; Preusser et al., 2002). In addition, the specificity of Nef with the clathrin adaptor protein AP-2 is conferred by a dileucine motif that has been demonstrated to be unique to CD4 downregulation and essential for proper sorting of the receptor (Aiken et al., 1994;

Bresnahan et al., 1998; Chaudhuri et al., 2007; Lindwasser et al., 2008; Mangasarian et al., 1997). Downregulation of CD4 has been postulated to serve a role in immune evasion by disrupting the antigen presenting cell-T cell interface and allowing for the infected T cell to circulate and engage in viral spread. In addition, because CD4 serves as the receptor for Env, CD4 downregulation may help to enhance release of HIV progreny during viral budding (reviewed in (Li et al., 2005a)).

In contrast to the downregulation of CD4 and MHC class I proteins, downregulation of surface TCR expression is only observed for HIV-2 and SIV Nef and represents one of the few functions of Nef that is lentiviral type-dependent. The inability of HIV-1 Nef to downregulate TCR expression has been suggested to be a consequence of cross-species evolution resulting in the loss of T cell activation suppression activity (Schindler et al., 2006). SIV Nef binds the ζ chain of the TCR at two unique sites (Howe et al., 1998; Schaefer et al., 2000) and mediates TCR downregulation binding of the clathrin-associated protein AP-2 through a unique cooperative mechanism (Swigut et al., 2003). Interestingly, HIV-1 Nef has also been demonstrated to interact with TCRζ *in vitro* (Fackler et al., 2001; Xu et al., 1999) suggesting that TCR-binding and TCR downregulation are separable functions and differentially conserved among HIV-1, HIV-2 and SIV Nef.

I.B.2.b. Modulation of T cell activation

As shown in Table I-1, Nef has been reported to bind multiple proteins involved in T cell signaling, including the Src family of protein tyrosine kinases (i.e. Fyn, Lck,

Src), PI-3 kinase and the signaling ζ chain of the T cell receptor. However, the functional consequences of those interactions are poorly understood. Furthermore, the reported effects of HIV-1 Nef on T cell activation has been inconsistent with some reports suggesting that Nef plays a positive enhancing role where other reports argue that Nef suppresses T cell activation in the presence of external stimuli (summarized in Table I-2). HIV-1 Nef has also been reported to induce a T-cell transcriptional program that closely resembles activation by anti-CD3 stimulation (Simmons et al., 2001). The discrepancy in the observed immunomodulatory effects suggests that Nef plays a significant role in modulating T cell signaling pathways but that its effect is pleiotropic. Each experimental condition may therefore highlight certain features of Nef's overall effect on T cell activation and result in aberrant functional outcomes.

Despite the controversy in Nef's immunomodulatory effect, one structural feature on Nef has consistently been demonstrated to be crucial for Nef's function in T cells: myristylation of the N-terminus. The myristylation modification directs Nef to the plasma membrane where it participates in the downregulation of surface molecules but additionally affects T cell signaling mechanisms, including the formation of the immunological synapse (IS) (Fenard et al., 2005; Thoulouze et al., 2006). Nef's recruitment to the IS has been demonstrated to potentiate TCR-mediated signaling events and reduce the stimulus threshold required for NFAT and NFkB (Fenard et al., 2005). Other studies have suggested that Nef associates with lipid rafts and primes the T cell for activation by increasing the local concentration of TCR molecules (Djordjevic et al., 2004; Wang et al., 2000). Disruption of the myristylation sequence results in drastic

abrogation of Nef's function at the IS (Fenard et al., 2005) and has also been described to result in inhibitition of TCR-mediated T cell signaling (Baur et al., 1994). Collectively, these data suggest that Nef imparts its immunomodulatory function primarily at the inner leaflet of the plasma membrane where it gains access to molecules that participate in the early events of T cell activation, namely the TCR and Src family kinases. Surprisingly, a highly pathogenic strain of SIV, SIVpbj14, is able to replicate by causing activation of resting peripheral blood mononuclear cells (PBMCs) (Fultz, 1991) and has been associated with an ITAM-like sequence present in Nef (Du et al., 1995). Reconstitution of the of ITAM YxxL motif (17RQ → 17YE) found in SIVpbj14 in SIVmac239 Nef resulted in increased tyrosine phosphorylation of SIVmac239 (17YE) Nef in addition to augmented T cell activation and acute disease, suggesting an extensive role of Nef in signal transduction and cellular activation (Du et al., 1995). Detailed investigation of Nef's interaction with different components of the T cell signaling machinery may therefore provide insight into the mechanisms of Nef-mediated immune modulation as well as provide a new perspective into the differential immune activation profiles observed during natural HIV-1 and SIV infection.

Table I-2. Modulation of T cell activation by Nef

Nef isolate	Cells	Mitogen	Activation Measurement	Reference
Suppression of T cell activity				
HIV-1 NL4-3	Jurkat	PMA + PHA, PMA + ionomycin	IL-2 mRNA	(Luria et al., 1991)
HIV-1 NL4-3	Jurkat	PHA + PMA	NFκB	(Niederman et al., 1992)
HIV-1 NL4-3	Jurkat	PHA + PMA	AP-1[1]	(Niederman et al., 1993)
HIV-1 NL4-3	Jurkat	anti-CD3	NFκB, AP-1	(Bandres and Ratner, 1994)
HIV-1 SF2[2]	Jurkat	anti-TCRβ, PMA	phosphorylation, Ca2+ flux, NFκB	(Baur et al., 1994)
HIV-1 NL4-3	Jurkat	PMA + PHA, PMA + ionomycin, PMA + CD3	IL-2, IFN	(Greenway et al., 1996)
HIV-1 BRU	Jurkat	PMA + ionomycin	IL-2 transcription	(Collette et al., 1996)
HIV-1 NA7	Jurkat	anti-CD3	CD69	(Iafrate et al., 1997)
No effect on T cell activity				
HIV-1 LAI	T cell clones, Jurkat	PMA, PHA + PMA, anti-CD3 + PMA, anti-CD3 + CD28	IL-2, TNF, cell proliferation	(Schwartz et al., 1992)
HIV-1 HxB3	T lymphocytes (transgenic)	CD3 + PMA	cell proliferation	(Skowronski et al., 1993)
HIV-1	Jurkat	PMA, PMA + PHA, TNF, anti-CD3	IL-2, TNF, IL-2R, NFκB, AP-1	(Carreer et al., 1994)
HIV-1 LAI	T cell clones	antigen-presenting cell	TNF, CSF, IFN, IL-6	(Page et al., 1997)
HIV-1 NL4-3	Jurkat	PMA, PHA	NFκB, AP-1	(Yoon and Kim, 1999)
Enhancement of T cell activity				
HIV-1 NL4-3	T lymphocytes (transgenic)	anti-CD3 + PMA	cell proliferation	(Skowronski et al., 1993)
HIV-1SF2	T cell hybridoma	anti-CD3	IL-2	(Rhee and Marsh, 1994)
HIV-1 SF2	Jurkat	anti-TCRβ, PMA	phosphorylation, Ca2+ flux, NFκB	(Baur et al., 1994)
SIVpbj14[3]	Jurkat	- - -	NFAT	(Luo and Peterlin, 1997)
HIV-1 NL4-3	T lymphocytes (transgenic)	anti-CD3	phosphorylation (LAT, MAPK)	(Hanna et al., 1998b)
HIV-1 SF2[3]	Jurkat	- - -	FasL	(Xu et al., 1999)
HIV-1 NL4-3	Jurkat	anti-CD3, anti-CD3 + anti-CD28	IL-2 secretion	(Schrager and Marsh, 1999)
HIV-1	Jurkat	anti-CD3 + anti-CD28, PMA	IL-2, PI3K activity	(Djordjevic et al., 2004)
HIV-1 R7	Jurkat	anti-CD3 + anti-CD28	IL-2 secretion, IL-2 transcription, NFAT, NFκB	(Wang et al., 2000)
HIV-1			NFkB NFAT	(Fenard et al., 2005)

[1] recruitment of AP-1 DNA-binding activity
[2] intracellular, not membrane-targeted Nef
[3] CD8-Nef fusion results in Nef-Nef dimer

Modifed from (Marsh, 1999)

.

CHAPTER II: Interaction of the HIV-1, HIV-2 and SIV Nef core domain with the T cell receptor zeta subunit

Abstract

Nef from HIV and SIV share a number of functions including downregulation of surface receptor molecules, modulation of T cell signaling pathways and enhancement of virion infectivity. However, recent studies have suggested that HIV-1 and SIV Nef are not interchangeable with respect to their ability to interact with the signaling ζ chain of the T cell receptor (TCRζ) or their ability to downmodulate TCR surface expression. Here we report that Nef from SIVmac239, HIV-2 ST and two isolates of HIV-1 (NL4-3, ELI) bind the cytoplasmic domain of TCRζ *in vitro* and that the conserved core domain of Nef mediates the interaction. The core domain of SIVmac239 Nef bound TCRζ with the highest affinity, followed by HIV-2 ST and HIV-1 ELI Nef. In addition, the Nef core domain from SIVmac239 and HIV-2 ST interacted with two distinct regions on TCRζ whereas the core domain of HIV-1 ELI Nef shared only the N-terminal binding site. However, the high affinity TCRζ-binding properties of the core domain of SIVmac239 Nef were found to be necessary but not sufficient to reduce TCR surface expression. An intact Nef protein, containing both the SIV N-terminal domain and the high affinity core domain was required for TCR downregulation. Collectively, these data suggest that the TCRζ-binding and downregulatory properties of Nef changed during the cross-species evolution of SIV to HIV-1 and may be responsible for the differential TCR-mediated activation profiles seen in naturally infected HIV-1 and SIV hosts.

II.A. Introduction

Human immunodeficiency virus 1 (HIV-1) infection and progression to acquired immunodeficiency syndrome (AIDS) is characterized by elevated immune activation, CD4+ lymphocyte depletion and high viral load. One of the critical determinants mediating HIV-1 pathogenesis is Nef, a myristoylated 27-35 kDa viral accessory protein unique to HIV and SIV that is expressed in abundance early in the viral life cycle. In studies where rhesus macaques were experimentally inoculated with SIV (Kestler et al., 1991), *nef*-deleted strains of SIVmac239 failed to promote accelerated disease and instead resulted in markedly low viremia and reduced pathogenicity. In humans, several patients infected with *nef*-defective HIV-1 exhibited a long-term nonprogressor phenotype with delayed disease progression (Kirchhoff et al., 1995; Salvi et al., 1998). HIV-1 Nef itself is capable of inducing virulent behavior: HIV-1 *nef*-transgenic mice present with severe AIDS-like phenotypes (Hanna et al., 2009; Lindemann et al., 1994; Simard et al., 2002; Skowronski et al., 1993) and HIV-1 *nef*-transfected T-cells display enhanced sensitivity to external stimuli (Baur et al., 1994; Schrager and Marsh, 1999) and a transcriptional state nearly identical to that of T cells stimulated by mitogenic anti-CD3 antibodies (Simmons et al., 2001). In contrast, natural infection of humans with HIV-2 or nonhuman primates with the orthologous simian immunodeficiency virus (SIV) is largely nonpathogenic and does not exhibit the augmented T cell activation profile nor progression to severe immunodeficiency observed with HIV-1 (Munch et al., 2005; Villinger et al., 1996). Understanding the differential effect of HIV-1 and HIV-2/SIV infection on T cell activation requires the elucidation and characterization of their

molecular targets. In this study, we investigate the interaction of HIV-1, HIV-2 and SIV Nef with the ζ chain of the T cell receptor (TCR), the primary signaling molecule in the TCR complex.

Nef's role in HIV-1 virulence is multifaceted but can be described as a combination of three distinct mechanisms that collectively determine the course of viral pathogenesis (reviewed in (Kirchhoff et al., 2008): (1) modulation of cell-surface expression of membrane proteins, (2) modulation of signal transduction pathways, and (3) enhancement of viral infectivity. Generally conserved among the HIV-1, HIV-2 and SIV Nef variants is the ability to downregulate surface expression of several type I membrane proteins including CD4 (Aiken et al., 1994; Anderson et al., 1993; Benson et al., 1993; Garcia and Miller, 1991; Mariani and Skowronski, 1993; Schindler et al., 2006), major histocompatability complex (MHC) class I molecules (Collins et al., 1998; Le Gall et al., 1997; Schindler et al., 2006; Schwartz et al., 1996) and CD28 (Bell et al., 2001; Schindler et al., 2006; Swigut et al., 2001). In contrast, downregulation of the TCR complex is not conserved among the different Nef variants; HIV-2/SIV Nef reduces TCR surface expression with high efficiency whereas HIV-1 Nef does not (Bell et al., 1998; Schindler et al., 2006). This disparity has been postulated recently (Schindler et al., 2006) to be the result of lentiviral evolution where the protective ability of SIV Nef to downregulate TCR expression and to suppress T-cell activation in its natural primate host was lost during zoonotic transfer to humans and development of virulent HIV-1.

Modulation of TCR surface expression by HIV-2/SIV Nef is mediated by interaction with the cytoplasmic domain of the ζ signaling subunit of the T cell receptor

(TCRζ) (Bell et al., 1998; Howe et al., 1998; Schaefer et al., 2000) and cooperative recruitment of the endocytotic machinery protein AP-2 (Swigut et al., 2003). Although it has been demonstrated that HIV-1 Nef does not downregulate TCR surface expression (Schindler et al., 2006), its ability to bind TCRζ and to subsequently alter downstream signaling consequences is unclear. Initial yeast two-hybrid and GST-pulldown binding studies (Bell et al., 1998; Howe et al., 1998) suggested that HIV-2 and SIV Nef but not HIV-1 Nef could bind to the cytoplasmic domain of TCRζ and that the core domain (residues 98-235) of SIV Nef was responsible for the interaction. Further studies demonstrated that SIV Nef bound TCRζ at two distinct sites, coined SIV Nef interaction domains (SNIDs) (Schaefer et al., 2000). However, subsequent co-immunoprecipitation studies have shown that HIV-1 Nef also specifically binds TCRζ (Fackler et al., 2001; Xu et al., 1999) and that the interaction is responsible for mediating HIV-induced TCR-dependent FasL expression (Xu et al., 1999). Confocal imaging studies have shown that HIV-1 Nef is recruited to the immunological synapse during engagement of the TCR and potentiates T-cell signaling (Fenard et al., 2005), a function largely attributed to HIV-1 Nef acting directly on TCRζ (Fackler et al., 2001; Sigalov et al., 2008). Studies involving HIV-1 Nef are complicated by the use of different HIV-1 Nef isolates where some reports investigate several strains from a number of viral clades (Howe et al., 1998; Schindler et al., 2006) and others focus on individual HIV-1 isolates such as SF2 (Simmons et al., 2001) or the laboratory strain NL4-3 (Fackler et al., 2001). Taken all together, it remains unclear whether or not the ability to bind TCRζ is a conserved function shared by Nef

proteins from a range of HIV and SIV isolates and if so, whether that interaction plays a role in both TCR downregulation and modulation of TCR-mediated T cell activation.

Here we demonstrate that Nef proteins from representative strains of HIV-1, HIV-2, and SIV all specifically bind the cytoplasmic domain of TCRζ *in vitro* and that the conserved core domain of Nef is responsible for mediating the interaction. SIVmac239 Nef and the homologous HIV-2 ST Nef variant bind to the same two regions on TCRζ whereas HIV-1 ELI Nef only interacts with the N-terminal binding region. In addition, SIVmac239 Nef binds to both binding regions with relatively similar affinities whereas a more discrete difference in affinity is seen for HIV-2 ST Nef. In contrast, HIV-1 ELI Nef binds to only one region on TCRζ and with the lowest affinity, suggesting that the ability of Nef to bind TCRζ was attenuated during evolution and in the species crossover from SIV to HIV-1. Therefore, the affinity of Nef for TCRζ may be one of the primary factors that determines whether Nef has a nonpathogenic or pathogenic role in modulation of T-cell signaling in SIV or HIV-1 infection, respectively.

II.B. Materials and Methods

II.B.1. Nef and TCRζ expression plasmids.

Prokaryotic *nef* expression plasmids were created by cloning the HIV-1 (ELI, NL4-3), HIV-2 ST and SIVmac239 genes into pET32a(+) (Novagen). Open reading frames of full-length HIV-1 isolate ELI (K4-N206), HIV-1 laboratory strain NL4-3 (K4-C206), HIV-2 ST (S4-S255) and SIVmac239 (A4-R263) *nef* and core domain HIV-1 ELI (A56-N206), HIV-1 NL4-3 (A56-C206), HIV-2 ST (D94-S234) and SIVmac239 (D95-S235) nef were amplified by PCR from HIV-1 (ELI, NL4-3) provirus (kindly provided by M. Stevenson) and HIV-2 ST and SIVmac239 Nef cloning vectors (NIH AIDS Reagent Repository). The *nef* amplification products included 5' *KpnI* and 3' *HindIII* restriction digestion sites and an engineered thrombin cleavage site immediately upstream of the nef coding region. The nef full-length and core domain amplification products were digested with *KpnI* and *HindIII* and ligated into the pET32a(+). Prior to ligation, pET32a(+) was mutated to remove the thrombin cleavage site included in the original parent vector by site directed mutagenesis. The final Nef-encoding gene product included an N-terminal thioredoxin (Thx) tag, 6xHis affinity tag, S-tag, single thrombin cleavage site and *nef* gene.

Eukaryotic *nef* expression plasmids encoding wildtype or mutant Nef-GFP fusion proteins were generated by cloning the HIV-1 ELI (M1-N206) and SIVmac239 (M1-S263) genes into pEGFP-N1 (Clontech). Open reading frames of full-length HIV-1 ELI and SIVmac239 were amplified by PCR from their respective pET32a-nef expression plasmids with 5' *EcoRI*-containing and 3' *BamHI*-containing primers. The nef

amplification products were digested with *EcoRI* and *BamHI* and ligated into pEGFP-N1 in frame with the downstream GFP sequence to allow for Nef-GFP fusion protein expression. In order to generate the mutant nef chimera expression plasmids, the *BamHI* restriction site downstream of the nef gene was removed by site directed mutagenesis, keeping the GFP gene still in frame with the nef gene. A *BamHI* restriction site was inserted by site-directed mutagenesis at the junction of the N-terminal domain and the core domain in HIV-1 ELI (W57) and SIVmac239 (D89). The N-terminal domains of HIV-1 ELI (M1-W57) and SIVmac239 (M1-D89) were amplified by PCR from their respective pEGFP-nef expression plasmids with 5' *EcoRI*-containing and 3' *BamHI*-containing primers and ligated into their partner plasmid to generate the HIV/SIV (M1-W57/V90-S263) and SIV/HIV (M1-D89/L58-N206) chimeric nef expression plasmids. In order to keep the N-terminal domain and C-terminal domain regions in frame, the internal *BamHI* restriction site was removed by site-directed mutagenesis. All of the primers used in the cloning and mutagenesis procedures are listed in Appendix A.1.

Construction of plasmids expressing the cytoplasmic domain (K54-R163) of TCRζ (pET32a-TCRζ_{cyt}) and an N-terminal cysteine-containing (cys-L51-R163) construct (pET32a-cys-TCRζ_{cyt}) has been described previously (Aivazian and Stern, 2000).

II.B.2.Recombinant protein expression, purification and modification.

Nef was expressed as a thioredoxin fusion protein in *E. coli* strain BL21 (DE3). Following induction at 37^{o}C with 0.75 mM isopropyl-β-D-thiogalactopyranoside (IPTG),

cell cultures were harvested by centrifugation at 5,000xg. The cell pellets were re-suspended in lysis buffer (100 mM NaH_2PO_4, 8M Urea, pH 8.0) and lysed at 4^oC by stirring. After clearance of the cell lysate by centrifugation at 10,000xg, the soluble fraction was loaded onto a Ni-NTA agarose (Qiagen) column and the target fusion protein was eluted by a pH gradient (pH 8.0-pH 4.5) under denaturing conditions (8 M urea). Elution fractions containing the thioredoxin-Nef fusion protein were identified by 12% SDS-PAGE and dialyzed against dialysis buffer (20 mM TRIS, 150 mM NaCl, 0.1 mM DTT, pH 8.0) at 4^oC. The dialysis products were then filtered through a 0.22 μm filter and total protein concentration was quantified by Bradford assay (Bio-Rad). Thrombin (MP Biomedicals) was added to each dialysis sample at a concentration of 5U thrombin/mg total protein and incubated at room temperature for 1 - 3 hrs. The digestion reactions were then quenched by addition of PMSF, diluted 4-fold with dilution buffer (20 mM Tris, pH 8.0) and loaded on a POROS 20 HQ (Applied Biosystems) anion exchange column. Cleaved Nef proteins were eluted with a salt gradient (0 - 600 mM NaCl) and fractions containing Nef were identified by 12% SDS-PAGE. Nef-containing fractions were pooled, concentrated and run over a Superdex 200 (Pharmacia) size exclusion chromatography column in PBS after which peak fractions were pooled and concentrated. Purification of $TCR\zeta_{cyt}$ was performed as described (Sigalov et al., 2004). Purified cys-$TCR\zeta_{cyt}$ was modified with an N-terminal biotin affinity tag by conjugating the free cysteine with maleimide-PEO_2-biotin (Pierce) as directed by the manufactuer's instructions. The TCRζ polypeptides DP1 (L51-D93) and DP2 (P94-R164) were purified

following trifluoroacetic acid (TFA)-mediated hydrolysis of the purified TCRζ_{cyt} protein by size exclusion chromatography.

II.B.3. Surface plasmon resonance (SPR) analysis.

SPR spectroscopy experiments were performed at 25^{o}C on a Biacore 3000 system (GE Healthcare). 5000-8000 resonance units (RU) of neutravidin were coupled to a CM5 sensor chip (GE Healthcare) in 10mM acetate buffer (pH 5.0) using standard amine coupling protocols; residual areas of activated surface were blocked with ethanolamine. For all binding experiments, 10-20 RU of each overlapping biotin-LC-TCRζ peptide (Anaspec) or 250 RU of biotin-cys-TCRζ_{cyt} were captured in different neutravidin-coupled experimental flow cells leaving one flow cell unmodified as a control surface. Each immobilized TCRζ peptide or polypeptide was directed uniformly in an N-terminal to C-terminal orientation away from the neutravidin-CM5 surface due to placement of the biotin tag at the N-terminus. Binding of each Nef analyte was monitored after equilibrating the instrument at 25^{o}C in PBS (150mM NaCl + 0.005% surfactant P20, pH 7.4) under reducing (5mM DTT) and non-reducing conditions and achieving a stable immobilized surface with no baseline drift. In the initial screening experiments, purified samples of full-length and core domain Nef proteins from HIV-1 (ELI, NL4-3), HIV-2 ST and SIVmac239 were injected at a flow rate of 30μl/min over each experimental flow cell for and the control flow cell, generating SPR sensorgrams. The sensorgram from the control neutravidin-only flow cell was subtracted from the experimental neutravidin-bio-TCRζ peptide flow cell sensorgram (reference subtraction), generating a resultant Nef

binding sensorgram that described the specific binding of Nef for the captured TCRζ peptide and removed any nonspecific interaction with the CM5 or neutravidin surface. All Nef proteins were allowed to bind until reaching binding equilibrium and then exchanged with PBS. In the kinetic and equilibrium interaction analyses, Nef was injected in a 2-fold concentration series ranging from 0 - 50 μM (SIV mac239, HIV-2 ST) or 0 - 200 μM (HIV-1 ELI). Each experiment was run in triplicate with each concentration injected at random. No regeneration step was required.

In order to determine the affinity of each Nef-TCRζ fragment interaction, equilibrium and kinetic analyses was performed when appropriate. In the equilibrium binding analysis, the RU binding levels at equilibrium were extrapolated from each sensorgram in the concentration series. The RU levels from each triplicate Nef concentration injection were averaged and plotted against concentration to derive a binding curve. Scatchard analysis and appropriate affinity rate constants were determined in Prism 4.0 (Graphpad). Kinetic analysis was also performed where the binding sensorgrams had measurable association and disassociation rates that could be calculated by global fitting. Evaluation of different kinetic binding models and determination of the appropriate kinetic affinity measurements were performed using BIAevaluation 4.1 (GE Healthcare). The quality of the kinetic fit for each binding model was assessed by inspecting the statistical χ^2 value and the residuals (observed - calculated) in order to determine the most accurate mode of interaction. The following binding models were used to describe the Nef-TCRζ interaction:

1. Simple model: single analyte-ligand interaction that corresponds to the 1:1 bimolecular Langmuir Equation.

$$A + B \underset{k_{off}}{\overset{k_{on}}{\leftrightarrow}} AB$$

$$K_D = \frac{k_{off}}{k_{on}}$$

where the affinity rate constant K_D is the ratio of the dissociation rate k_{off} and association rate k_{on}.

2. Heterogenous ligand model: heterogeneity in the ligand results in two unique interaction sites, each of which binds the same analyte with different association and diassociation rates.

$$A + B_1 \underset{k_{off\,1}}{\overset{k_{on1}}{\leftrightarrow}} AB_1;\ A + B_2 \underset{k_{off\,2}}{\overset{k_{on\,2}}{\leftrightarrow}} AB_2$$

$$K_{D1} = \frac{k_{off\,1}}{k_{on1}} \qquad K_{D2} = \frac{k_{off\,2}}{k_{on2}}$$

where the ligands B_1 and B_2 refer to two unique ligand subset populations and AB_1 and AB_2 represent the resulting complexes when the homogenous analyte A binds each ligand binding site. Rate constants K_{D1} and K_{D2} represent the affinity of each ligand population for the single analyte.

II.B.4. Size exclusion chromatography.

Analytical size exclusion chromatography was performed at room temperature using a BioSep-SEC-S2000 column (Phenomenex) on a BioCad Sprint Perfusion

Chromatography System. Samples containing SIV mac239 Nef_{core}, $TCR\zeta_{cyt}$, $TCR\zeta_{cyt}$ DP1, $TCR\zeta_{cyt}$ DP2 and Nef in the presence of each $TCR\zeta_{cyt}$ sample were flowed at 0.5 ml/min in PBS and elution was monitored by recording of the absorbance at 280 nm. Peak fractions for each experimental sample were collected for analysis by 12% SDS-PAGE. For calibration of the BioSep-SEC-S2000 column, the following molecular mass markers (Bio-Rad Laboratories, Hercules, CA) were used: bovine thyroglobulin (670 kDa), bovine γ-globulin (158 kDa), chicken ovalbumin (44 kDa), horse myoglobulin (17 kDa), and vitamin B_{12} (1.35 kDa). A calibration curve correlating retention time and molecular weight was generated and used to translate the peak retention time for each experimental sample to a calculated molecular weight. The stoichiometries of the different Nef-TCRζ peptide interactions were determined by comparing the different calculated molecular weights for each experimental sample.

II.B.5. Cell culture and DNA transfections.

CH7C17 Jurkat T cells (Hewitt et al., 1992) were cultured in RPMI 1640 medium supplemented with 2mM glutamine and 10% fetal bovine serum (FBS) and passaged 1:5 every 3-4 days. Cells were transfected by electroporation at 262V, 1500uFd, 725ohms with 10ug of DNA on a BTX ECM 830 (Harvard Apparatus) electroporation generator. Following transfection, the cells cultured for 42-48h prior to flow cytometric analysis of Nef-GFP and surface CD3 expression.

II.B.6. Flow cytometry analysis.

Transfected CH7C17 Jurkat T cells were stained for surface CD3 expression. Aliquots of $1x10^6$ cells were incubated with saturating amounts of phycoerythrin (PE)-conjugated anti-CD3ε monoclonal antibody (Sigma) at 4^oC, washed with staining buffer (1xPBS, 0.5% BSA, 0.02% NaN_3) and analyzed on a FACSCalibur flow cytometer (BD Biosciences). The effect of wildtype and mutant Nef expression on surface CD3 expression was determined by correlating GFP and PE fluorescence. Flow cytometric plots were generated and analyzed in FlowJo (Treestar).

II.C. Results

II.C.1 Full length and core domains of HIV-1 ELI, HIV-1 NL4-3, HIV-2 ST and SIVmac239 Nef bind the cytoplasmic domain of TCRζ in vitro.

Previous studies have been contradictory with regard to the ability of Nef from HIV-1 strains to interact with TCRζ in comparison to the better characterized binding activity of HIV-2 and SIV Nef (Bell et al., 1998; Fackler et al., 2001; Howe et al., 1998; Schaefer et al., 2000; Xu et al., 1999). To directly address the discrepancy regarding the ability of Nef to specifically interact with TCRζ, surface plasmon resonance (SPR) binding studies were performed with representative strain variants of HIV-1, HIV-2 and SIV Nef (Figure II-1A) and the cytoplasmic domain of human TCRζ (Figure II-1B), expressed and purified as recombinant proteins. HIV-1 Nef variants from the HIV-1 laboratory strain NL4-3 (clade B) and HIV-1 isolate ELI (clade D) were selected as representative HIV-1 strains based on an arginine/threonine polymorphism at residue 71 (Figure II-1A) that has been suggested to be a determining factor in the specificity of HIV-1 Nef for TCRζ (Fackler et al., 2001). An arginine present at residue 71, found in HIV-1 ELI Nef, has been reported to confer specificity for TCRζ whereas a threonine, present in HIV-1 NL4-3 Nef, does not. The cytoplasmic domain of TCRζ (L51-R164), modified with an N-terminal biotin affinity tag, was immobilized on a neutravidin-coupled CM5 sensor chip to mimic the native orientation of TCRζ on the inner leaflet of the cell membrane. Full-length Nef proteins (50μM) were flowed over the sensor chips under reducing conditions to prevent adventitious disulfide-mediated dimerization observed for HIV-1, HIV-2 and SIV Nef. All four Nef variants from HIV-1, HIV-2 and

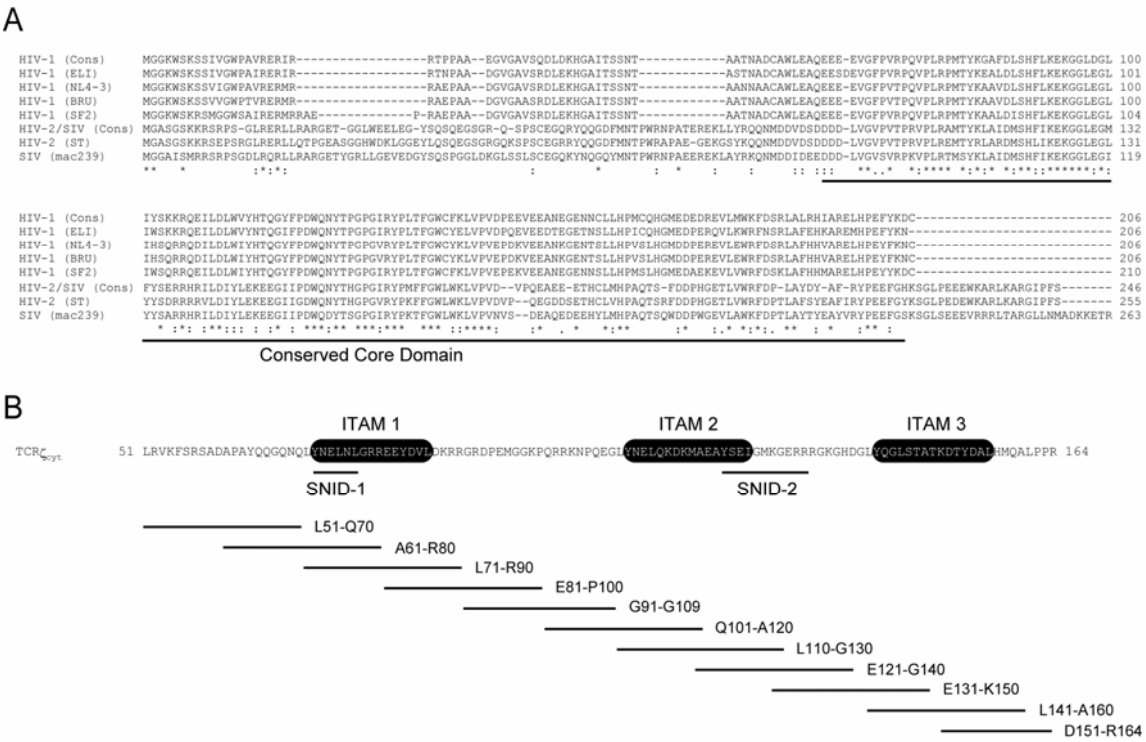

Figure II-1. Primary sequence analysis of Nef and TCRζ. (A) Sequence homology of Nef from representative HIV-1, HIV-2, SIV and consensus sequences. The conserved core domain shared by all isolates shown is denoted by the solid line. Similar and identical residues are denoted by colons (:) and asterisks (*), respectively. (B) The primary sequence of the cytoplasmic domain of TCRζ ($TCR\zeta_{cyt}$) is shown with immunoreceptor tyrosine activation motifs (ITAMS) denoted by black ovals. The previously reported SIV Nef interaction domains (SNIDs) (Schaefer et al., 2000) are denoted by black lines. Overlapping 14-21 amino acid peptides spanning the length of $TCR\zeta_{cyt}$ are illustrated by bars with their respective residue position labels.

SIV were observed to bind to immobilized TCRζ with resonance signals 10-200 RU above the neutravidin control surface (Figure II-2A, top panel). Since Nef from ELI and NL4-3 strains of HIV-1 are able to bind TCRζ, neither the R/T polymorphism at residue 71 in HIV-1 Nef nor the HIV-1/HIV-2 subtype variation are crucial factors in the interaction of Nef with TCRζ.

A previous study reported that the core domain (residues 98-235) of SIVmac239 Nef is the primary region responsible for binding TCRζ (Howe et al., 1998). Alignment of the primary sequences from various HIV-1, HIV-2 and SIV Nef variants (Figure II-1A) reveals that the core domain is highly conserved. In addition, the core domain spans the structurally ordered region of the HIV-1 protein as observed by crystallography (Arold et al., 1997; Lee et al., 1996) and NMR (Grzesiek et al., 1996a). Therefore, we investigated the possibility that TCRζ specificity was conferred by the conserved core domain present in all HIV-1, HIV-2 and SIV Nefs. We expressed and purified the Nef core domain (Nef_{core}) from HIV-1, HIV-2, and SIV strains described above, and analyzed their binding to immobilized TCRζ as was done with their respective full-length forms. Each Nef core domain bound to TCRζ with SPR signals of 25-160 RU, similar to that observed for the full-length proteins (Figure II-2A). Therefore, not only does Nef from HIV-1 ELI, HIV-2 ST and SIVmac239 show the ability to bind TCRζ, but the structured core domain that is conserved among the different subtypes seems to be sufficient for binding.

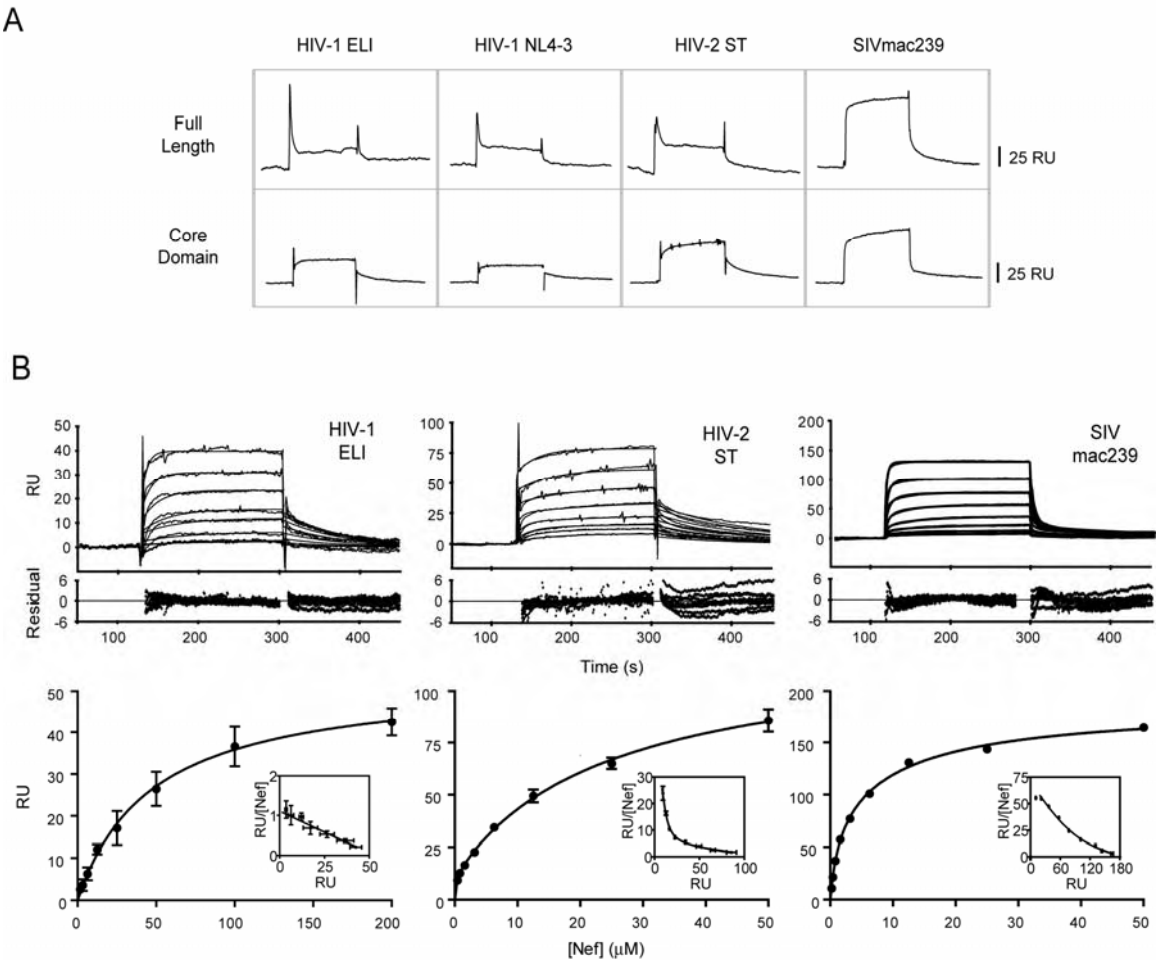

Figure II-2. HIV-1, HIV-2 and SIV Nef bind TCRζ_{cyt}. A. Full-length and core domain Nef proteins from HIV-1 ELI, HIV-1 NL4-3, HIV-2 ST and SIVmac239 were flowed at a concentration of 50μM over TCRζ_{cyt} immobilized on a CM5 bionsensor chip. Binding was recorded by changes in the SPR resonance unit (RU) signal. B. Core domain Nef (Nef_{core}) proteins from HIV-1 ELI, HIV-2 ST and SIVmac239 were injected at various concentrations (0-200μM for HIV-1 ELI Nef_{core} and 0-50μM for HIV-2 ST and SIVmac239 Nef_{core} were flowed over immobilized TCRζ_{cyt}. Binding models for simple 1:1 Langmuir binding and heterogenous parallel reaction binding were fit to HIV-1 ELI Nef_{core} and HIV-2 ST/SIVmac239 Nef_{core}, respectively. Residuals of model fit are shown below the binding curves. The RU values measured at binding equilibrium (250-300s) were used to generate the binding plots (lower panel) and for Scatchard analysis (inset).

II.C.2. The conserved core domain of HIV-1 ELI, HIV-2 ST and SIV mac239 Nef bind TCRζ with different binding region specificities and affinities.

In order to further characterize the Nef-TCRζ interaction and investigate any strain-dependent differences in binding, detailed SPR studies were performed with the Nef_{core} proteins. Two-fold dilution series of HIV-1 ELI (0-200μM), HIV-2 ST (0-50 μM) and SIVmac239 (0-50 μM) Nef core domains were flowed over immobilized TCRζ and changes in resonance signal were recorded. As illustrated in the binding sensorgrams (Figure II-2B), the core domains from all three Nef variants bound TCRζ with measurable association (k_{on}) and dissociation (k_{off}) phases, reaching apparent binding equilibrium during the experiment. To characterize the binding kinetics, we considered a number of different binding models for each Nef_{core} domain, as described below.

In a previous study, SIVmac239 Nef was demonstrated to bind TCRζ at two unique regions (Schaefer et al., 2000), indicated as SNID-1 and SNID-2 in Figure II-1B. Therefore, we evaluated a heterogenous ligand binding model ($A + B_1 = AB_1$; $A + B_2 = AB_2$) that would account for the two binding regions. As shown in Figure II-2B, the SIVmac239 Nef_{core}-TCRζ binding sensorgrams fit well to the heterogenous ligand binding model with random and compact residuals. Other binding models, including bivalent analyte ($A + B \leftrightarrow AB$; $AB + B \leftrightarrow AB_2$), conformational change ($A + B \leftrightarrow AB$; $AB \leftrightarrow AB^*$), hetereogenous analyte ($A_1 + B \leftrightarrow A_1B$; $A_2 + B \leftrightarrow A_2B$) and simple langmuir bimolecular ($A + B \leftrightarrow AB$) models, did not fit the data as well; the respective modeled curves deviated significantly from the binding data and exhibited higher $\chi 2$ values. Using the kinetic association and dissociation parameters, the equilibrium

dissociation constants of the binding of SIVmac239 Nef_{core} to TCRζ were calculated to be 0.3μM ± 0.1 (K_{D1}) and 3.9μM ± 0.4 (K_{D2}) (Table 1). We also estimated the equilibrium dissociation constants from the binding plot and accompanying scatchard analysis (Figure II-2) of the equilibrium binding values measured at 250-300s of each experiment. As observed from the kinetic analysis, the equilibrium binding curve of the SIVmac239 Nef_{core}-TCRζ interaction fit best to a two site binding model with the calculated affinity constants K_{D1} = 1.3μM ± 0.6 and K_{D2} = 11.8μM ± 6.6, closely matching the values from the kinetic analysis (Table 1).

Previous work has suggested that HIV-2 Nef might also bind to two regions on TCRζ (Schaefer et al., 2002). In our studies, the SPR sensorgrams of HIV-2 ST Nef_{core} binding TCRζ also fit best to a heterogenous ligand binding model in both the kinetic and equilibrium analyses. Consistent with the pronounced curvilinear fit of the scatchard plot, TCRζ has one high affinity binding site (K_{D1} = 0.2- 4.7μM) and one markedly weaker one (K_{D2} = 24.3 - 37.2μM). The presence of a strong and weak binding site on TCRζ correlates well with previous GST pull-down experiments that demonstrated that HIV-2 ST Nef only weakly interacted with SNID-1 and exhibited more prominent binding to SNID-2 (Schaefer et al., 2002). In contrast, HIV-1 ELI Nef_{core} exhibited completely different TCRζ-binding behavior. Following evaluation of the different binding models with the binding sensorgrams, a simple langmuir bimolecular model (A + B ↔ AB) fit the best, suggesting that the hetereogeneity in the ligand population seen in the presence of SIVmac239 and HIV-2 ST Nef is absent and only a homogenous ligand surface exists. The linear regression curve observed on the scatchard plot of the equilibrium binding

data verified the simple bimolecular model and resulted in a calculated affinity measurement (K_D = 47.8μM ± 3.5) that corresponded with the observed kinetically-derived affinity constant K_D = 20.2μM ± 5. (Figure II-2B).This suggests that TCRζ either 1) has one weak affinity binding site specific for HIV-1 ELI Nef_{core} with any second site either absent or having affinity too weak to detect in our assays or 2) that the weak and strong binding sites on TCRζ seen with HIV-2 ST and SIVmac239 Nef_{core} have an identical affinity for HIV-1 ELI Nef and are thus indistinguishable. Collectively, these data demonstrate that TCRζ-binding is a conserved function among the core domains of HIV-1 ELI, HIV-2 ST and SIVmac239 Nef, and that each Nef variant binds TCRζ in a slightly different manner where the affinity of the interaction decreases from SIV ~ HIV-2 > HIV-1.

II.C.3. HIV-2 ST and SIV mac239 Nef_{core} bind to two regions on $TCR\zeta_{cyt}$ whereas HIV-1 ELI Nef_{core} binds to only one.

Due to its structural intrinsic disorder in solution (Sigalov et al., 2004), the recombinant TCRζ proteins used in the SPR spectroscopy experiments are highly unlikely to contain conformational epitopes that participate in binding Nef. Alternatively, it is more likely that $TCR\zeta_{cyt}$ interacts with Nef through linear epitopes that can be characterized through straightforward regional mapping studies. Therefore, in order to further investigate the nature of the two site and single site binding models describing HIV-2 ST/SIVmac239 and HIV-1 ELI Nef_{core} binding of $TCR\zeta_{cyt}$, respectively, the regions on TCRζ responsible for binding each Nef variant were identified. Overlapping,

N-terminally biotinylated 14-21-mer peptides spanning the length of TCRζ_{cyt} (Figure I-1B) were immobilized on neutravidin-coupled CM5 chips. Each TCRζ peptide was then screened for positive Nef-binding by flowing over HIV-1 ELI, HIV-2 ST and SIVmac239 Nef_{core} proteins and observing changes in the SPR signal. As shown in Figure II-3A, HIV-2 ST and SIVmac239 Nef_{core} both bind to one peptide near the N-terminus (A61-R80) and two peptides located closer to the C-terminus (L110-G130, E121-G140), consistent with previous reports characterizing SNID-1 and SNID-2 (Schaefer et al., 2000). In contrast, HIV-1 ELI Nef_{core} showed exclusive binding (RU = 125) to only one (A61-R80) of the three TCRζ peptides that bound HIV-2 ST and SIVmac239 Nef_{core}.

To determine the affinity of each Nef_{core} variant for their respective TCRζ-binding preptide partners, a 2-fold concentration series of each Nef_{core} protein were flowed over each peptide and allowed to reach equilibrium. Due to the association and disassociation rates being too rapid to fit to kinetic models (Figure II-3A), equilibrium analysis was performed on the binding data by plotting the measured equilibrium RU binding levels against the concentration of the injected Nef_{core} sample. Binding model curves were applied and assessed for best fit by evaluating the correlation coefficient R^2 for each model. For all of the Nef_{core}-TCRζ peptide binding plots, the binding data fit best to a simple langmuir bimolecular binding curve (Figure II-3B) with R^2 values ranging from 0.974 to 0.992. SIVmac239 Nef_{core} displayed the highest affinity for each of the two TCRζ binding regions with K_D affinity measurements of 5.9μM ($\pm$ 0.2) for the SNID-2-containing region and 8.5μM ($\pm$ 0.5) for the SNID-1-containing region. In contrast, HIV-

2 Nef_{core} displayed markedly reduced affinity for both TCRζ regions in comparison to SIVmac239 but more importantly revealed an approximate five-fold increase in affinity for the C-terminal SNID-2-containing region (K_D = 21.9μM vs. 94.9μM) as compared to the N-terminal SNID-1-containing region. This preference for the C-terminal binding region is unique to HIV-2 as it was not observed for SIVmac239 nor HIV-1 ELI Nef_{core} which only showed specificity for the N-terminal SNID-1-containing domain. Interestingly, while HIV-1 ELI Nef_{core} displayed the weakest affinity for TCRζ among the Nef variants, it also bound to the weaker of the two interaction sites observed for HIV-2 ST Nef_{core} with even weaker affinity (K_D > 100μM). These measurements support the experiments performed on the full $TCR\zeta_{cyt}$ proteins where two site binding was observed for SIVmac239 and HIV-2 ST Nef and one site binding was observed for HIV-1 ELI Nef_{core}. Taken together, these data suggest that the number of binding sites on TCRζ that Nef_{core} recognizes and the affinities associated with them are lentiviral subtype dependent where SIVmac239 Nef_{core} is the most specific and HIV-1 ELI Nef_{core} is the least.

To further confirm the presence of two distinct binding regions on TCRζ specific for SIVmac239 Nef_{core} and to further characterize the stoichiometry of the interaction, size exclusion chromatography experiments were performed. Two fragments of the cytoplasmic domain of TCRζ, $TCR\zeta_{DP1}$ (L51-D93) and $TCR\zeta_{DP2}$ (P94-R164), were generated by self cleavage under acidic conditions with each containing one of the two SIVmac239 Nef_{core}-binding regions. During size exclusion chromatography, $TCR\zeta_{DP1}$ (20μM) and $TCR\zeta_{DP2}$ (20μM) eluted as 9.9 kDa and 15.6kDa species, respectively,

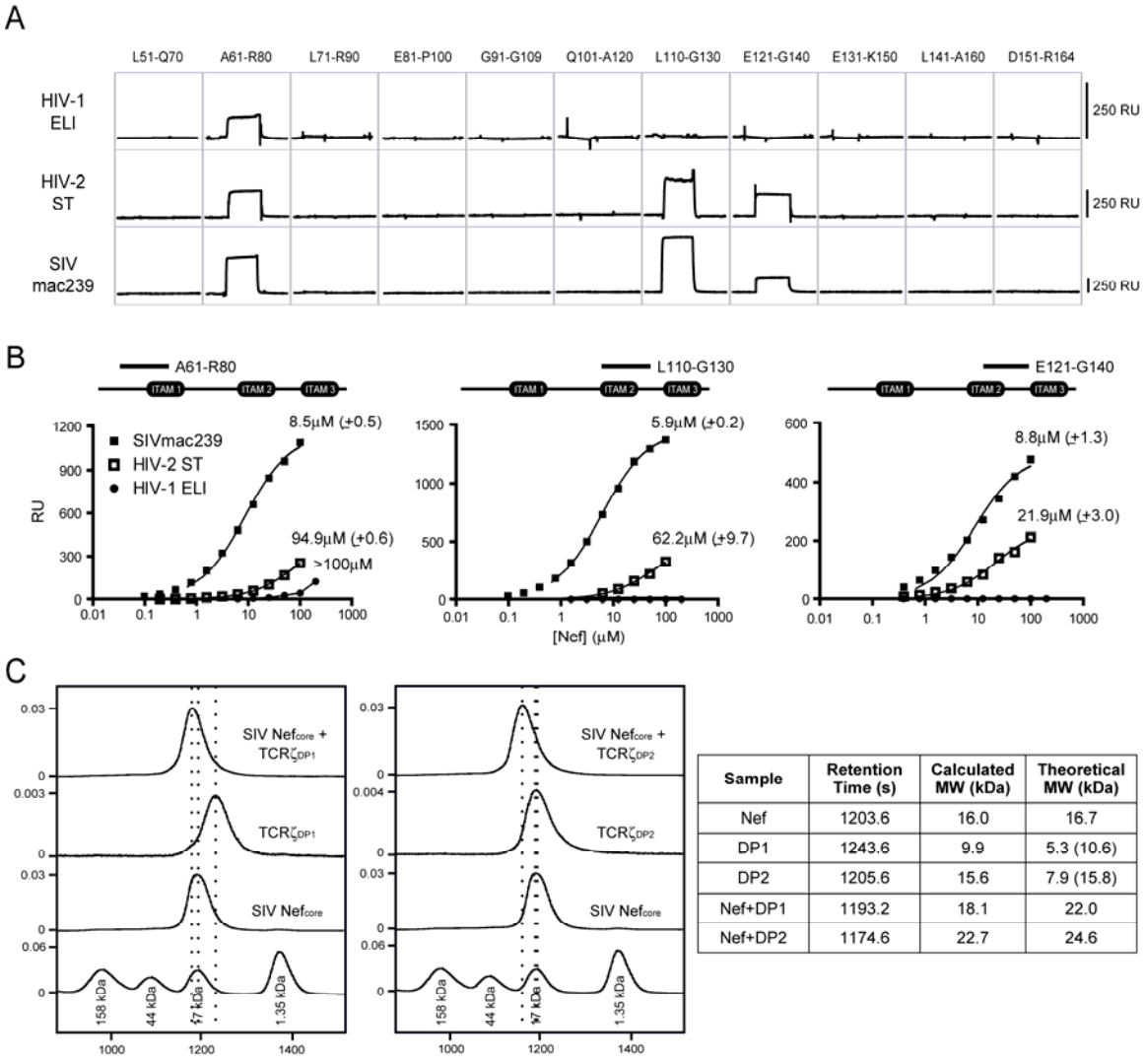

Sample	Retention Time (s)	Calculated MW (kDa)	Theoretical MW (kDa)
Nef	1203.6	16.0	16.7
DP1	1243.6	9.9	5.3 (10.6)
DP2	1205.6	15.6	7.9 (15.8)
Nef+DP1	1193.2	18.1	22.0
Nef+DP2	1174.6	22.7	24.6

Figure II-3. SIVmac239 and HIV-2 Nef_{core} bind to two regions on TCRζ where HIV-1 ELI binds to only one. A. HIV-1 ELI, HIV-2 ST and SIVmac239 Nef_{core} (50μM) were flowed over a series of overlapping 14-21 amino acid peptides spanning the length of $TCR\zeta_{cyt}$, each immobilized separately. Binding was detected by changes in the SPR signal (RU). B. Equilibrium affinity analysis. Bound (RU) levels of Nef core domain proteins from HIV-1 ELI, HIV-2 ST and SIVmac239 Nef were recorded for each peptide and plotted against Nef concentration. Affinity measurement (KD) was calculated by fitting a simple 1:1 langmuir binding model. Standard deviation is shown in parenthesis. C. SIVmac239 Nef_{core} (20μM) and the $TCR\zeta_{cyt}$ polypeptides DP1 and DP2 (20μM) were injected alone and in combination over a BioSep-SEC-S2000 column.

consistent the calculated molecular weights of TCRζ_{DP1} and TCRζ_{DP2} homodimers (Figure II-3C). This was similar to the dimerization behavior described for the full cytoplasmic domain of TCRζ (Sigalov et al., 2004). In the presence of equimolar SIVmac239 Nef_{core}, both Nef + TCRζ_{DP1} and Nef + TCRζ_{DP2} samples eluted as a heterodimeric species with simple 1:1 stoichiometry, validating the SPR finding that SIVmac239 Nef_{core} was specific for an N-terminal and C-terminal binding site on TCRζ_{cyt}. The formation of a simple heterodimeric Nef- TCRζ_{DP1} and Nef- TCRζ_{DP2} species supports our previous finding that SIVmac239 Nef_{core} disrupts the TCRζ homodimer during the formation of the heterodimeric Nef-TCRζ complex (Sigalov et al., 2008).

II.C.4. SIV Nef-mediated TCR downregulation is dependent on both the high affinity core domain and the N-terminal domain.

A previous study suggested that HIV-1 and SIV Nef differ in their ability to modulate TCR surface expression where the majority of SIV isolates of Nef robustly downregulates TCR from the cell surface and HIV-1 Nef has no effect (Schindler et al., 2006). Having demonstrated that the conserved core domains of HIV-1 ELI and SIVmac239 Nef share TCRζ-binding activity, we investigated the role of the non-conserved N-terminal domain in TCR downregulation by generating HIV-1/SIV and SIV/HIV-1 Nef chimeras and measuring their effect on TCR surface expression. As shown in Figure II-4, SIVmac239 Nef-GFP reduces surface TCR levels whereas HIV-1 ELI Nef-GFP and GFP alone do not. Surprisingly, both the HIV-1/SIV Nef-GFP

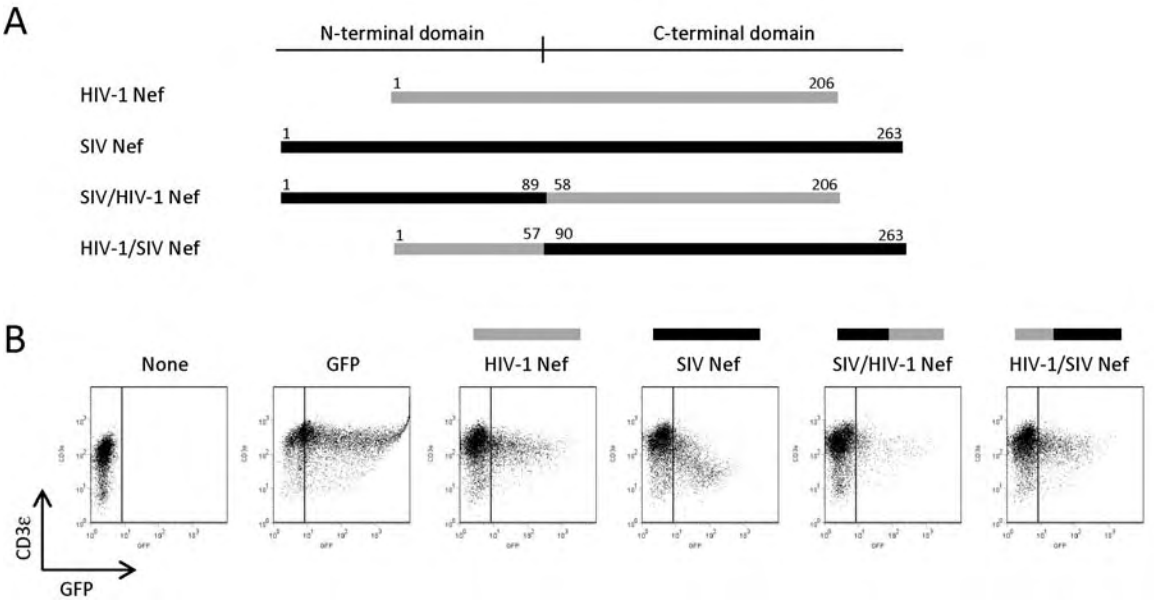

Figure II-4. TCR downregulation by wildtype and chimeric Nef. A. Schematic representation of wildtype and chimeric Nef transfection constructs. Full-length Nef from HIV-1 ELI and SIVmac239 are depicted in grey and black, respectively, with terminal residue positions labeled. SIV/HIV-1 and HIV-1/SIV Nef chimeric constructs, containing the HIV-1 or SIV unconserved N-terminal domain or conserved C-terminal domain, are illustrated with the corresponding residue positions. B. The N-terminal domain and C-terminal domain of SIVmac239 Nef is necessary for downregulation of TCR. Flow cytometry analysis of CD3ε surface expression in JJK Jurkat T cells transiently expressing wildtype or chimeric Nef-GFP fusion proteins is shown.

chimera, containing the N-terminal domain of HIV-1 ELI Nef (M1-W57) fused to the high affinity TCRζ-binding C-terminal domain of SIVmac239 Nef (V90-S263), and the SIV/HIV-1 Nef-GFP chimera, containing the N-terminal domain of SIVmac239 Nef (M1-D89) fused to the low affinity TCRζ-binding C-terminal domain of HIV-1 ELI Nef (L58-N206), failed to downregulate TCR. It has been suggested that SIV Nef may bind endocytotic factors, namely clathrin associated protein AP-2, through a cooperative binding mechanism with TCRζ exclusive from the classical AP-2 interaction domains (CAIDs) found in the SIV Nef N-terminal domain (Swigut et al., 2003). Our studies suggest that the SIVmac239 N-terminal domain is in fact necessary for SIV Nef's ability to downregulate the TCR. However, because the SIV/HIV-1 Nef chimera was unable to reduce surface TCR expression, the N-terminal domain of SIVmac239 Nef is not sufficient for TCR downregulation. Therefore, TCR-downregulatory function and TCRζ-binding activity are distinct functional properties but mutually dependent: Nef-mediated TCR downregulation not only requires the high affinity binding property of the core domain of SIVmac239 Nef but also the non-conserved N-terminal domain from SIVmac239 Nef.

Table II-1. Affinity measurements of the HIV-1, HIV-2 and SIV Nef_{core}-$TCR\zeta_{cyt}$ interaction.

	Kinetic Analysis			*Equilibrium Analysis*
Nef_{core}	k_a, 1/Ms	k_d, 1/s	K_D, μM	K_D, μM
HIV-1 ELI	$6.74x10^2$ (± 25.1)	$1.36x10^{-2}$ (± 0.002)	20.2 (± 5.1)	47.8 (± 3.5) [100%]
HIV-2 ST	$6.0x10^2$ (± 8.3)	$2.81x10^{-3}$ (± 0.02)	4.7 (± 0.7)	0.2 (± 0.2) [10%]
	$4.05x10^4$ (± 40.5)	$1.51x10^{-2}$ (± 0.001)	37.2 (± 5.4)	24.3 (± 4.1) [90%]
SIVmac239	$2.26x10^4$ (± 18.2)	$8.72x10^{-2}$ (± 0.01)	0.3 (± 0.1)	1.3 (± 0.6) [43%]
	$1.71x10^4$ (± 16.7)	$5.51x10^{-3}$ (± 0.003)	3.9 (± 0.4)	11.8 (± 6.6) [57%]

Association (k_a), dissociation rates (k_d) and affinity constants (K_D) calculated from kinetic analysis, on left, as well as affinity constants (K_D) derived from equilibrium analysis, on right, are indicated for each Nef_{core} protein. Standard deviation is indicated in parentheses, (), and percentage of total binding is indicated in brackets, [].

II.D. Discussion

In this study we demonstrate that the core domains of Nef from HIV-1 ELI, HIV-2 ST and SIVmac239 collectively bind the cytoplasmic domain of TCRζ but with different affinities and site specificities. The core domain of HIV-1 ELI Nef bound TCRζ with the lowest affinity (K_D = 20.2 - 47.8μM) and at only one region containing elements of ITAM 1. In contrast, the core domains of HIV-2 ST and SIVmac239 Nef bound TCRζ at two distinct regions containing elements of ITAM 1 (shared with HIV-1 ELI Nef) and ITAM 2, consistent with previous findings (Schaefer et al., 2000). Analysis of the SPR sensorgrams suggests that the core domains of HIV-2 ST and SIVmac239 Nef binds to each region with different affinity: one strong binding site (SIVmac239 Nef, K_D = 0.3 - 1.3μM; HIV-2 ST Nef, K_D = 0.2 – 4.7μM) and one weaker binding site (SIVmac239 Nef, K_D = 3.9 – 11.8μM; HIV-2 ST Nef, K_D = 24.3 - 37.2μM) that corresponds closely with HIV-1 ELI Nef's affinity for the full cytoplasmic domain of TCRζ.

Previous studies based on yeast two-hybrid and GST-pulldown experiments suggested that the interaction of Nef with TCRζ was limited to SIV and HIV-2 (Bell et al., 1998; Howe et al., 1998). Co-immunoprecipitation experiments from Nef-transfected Jurkat T cells later refuted those findings and demonstrated that HIV-1 Nef was capable of binding TCRζ (Fackler et al., 2001; Xu et al., 1999) and that the R/T polymorphism at residue 71 on Nef determined its specificity (Fackler et al., 2001). Our results confirm the co-immunoprecipitation results but additionally demonstrate that the amino acid occupying residue 71 is not a primary determinant of the binding reaction between Nef and TCRζ as both the laboratory strain NL4-3 (T71) and the ELI isolate (R71) of Nef

bound TCRζ. Curiously, contradictory experimental findings were also observed for HIV-1 Nef regarding its ability to bind the SH3 domain of Src family protein tyrosine kinases. In SPR experiments, HIV-1 NL4-3 Nef was demonstrated to bind the SH3 domain of Hck with high affinity (K_D = 0.25μM) but only weakly to the SH3 domain of wildtype Fyn (K_D > 20μM) (Lee et al., 1995). However, GST-pulldown experiments performed in parallel resulted in co-precipitation of only the SH3 domain of Hck and not Fyn in the presence of Nef, refuting their SPR binding results. Co-precipitation of the Fyn SH3 domain with Nef was later observed but only after the introduction of a point mutation in Fyn (F96I) that increased its affinity for Nef by over 50-fold (K_D = 0.38μM). Therefore, co-precipitation studies may not be a reliable assay to measure the weaker interactions of Nef with its cellular partners that instead require more sensitive methods.

HIV-1 Nef may also bind TCRζ through a cooperative mechanism that involves other binding partners. In co-immunoprecipitaton experiments, the interaction of HIV-1 Nef with TCRζ was abrogated following mutation of the PxxP sequence found near the N-terminus of the core domain (Xu et al., 1999). Although the PxxP motif has been demonstrated to interact with the SH3 domains of Src family kinases (Arold et al., 1997; Lee et al., 1996), it is not expected to interact with TCRζ in the same manner. Therefore, HIV-1 Nef may bind TCRζ cooperatively with a Src family kinase to form a stable heterotrimeric complex that is within the detection range of co-precipitation binding studies. This would explain the discrepancy in the co-precipitation studies since TCRζ should only co-immunoprecipitate with HIV-1 Nef from Nef-transfected T cells that contain Src family kinases and not with Nef alone as was performed in the yeast-two

hybrid and GST-pulldown studies. A similar cooperative binding mechanism has been proposed for SIVmac239 Nef, TCRζ and the clathrin-associated adaptor protein AP-2 (Swigut et al., 2003) based on the observation that Nef co-precipitated increased amounts of TCRζ and AP-2 when all three components were present as compared to TCRζ and AP-2 alone (Swigut et al., 2003). None of the classical AP-2 binding elements on Nef were found to be involved in the interaction with AP-2 thus raising the possibility that the SIV Nef-TCRζ interaction forms a high affinity binding site for AP-2 and vice-versa. Interestingly, the SH3 domain of Fyn has been demonstrated to order the N-terminus of the core domain of HIV-1 Nef into a polyproline type II helix that is not observed in the unliganded Nef_{core} protein (Arold et al., 1997). Therefore, HIV-1 Nef and Src family kinases may be acting in a similar fashion to SIVmac239 and AP-2 by coupling binding to the formation of a novel interaction interface that exhibits increased affinity for TCRζ.

The cooperative binding mechanism of SIVmac239-TCRζ-AP-2 complex formation may also help to explain the differences in TCR downregulation observed for HIV-1 and SIV Nef. Our studies demonstrate that SIV Nef is only capable of downregulating TCR surface expression in its full length form that contains both the highly variable N-terminus and strong TCRζ-binding C-terminal domain. When either domain was swapped with HIV-1 Nef, downregulation was abrograted. Therefore, the AP-2 binding interface formed by the SIVmac239 Nef-TCRζ interaction likely contains elements of both domains that are not conserved with HIV-1. Therefore, we suggest that TCRζ-binding is a shared function of HIV-1, HIV-2 and SIV Nef and that TCRζ-binding does not directly lead to downregulation.

Nef functions primarily as an adaptor protein that forms multimeric complexes with host cellular proteins resulting in dysregulation of normal function. SIV Nef has been demonstrated extensively to bind TCRζ and AP-2 and induce downregulation of the T cell receptor. TCR downregulation has been suggested to serve as a protective mechanism that attenuates T cell activity and promotes commensal viability with its infected host (Schindler et al., 2006). In humans, this protective function is lost allowing HIV-1 Nef to potentially recruit proteins other than AP-2 to TCRζ. One intriguing group of candidates includes members of the Src family of protein kinases that initiate the T-cell signaling cascasde following external stimulation of the TCR [reviewed in (Smith-Garvin et al., 2009)]. By binding TCRζ and Src family kinases, HIV-1 Nef may enhance TCRζ phsophorylation and modulate downstream T cell activation events conducive to elevated viral replication.

CHAPTER III: Pseudo-merohedral twinning and non-crystallographic symmetry in orthorhombic crystals of SIVmac239 Nef core domain bound to different length TCR zeta fragments

Abstract

HIV/SIV Nef mediates many cellular processes through interactions with various cytoplasmic and membrane-associated host proteins, including the signalling zeta subunit of the T cell receptor (TCRζ). Here, the crystallization strategy, methods and refinement procedures used to solve structures of the core domain of the SIVmac239 isolate of Nef (Nef_{core}) in complex with two different TCRζ fragments are described. The structure of SIVmac239 Nef_{core} bound to the longer TCRζ polypeptide (L51-D93) was determined to 3.7 Å (R_{work} = 28.7%) in the tetragonal space group $P4_32_12$. The structure of SIVmac239 Nef_{core} in complex with the shorter TCRζ polypeptide was determined to 2.05 Å (R_{work} = 17.0%) but only after the detection of nearly perfect pseudo-merohedral crystal twinning and proper assignment of the orthorhombic space group $P2_12_12_1$. The reduction in crystal space group symmetry induced by the truncated TCRζ polypeptide appears to be caused by the rearrangement of crystal contact hydrogen bonding networks and the substitution of crystallographic symmetry operations with similar non-crystallographic symmetry (NCS) operations. The combination of NCS rotations nearly parallel to the twin operation (*k*,*h*,-*l*) and unit cell lengths a and b nearly identical predisposed the $P2_12_12_1$ crystal form to pseudo-merohedral twinning.

III.A. Introduction

Protein crystallization occurs under supersaturating conditions where protein molecules organize by either non-crystallographic or crystallographic symmetry operations into repeating unit cells that pack to form a crystal lattice. Crystal twinning occurs when two or more crystal packings intersperse in one larger aggregate crystal. This has been reported to occur as a result of polymorphic transformation during physical stress (Govindasamy et al., 2004; Yeates, 1997) but occurs more commonly as a pathology of crystal growth. When the lattice of each crystal packing in the aggregate crystal do not overlap in three dimensions, the crystal exhibits epitaxial, or non-merohedral, twinning that can be easily detected by the presence of split reflections on the crystal's x-ray diffraction pattern. However, when the lattice axes of the individual crystals are parallel, the crystal is considered to be merohedrally twinned and the x-ray diffraction pattern will not provide any visual cues of crystal twinning. For protein molecules, merohedrally twinned crystals exist predominately as hemihedrally twinned crystals (Yeates, 1997) that contain two distinct twin domains that are related to each other by a twin law operation. The twin fraction α represents the fractional contribution of the less prevalent twin domain. The diffraction pattern of a hemihedrally twinned crystal is therefore the superimposition of two unique diffraction patterns, one of each twin domain, where each reflection intensity is the weighted sum of two twin-related intensities (Equations 1a, 1b) (Grainger, 1969).

$$I_{obs}(\mathbf{h1}) = (1-\alpha)\, I(\mathbf{h1}) + \alpha\, I(\mathbf{h2}) \qquad (1a)$$

$$I_{obs}(\mathbf{h2}) = \alpha\, I(\mathbf{h1}) + (1-\alpha)\, I(\mathbf{h2}) \qquad (1b)$$

The individual intensities I(**h1**) and I(**h2**) can be solved by combining the linear equations (Equations 2a, 2b).

$$I(h1) = \frac{(1-\alpha)\, I_{obs}(h1) - \alpha\, I_{obs}(h2)}{1-2\alpha} \qquad (2a)$$

$$I(h2) = \frac{-\alpha\, I_{obs}(h1) + (1-\alpha)\, I_{obs}(h2)}{1-2\alpha} \qquad (2b)$$

As the twin fraction α approaches 1/2, the crystal is considered to be perfectly twinned and the calculation of the intensities I(**h1**) and I(**h2**) begins to fail as the term (1-2α) begins to approach zero. This complicates the process of twin-related reflection intensity calculation, commonly referred to as detwinning. Structure determination has therefore has been preferentially performed for hemihedral crystals that exhibit non-perfect twinning.

Rare cases of twinning have been described where a twin law operation supports a higher Laue symmetry than that of the crystal unit cell (Rudolph et al., 2004). This type of twinning, referred to as pseudo-merohedral twinning, can occur in special circumstances such as a monoclinic system where the β angle approaches 90^o (Larsen et al., 2002) or an orthorhombic system where the unit cell axes a and b are fortuitously similar in length ($a \approx b$), resulting in the emulation of higher apparent tetragonal symmetry (Brooks et al., 2008). In this report we describe such a case, for crystals of the the complex of the Nef (negative factor) protein from simian immunodeficiency virus bound to a fragment of the one of Nef's cellular targets, the cytosolic domain of the TCR zeta subunit (TCRζ).

Nef from human immunodeficiency virus (HIV) or simian immunodeficiency virus (SIV) is a 27-35 kDa viral accessory protein dispensable for replication but required for high infectivity and virulence (reviewed in (Arien and Verhasselt, 2008)). Expressed in abundance early in the viral life cycle, Nef performs a number of functions that can be generalized into three activities: enhancement of viral infectivity, downregulation of surface receptors and modulation of T cell activation. Notable among Nef's functions is the interaction of Nef with the TCRζ (Bell et al., 1998; Fackler et al., 2001; Howe et al., 1998; Schaefer et al., 2000; Sigalov et al., 2008; Swigut et al., 2000; Xu et al., 1999), the principal signaling component of the T cell antigen receptor. This interaction has been suggested to play a role in HIV-mediated modulation of membrane proximal T cell sigaling events (Fenard et al., 2005; Thoulouze et al., 2006) and in SIV-mediated downregulation of the T cell receptor (Munch et al., 2002; Schaefer et al., 2002; Schindler et al., 2006; Swigut et al., 2003; Willard-Gallo et al., 2001). In previous work (Schaefer et al., 2000) as well as studies described in Chapter II of this thesis, Nef has been shown to bind TCRζ at two unique sites, the first containing elements of immunoreceptor tyrosine activation motif (ITAM) 1 that is shared by HIV-1 and SIV Nef and the second containing elements of ITAM 2 that is unique to SIV Nef. However, the structural features on Nef that determine its specificity for TCRζ remain unknown.

Nef contains two domains, an unstructured, highly variable, myristylated N-terminal domain and a C-terminal structured core domain (Arold et al., 1997; Grzesiek et al., 1997; Lee et al., 1996) that exhibits high sequence conservation among different HIV-1, HIV-2 and SIV isolates. The Nef conserved core domain (Nef_{core}) has been

described to be responsible for the majority of Nef's interactions (Peter, 1998), including SIV Nef's TCRζ-binding activity. For HIV-1 Nef, the core domain has been shown to be amenable to crystallization (Arold et al., 1997; Lee et al., 1996; Li et al., 2002). In this study, we aimed to determine the crystal structure of the Nef-TCRζ complex by crystallizing the high-affinity complex of the Nef_{core} protein, SIVmac239 Nef_{core} (Chapter 2), with TCRζ fragment polypeptides containing the putative binding regions.

Here, we describe the crystallization and structure determination of two complexes of SIVmac239 Nef_{core} with two different TCRζ polypeptides, $TCR\zeta_{L51\text{-}D93}$ and $TCR\zeta_{A63\text{-}R80}$. Structure determination of the SIVmac239 Nef_{core}- $TCR\zeta_{L51\text{-}D93}$ complex was hampered by the poor electron density maps calculated from the low resolution diffraction data phases derived from molecular replacement using the published HIV Nef core domain model. Eventually we were able to determine this structure using the higher-resolution SIVmac239 Nef_{core}- $TCR\zeta_{A63\text{-}R80}$ complex as a starting model. However, determination of the high resolution SIVmac239 Nef_{core}- $TCR\zeta_{A63\text{-}R80}$ complex structure was hindered by the nearly perfect pseudo-merohedral crystal twinning that was detected by analysis of intensity statistics. Ultimately, a partially twinned crystal with a twin fraction of 0.424 was used to solve the structure of the SIVmac239 Nef_{core}-$TCR\zeta_{A63\text{-}R80}$ complex to 2.05 Å. The structures of the two complexes revealed that crystallization of SIVmac239 Nef_{core} with the shorter TCRζ polypeptide had reduced the space group symmetry from tetragonal to orthorhombic and introduced non-crystallographic symmetry (NCS). Because the unit cell axes a and b were still nearly identical in the orthorhombic crystal form, the crystal was prone to twinning. This study

presents a unique case where pseudo-merohedral crystal twinning was a consequence of reduction in crystal symmetry induced by the truncation of a protein ligand.

III.B. Materials and methods

III.B.1. Protein expression and purification

The core domain of SIVmac239 Nef with a two residue linker, GS-Nef [D95-S235] (Nef_{core}), was expressed and purified as described (Chapter II, Sigalov et al., 2008a). Briefly, Nef was expressed as a 6xHis-thioredoxin fusion protein in BL21 (DE3) *E. coli*. Following cell lysis, the Nef fusion protein was isolated by Ni-NTA affinity chromatography (Qiagen) under denaturing conditions (8M urea) and then dialyzed against a non-denaturing buffer containing 20mM Tris, 150mM NaCl, 100uM DTT at pH 8.0. The soluble fusion protein was then subjected to proteolysis with thrombin (MP Biochemicals), resulting in the cleaved Nef_{core} protein. SIVmac239 Nef_{core} was purified by anion exchange and size exclusion chromatography and concentrated to 700μM by ultrafiltration (Amicon) in PBS.

$TCR\zeta_{cyt}$ includes and acid-labile Asp-Pro sequence (Landon, 1977) at positions 93-94. We made use of this to prepare two fragments of TCRζcyt, termed DP1 (L51-D93) and DP2 (P94-R164). $TCR\zeta_{cyt}$, purified as described (Sigalov et al., 2004), was incubated at 1.3 mg/ml (0.1 mM) in 30% acetonitrile, 0.5% TFA (v/v) for 48 hrs at 50^{o}C. Fragments were isolated by reverse-phase chromatography on a Vydac c18 300A pore size column using an acetonitrile gradient in 0.1% TFA, and recovered by lyophilization. Mass spectrometry was used to verify the identity of the fragments and lack of any additional chemical modification other than the desired amide hydrolysis. All TCRζ polypeptides were solubilized in 20mM Tris pH 8.0 to a final concentration of 700μM.

Full-length TCRζ was expressed and purified as reported previously (Sigalov et al., 2004).

III.B.2. Crystallization

Crystals of SIVmac239 Nef_{core} in complex with the TCRζ polypeptides $TCR\zeta_{DP1}$ and $TCR\zeta_{A63\text{-}R80}$ were grown at 4^{o}C using the hanging-drop vapor diffusion method (McPherson, 1982). Crystals of the Nef_{core}- $TCR\zeta_{DP1}$complex were grown in a 2μl hanging drop by mixing 0.5μl SIVmac239 Nef_{core} (700μM), 0.5μl $TCR\zeta_{DP1}$ (700μM) and 1μl crystallization buffer (15% PEG 3,350, 150mM KF, 100mM HEPES, pH 8.2). Crystals of the Nef_{core}- $TCR\zeta_{A63\text{-}R80}$ complex were grown in a 3μl hanging drop by mixing 1μl SIVmac239 Nef_{core} (700μM), 1μl $TCR\zeta_{63\text{-}80}$ (700μM) and 1μl crystallization buffer (10-14% PEG 3,350, 200mM NH_4F, 100mM HEPES, pH 7.4-7.5). The hanging drops were suspended on siliconized glass coverslips over 1ml crystallization buffer in 24 well plates (Vydax). Crystals of the Nef_{core}-TCRζ polypeptide complexes grew to maximal size (750 x 150 x 150 μm) in 3-7 days. Prior to x-ray diffraction experiments, the Nef_{core}- $TCR\zeta_{DP1}$and Nef_{core}- $TCR\zeta_{A63\text{-}R80}$ crystals were transferred into cryoprotectant solutions containing 20-25% ethylene glycol in their respective crystallization buffers and then flash-cooled in liquid nitrogen.

III.B.3. Data collection and processing

Sixteen data sets from various Nef_{core}- TCRζ crystals were collected, of which three were

used for data collection. One low resolution data set (3.7 Å) of the SIVmac239 Nef_{core}-$TCR\zeta_{DP1}$complex and two high resolution data sets (1.9 Å, 2.05 Å) of the SIVmac239 Nef_{core}- $TCR\zeta_{A63\text{-}R80}$ complex were collected from single crystals at the National Synchrotron Light Source (beamline X29) using an ADSC Quantum-315r CCD detector system. The crystal-to-detector distance for the Nef_{core}- $TCR\zeta_{DP1}$complex and Nef_{core}-$TCR\zeta_{A63\text{-}R80}$ crystals were 275mm and 250mm, respectively. The crystals were exposed for 1s with an oscillation of 1^{o} per image. A total of 180 images were collected for each data set which were separately indexed, integrated and scaled in HKL2000 (Otwinowski et al., 1997). Detection and analysis of crystal twinning was performed in *phenix.xtriage* of the *PHENIX* software package (Adams et al., 2002). Determination of the twin law governing the pseudo-merohedrally twinned SIVmac239 Nef_{core}- $TCR\zeta_{A63\text{-}R80}$ crystals was performed following proper assignment of the crystal space group as described below.

III.B.4. Structure determination and refinement

The structures of the SIVmac239 Nef_{core}- $TCR\zeta_{A63\text{-}R80}$ and SIVmac239 Nef_{core}-$TCR\zeta_{DP1}$ complexes were determined by molecular replacement. First, atomic coordinates of the Nef core domain from HIV-1 were extracted from the crystal structures of the unliganded HIV-1 isolate LAI Nef structure (PDB ID code 1AVV) (Arold et al., 1997), the HIV-1 isolate LAI Nef-Fyn SH3 domain complex (PDB ID code 1AVZ) (Arold et al., 1997) and HIV-1 isolate NL4-3 Nef-Fyn SH3 (R96I) domain complex (PDB ID code 1EFN) (Lee et al., 1996), and were modified with *CHAINSAW*

[CCP4, (1994)] to trim the side chains not shared by SIVmac239 Nef to methyl groups. The modified Nef coordinate sets were used as an ensemble search model for molecular replacement in *PHASER* (Storoni et al., 2004) and single solutions with translation z scores (TFZ) greater than 8.0 were as starting models. The structure of the Nef_{core}-$TCR\zeta_{A63\text{-}R80}$ complex was solved by multiple rounds of twinned refinement using *phenix.refine* of the *PHENIX* software package (Adams et al., 2002) interspersed with rounds of manual model building and fitting of F_o - F_c and $2F_o$ - F_c electron density maps in Coot (Emsley and Cowtan, 2004). The twin operator *k, h, -l* was applied during each round of refinement which included three cycles of individual atomic displacement factor refinement and individual energy-minimization procedures, accompanied by refinement of the twin fraction α. Water molecules were added to the refined model using both *phenix.refine* and Coot. The quality of the final and refined SIVmac239 Nef_{core}- $TCR\zeta_{A63\text{-}R80}$ structure was validated in *PROCHECK* (Laskowski et al., 1993).

The structure of the refined SIVmac239 Nef_{core}- $TCR\zeta_{A63\text{-}R80}$ complex was used as a search model to find a molecular replacement solution for the SIVmac239 Nef_{core}-$TCR\zeta_{DP1}$data. A single top molecular solution (TFZ = 10.5, LLG = 266) was found and used as starting model. The structure of the SIVmac239 Nef_{core}- $TCR\zeta_{DP1}$ structure was solved by refinement with several rounds of individual atomic displacement factor refinement and individual energy-minimization procedures using *phenix.refine*. Model inspection was performed between each round of refinement and the model was modified in Coot. The final refined structure was validated for acceptable chemical properties with

PROCHECK. Final model and refinement statistics for both SIVmac239 Nef_{core}-TCRζ polypeptide structures are shown in Table III-1.

III.C. Results and discussion

III.C.1. Crystallization and data collection of two SIVmac239 Nef$_{core}$-TCRζ polypeptide complexes

In order to determine the structure of the Nef-TCRζ complex, mixtures of the structured core domain of SIVmac239 Nef (D95-S235) with various polypeptides spanning the putative binding regions on TCRζ (Chapter II, Schaefer et al., 2000) were screened for crystal formation. Initial crystallization experiments were aimed at crystallizing the complex of Nef$_{core}$ (SIVmac239, HIV-1 ELI and NL4-3) with the full-length cytoplasmic domain of TCRζ (TCRζ$_{cyt}$), but these were unsuccessful as the complex precipitated at high concentration, possibly due to the largely unstructured nature of TCRζ$_{cyt}$ (Aivazian and Stern, 2000; Sigalov et al., 2004). Therefore, a polypeptide crystallization screening strategy was employed to identify a minimal TCRζ polypeptide that bound SIVmac239 Nef$_{core}$, which among the SIV, HIV-1, and HIV-2 variants tested (SIVmac239, HIV-1 ELI and NL4-3, respectively), exhibited the highest affinity TCRζ$_{cyt}$ binding (Chapter II) .

Crystallization efforts focused on TCRζ fragments containing the N-terminal of the two SIV interaction domains (Figure III-1). Of a series of polypeptides spanning TCRζcyt a peptide included in this region, TCRζ$_{A61-R80}$, bound to Nef$_{core}$ from HIV-1, HIV-2 and SIV strains (Chapter II), and structural information obtained on the higher-affinity SIV variant might be relevant for HIV-1 as well as the more homologous HIV-2 Nef proteins. Moreover, the TCRζ$_{DP1}$ (i.e. the N-terminal acid-cleavage fragment residues L51-D93) formed a 1:1 stoichiometric complex with SIVmac239 Nef$_{core}$,

(Chapter II) as did intact TCRζ_{cyt} (Sigalov et al., 2008). Therefore a series of polypeptides containing the original TCRζ_{DP1} polypeptide, the shorter TCR$\zeta_{A61\text{-}R80}$ polypeptide and several peptides containing the proposed SNID-1 (Schaefer et al., 2000) sequence, were either prepared from full-length TCRζ_{cyt} (TCRζ_{DP1}) or chemically synthesized (TCR$\zeta_{A61\text{-}R80}$ and variants) and used in crystallization experiments with SIVmac239 Nef$_{core}$.

SIVmac239 Nef$_{core}$ was previously demonstrated to bind to the TCRζ polypeptide spanning residues L51-D93 (i.e. the N-terminal acid-cleavage fragment TCRζ_{DP1}), forming a simple 1:1 heterodimeric complex in solution (Chapter II). SIVmac239 Nef$_{core}$ was also shown to bind a smaller binding region on TCRζ (A61-R80) that contained the first YxxL motif of the N-terminal immunoreceptor tyrosine-based activation motif (ITAM), consistent with previous reports characterizing this region as one of the two SIV Nef interaction domains (Schaefer et al., 2000). Because Nef$_{core}$ proteins from HIV-1, HIV-2 and SIV all bound the A61-R80 binding region on TCRζ (Chapter II), structural information of SIVmac239 Nef$_{core}$ in complex with the N-terminal binding site might be relevant for HIV-1 as well as the more homologous HIV-2 Nef proteins. Therefore a series of polypeptides containing the original TCR$\zeta_{L51\text{-}D93}$ polypeptide, the shorter TCR$\zeta_{A61\text{-}R80}$ polypeptide and several peptides containing the proposed SNID-1 (Schaefer et al., 2000) sequence, were either expressed and purified from *E.coli* (for TCRζ_{DP1}) or chemically synthesized (TCR$\zeta_{A61\text{-}R80}$ and variants) and used in crystallization experiments with SIVmac239 Nef$_{core}$ (Figure III-1).

SIVmac239 Nef_{core} crystallized in complex with $TCR\zeta_{DP1}$ and $TCR\zeta_{A63\text{-}R80}$, under similar conditions. Crystals of the SIVmac239 Nef_{core}- $TCR\zeta_{DP1}$ complex grew readily as long tetragonal pyramids (Figure III-2A) but diffracted x-rays to low resolution (3.7 Å) (Figure III-2B), and could not be improved further by optimization of crystallization conditions. In contrast, crystals of SIVmac239 Nef_{core} bound to $TCR\zeta_{A63\text{-}R80}$ adopted a bi-pyramidal shape (Figure III-2A) and diffracted x-rays to high resolution (1.9 – 2.05 Å) (Figure III-2B). Neither crystal form exhibited the concave or "re-entrant" features that have been suggested to predict the presence of twinned crystals (Yeates, 1997) nor did their diffraction patterns contain split reflections (Figure III-2B).

III.C.2. Space group determination and molecular replacement for SIVmac239 Nef_{core}-$TCR\zeta_{DP1}$

The low resolution diffraction data for the SIVmac239 Nef_{core}- $TCR\zeta_{DP1}$ complex was indexed in the tetragonal Laue group 4/mmm (422 point group) with unit cell parameters a = b = 51.638, c = 189.449 Å and an R_{merge} of 0.051. The Matthews coefficient V_M (Matthews, 1968) was calculated to be 2.86 (57.1% solvent), indicating the presence of one SIVmac239 Nef_{core}- $TCR\zeta_{DP1}$ hetereodimer per asymmetric unit. After analysis of the h00, 0k0 and 00l reflection intensities, the space group was further assigned to $P4_32_12$ or $P4_12_12$ based on the indicated presence of screw axes along a and c. Using an ensemble of HIV-1 Nef core domain structures as a search model, a single molecular replacement solution (TFZ = 9.4, LLG = 63) was found in space group $P4_32_12$. However, model refinement and building were hindered by the poor quality of the σ_A-

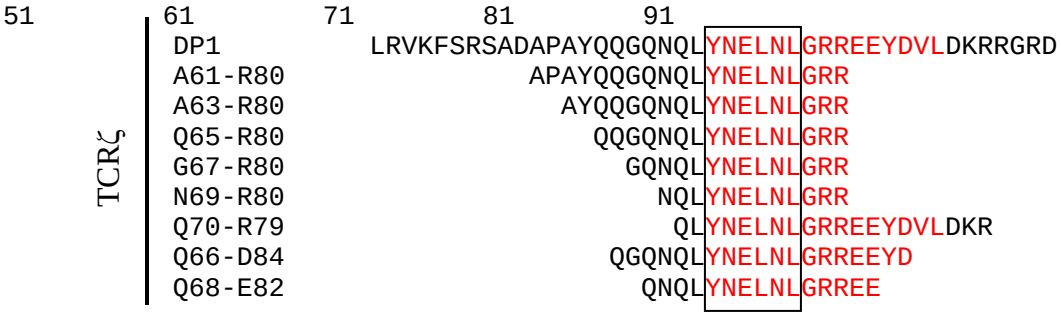

Figure III-1. TCRζ polypeptide crystallization screen. The polypeptide sequences are shown with residue position numbers assigned on the left. The boxed region contains the sequence of the first of the two reported SIV Nef interaction domains (Schaefer et al., 2000). The sequence of ITAM 1 is colored red.

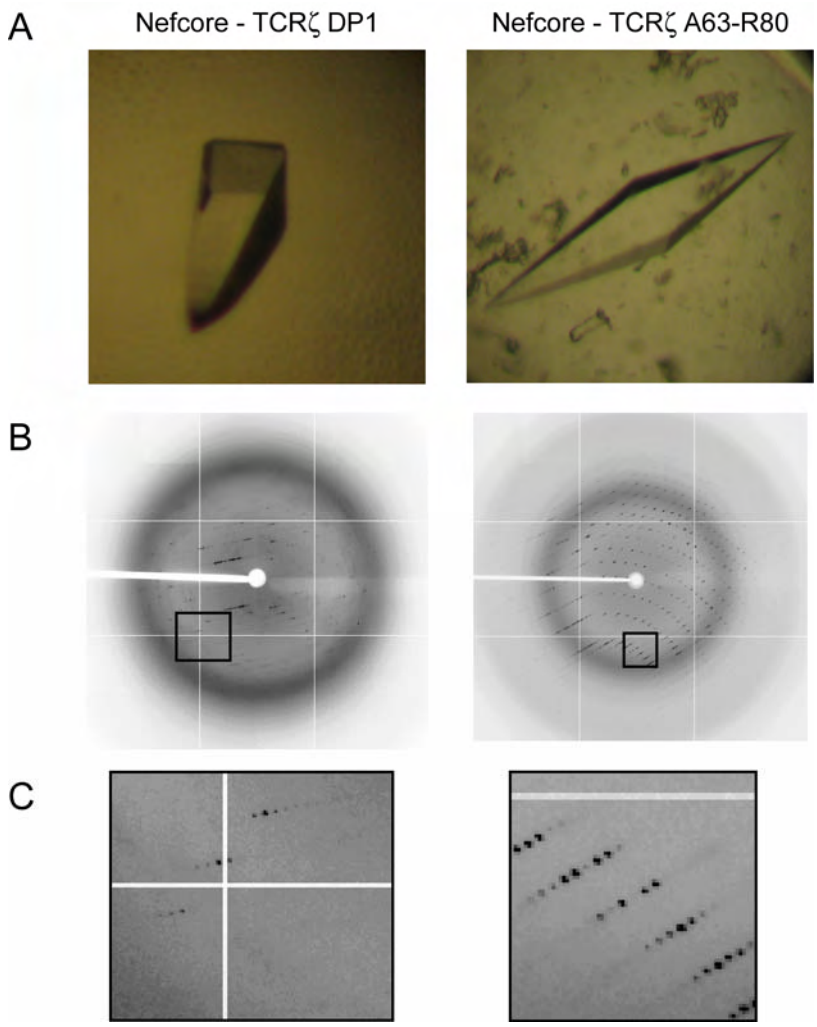

Figure III-2. Crystallization and diffraction. A. Crystals of the SIVmac239 Nef_{core}-$TCR\zeta_{L51\text{-}D93}$ and the SIVmac239 Nef_{core}- $TCR\zeta_{A63\text{-}R80}$ complex. Both crystals grew to 750 x 150 x 150μm at 4°C. B. Diffraction patterns of crystals of the SIVmac239 Nef_{core}-TCRζ polypeptide complexes collected at beamline X29 at the National Light Synchrotron Light Source, Brookhaven National Laboratories. C. Zoom view of the diffraction patterns. The diffraction pattern spot profiles are singular with no evidence of split spots.

weighted F_o - F_c and $2F_o$ - F_c electron density maps, resulting in the R_{free} which could not be reduced below at 41%. Despite the difficulty in model refinement, crystal twinning was not suspected due to the lack of twinning possibilities in $P4_32_12$ crystals.

III.C.3. Initial space group determination and molecular replacement for SIVmac239 Nef_{core}-TCR$\zeta_{A63\text{-}R80}$

Two crystals of SIVmac239 Nef_{core} bound to the shorter TCR$\zeta_{A63\text{-}R80}$ diffracted x-rays to higher resolution (1.9 - 2.05 Å) but space group determination proved to be more complicated than for the $P4_32_12$ crystal form of the Nef_{core}-TCRζ_{DP1}described above . Diffraction patterns observed for the Nef_{core}-TCR$\zeta_{A63\text{-}R80}$ appeared to be consistent with the lattice previously observed for the lower resolution Nef_{core}-TCRζ_{DP1} crystals, and initially the TCR$\zeta_{A63\text{-}R80}$ data (crystal 1) was indexed in the same tetragonal Laue group 4/mmm with unit cell parameters a = b = 47.203, c = 182.939 Å. Integration statistics were similar to those observed previously (R_{merge} = 7.6%). All of the unit cell parameters were reduced 4-10% as compared to the SIVmac239 Nef_{core}-TCRζ_{DP1}crystals, potentially consistent with the shorter length of the TCRζ polypeptide ligand. Analysis of the h00, 0k0 and 00l intensities indicated the presence of 2_1 screw axes along a, b and c, suggesting a lower symmetry than the SIVmac239 Nef_{core}-TCRζ_{DP1}crystals. In turn, the search for a molecular replacement solution in all P422 space groups yielded no results. A data set collected for a second SIVmac239 Nef_{core}-TCR$\zeta_{A63\text{-}R80}$ crystal (crystal 2) resulted in similar difficulties with molecular replacement. The ambiguous space group assignment and inability to find a molecular replacement solution for the SIVmac239

Nef_{core}-$TCR\zeta_{A63\text{-}R80}$ complex in the tetragonal Laue symmetry group suggested the possibility of crystal twinning and required space group re-evaluation.

III.C.4. Detection and analysis of twinning

A number of statistical methods have been developed to characterize crystal twinning, including the recently developed Padillia-Yeates algorithm to detect the presence of crystal twinning (Padilla and Yeates, 2003) and the Britton plot to estimate the twin fraction α (Britton, 1972). To assess twinning of the SIVmac239 Nef_{core}-TCRζ polypeptide crystals, several intensity statistics analyses were performed in *phenix.xtriage*. First, the second moment of intensities of acentric data ($\langle I^2\rangle/\langle|I|^2\rangle$) was calculated for all three SIVmac239 Nef_{core}-TCRζ polypeptide complexes. Untwinned and twinned data are expected to have $\langle I^2\rangle/\langle|I|^2\rangle$ values of 2.0 and 1.5 respectively. The SIVmac239 Nef_{core}-$TCR\zeta_{L51\text{-}D93}$ crystal had an $\langle I^2\rangle/\langle|I|^2\rangle$ value of 2.106, suggesting the absence of twinning, whereas the SIVmac239 Nef_{core}-$TCR\zeta_{A63\text{-}R80}$ crystals had $\langle I^2\rangle/\langle|I|^2\rangle$ values of 1.676 (crystal 1) and 1.628 (crystal 2), indicating the presence of twinning in both crystals. A more robust method of twin detection that uses cumulative local intensity deviation distribution statistics as determined by the Padilla-Yeates algorithm (Padilla and Yeates, 2003) was also employed. In a plot of the local intensity difference |L| of non twin-related intensities versus the distribution of the local intensity differences, N|L|, the presence of twinning can be deduced by comparing the experimental plots to the expected plots for twinned and untwinned data (Padilla and Yeates, 2003). The SIVmac239 Nef_{core}-$TCR\zeta_{DP1}$ data plot was linear, consistent with the expected curve for

untwinned data (Figure III-3, top). In contrast, both SIVmac239 Nef_{core}-$TCR\zeta_{A63\text{-}R80}$ crystals 1 and 2 data plots were curved, suggesting the presence of crystal twinning (Figure III-3, top). The L test, also based on the local intensity differences of non twin-related reflection pairs, was additionally employed to confirm twinning in the SIVmac239 Nef_{core}-$TCR\zeta_{A63\text{-}R80}$ crystals; for untwinned data, |L| and mean L^2 are expected to equal 1/2 and 1/3, respectively, and for twinned data, 3/8 and 1/5. The SIVmac239 Nef_{core}-$TCR\zeta_{DP1}$ data had calculated |L| and L^2 values of 0.473 and 0.307, consistent an absence of appreciable twinning. The SIVmac239 Nef_{core}-$TCR\zeta_{A63\text{-}R80}$ crystals had calculated |L| and L^2 values of 0.402 and 0.229 for crystal 1 and 0.390 and 0.218 for crystal 2, further supporting the presence of crystal twinning. All of the twinning tests suggested that the low resolution SIVmac239 Nef_{core}-$TCR\zeta_{DP1}$ crystal was not appreciably twinned whereas the high resolution SIVmac239 Nef_{core}-$TCR\zeta_{A63\text{-}R80}$ crystals were pseudo-merohedrally twinned with a twin fraction near 0.5.

In order to estimate the twin fraction α in the two SIVmac239 Nef_{core}-$TCR\zeta_{A63\text{-}R80}$ pseudo-merohedrally twinned crystals, Britton plot (Britton, 1972) and H plot (Yeates, 1988) analyses were performed (Figure III-3, middle and bottom). Crystal 1 exhibited near perfect twinning with an estimated twin fraction of 0.452 from the Britton plot and 0.477 from the H plot. In contrast, crystal 2 seemed to be only partially twinned with estimated twin fractions of 0.344 and 0.356 from the Britton plot and H plot, respectively. These initial estimates of the twin fraction refined upwards during structure determination to 0.500 and 0.426 for crystals 1 and 2, respectively (see below).

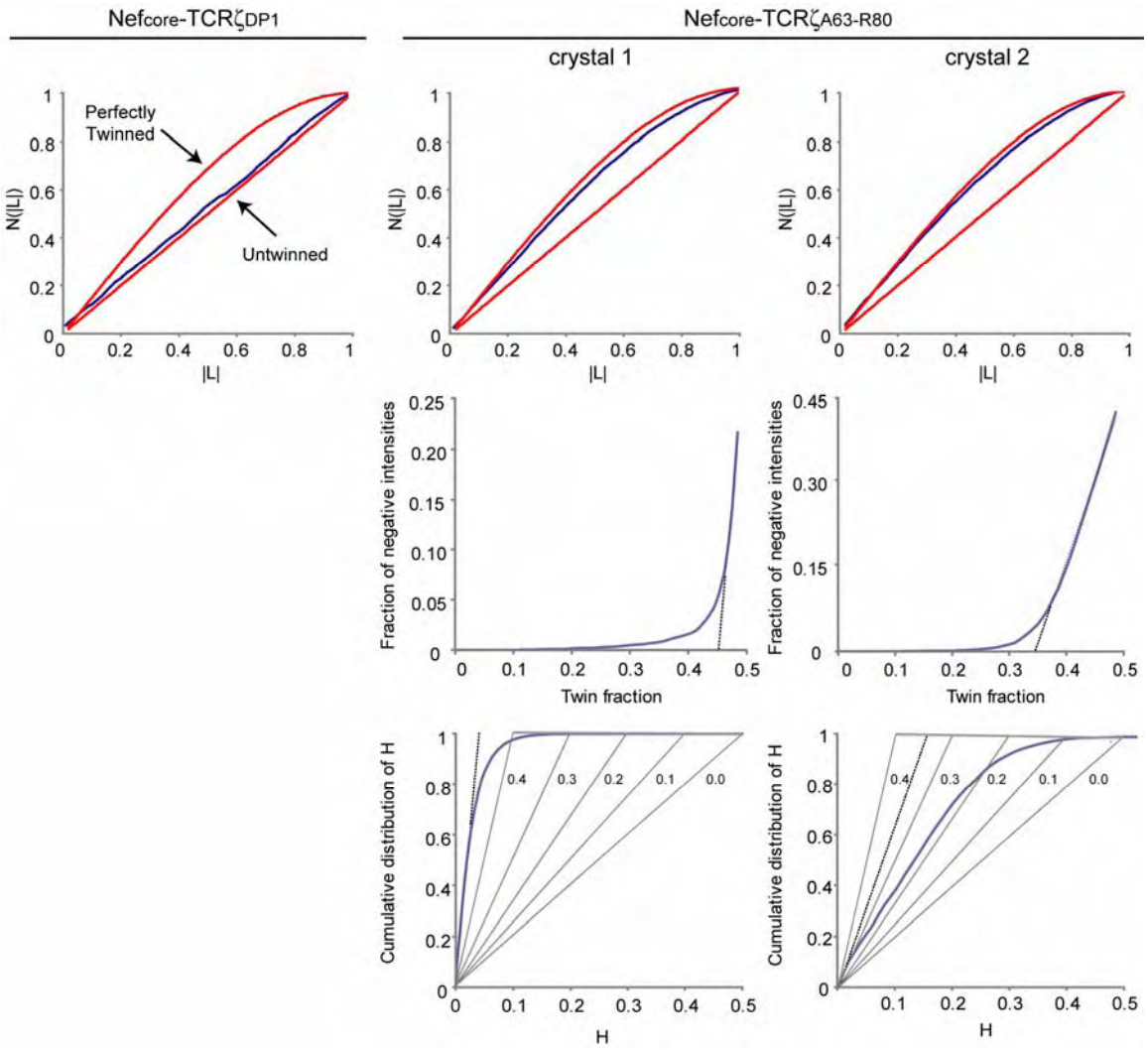

Figure III-3. Detection of twinning and estimation of the twin fraction α. Top, cumulative intensity difference plot of the intensity difference of local pairs of intensities that are not twin related |L| {L = [I(h1) – I(h2)]/[I(h1) + I(h2)]} against the cumulative probability distribution, *N*(*L*), of the parameter *L* (Yeates, 2003). The expected plots of untwinned and twinned acentric data (red) and calculated plots of the SIVmac239 Nefcore-TCRζ polypeptide data (blue) are shown. Middle, estimation of the twin fraction α by Britton plot analysis (Britton, 1972). The percentage of negative intensities after detwinning is plotted as a function as a function of the assumed value of a. Overestimation of the twin factor a results in an increase in the percentage of negative intensities. The estimated value for α is extrapolated from the linear fit (dashed line). Bottom, estimation of the twin fraction a using the H plot (Yeates, 1988). The cumulative fractional intensity difference of acentric twin-related intensities H {H = |I(h1) – I(h2)|/[I(h1) + I(h2)]} is plotted against H. The initial slope (dashed line) of the distribution is a measure of α. The expected slopes for the indicated twin fractions 0.0-0.4 are shown (dotted lines).

Because the tetragonal $P4_32_12$ space group does not support merohedral twinning, we explored the possibility that the twinned SIVmac239 Nef_{core}-$TCR\zeta_{A63\text{-}R80}$ crystals were orthorhombic crystals that emulated tetragonal symmetry due to pseudo-merohedral crystal twinning. The twinned SIVmac239 Nef_{core}-$TCR\zeta_{A63\text{-}R80}$ diffraction data was therefore re-indexed in the orthorhombic point group 222. The unit cell parameters, a and b, constrained to be equal in point group 422 (Laue group 4/mmm), refined to slightly different values, a = 47.197, b = 47.208 for crystal 1 and a = 47.417, b = 47.421 for crystal 2, with no significant changes in R_{merge} values (Table III-1). Inspection of the h00, 0k0 and 00l intensities indicated the presence of 2_1 screw axes along each axis, suggesting a $P2_12_12_1$ crystal space group. The Matthews coefficient V_M (Matthews 1968) was calculated to be 2.64 (53.42% solvent) for crystal 1 and 2.64 (53.99% solvent) for crystal 2, consistent with two SIVmac239 Nef_{core}-$TCR\zeta_{A63\text{-}R80}$ heterodimers comprising the asymmetric unit. The reduction in symmetry from a fourfold axis along c to a twofold symmetry in the orthorhombic unit cell cell led to the identification of the pseudo-merohedral twin operation (*k, h, -l*) that accounted for the apparent fourfold Laue symmetry observed in the diffraction data.

The reduction in symmetry from a fourfold axis along c in the tetragonal unit cell to a twofold axis in the orthorhombic unit cell, together with an increase in the number of molecules per asymmetric unit, helped us to identify the pseudo-merohedral twin operation (*k, h, -l*) that accounted for the apparent fourfold Laue symmetry observed in the diffraction data. Consider a $P2_12_12_1$ unit cell with unit cell length a approximately equal to unit cell length b (Figure III-4). Pseudo-merohedral twinning can exchange the a

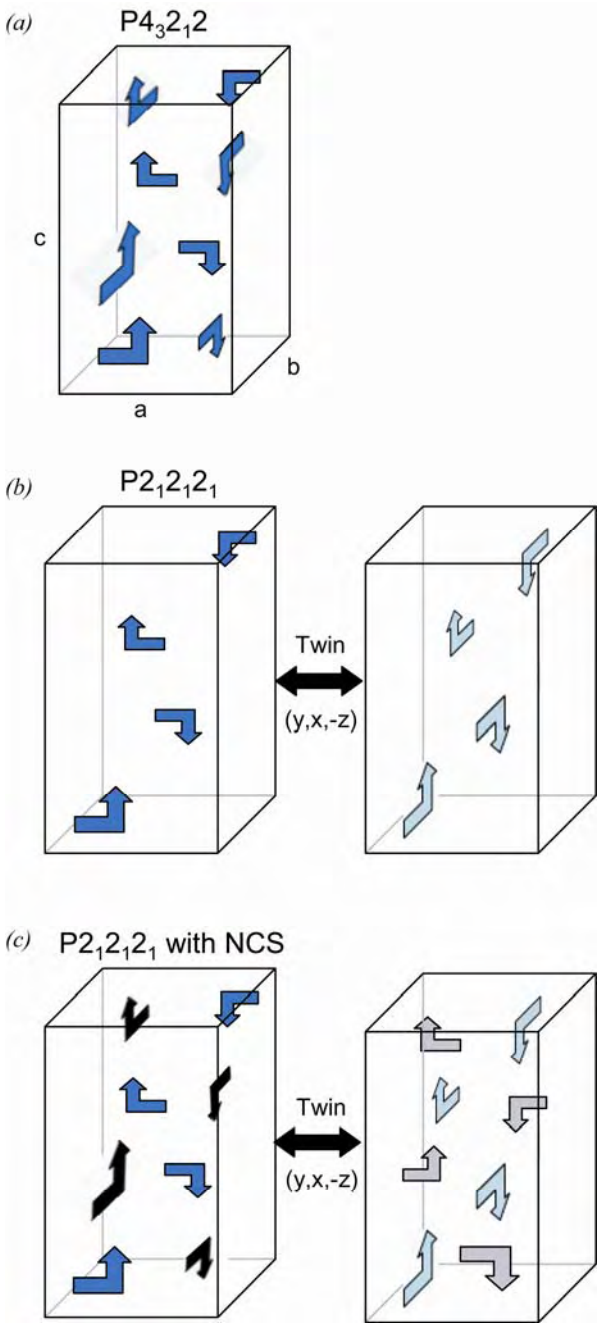

Figure III-4. Twinning in an orthorhombic $P2_12_12_1$ crystal. A $P4_32_12$ space group unit cell with 1 molecule (arrow) per asu (8 per unit cell) is shown with axes a, b, and c labeled. B. A $P2_12_12_1$ space group unit cell with 1 molecule per asu (4 per unit cell) is shown (left) with its twin unit cell (right) related by the twin operator (*y*,*x*,-*z*). C. A $P2_12_12_1$ space group unit cell with 2 molecules per asu (4 per unit cell) is shown (left) with its twin unit cell (right) related by the twin operator (*y*,*x*,-*z*). The asu is comprised of one blue and one black arrow related by non-crystallographic symmetry.

and b axis under the twin relationship (*h,k,l*) -> (*k,h,-l*), resulting in apparent tetragonal symmetry around the c axis (Figure III-4). The apparent symmetry observed in this case will be indistinguishable from a non-twinned $P4_32_12$ (or $P4_12_12$,) unit cell (Figure III-4). Note that in this case the twinned $P2_12_12_1$ unit cell is less tightly packed with one molecule per asymmetric unit (4 per unit cell) than is the corresponding non-twinned tetragonal $P4_32_12$ (or $P4_12_12$,) cell with one molecule per asymmetric unit (8 per unit cell). Based on the Matthews coefficient, we expected 2 molecules per asymmetric unit for the twinned a $P2_12_12_1$ unit cell. Note that the non-twinned crystals of the SIVmac239 Nef_{core}-$TCR\zeta_{DP1}$ complex, which did adopt true tetragonal symmetry with unit cell parameters similar to those of the twinned a $P2_12_12_1$ crystal, had a Matthews coefficient consistent with 1 molecule per asymmetric unit. Because the SIVmac239 Nef_{core}-$TCR\zeta_{DP1}$ and the SIVmac239 Nef_{core}-$TCR\zeta_{A63\text{-}R80}$ complexes had similar molecular sizes and crystallized in related unit cells with similar lengths and angles, we expected similar packing, but this was inconsistent with the different packing expected for the related twinned $P2_12_12_1$ and non-twinned $P4_32_12$ (or $P4_12_12$,) unit cells shown in Figure 4. Non-cystallographic symmetry relationships similar to crystallography symmetry operators also can result in observed symmetry higher than that actually present in the crystal. For example, breakdown of the crystallographic four-fold axis in a tetragonal cell could result in an orthorhombic cell with pseudo-fourfold symmetry. In this case the non-crystallographic symmetry relationship is similar to the missing crystallographic operator, and the related tetragonal and orthorhombic unit cells would have similar packing (Figure III-4). This arrangement can be particularly prone to pseudo-merohedral twinning as a

result of the similarity of crystal packing along the a and b unit cell axes (Figure III-4). We explored this scenario as an explanation for the observed twinning in the $P2_12_12_1$ crystals with packing similar to non-twinned $P4_32_12$ (or $P4_12_12$,) crystals.

III.C.5. Structure determination and refinement for SIVmac239 Nef_{core}-TCR$\zeta_{A63\text{-}R80}$ using twinned data

After assignment of the SIVmac239 Nef_{core}-TCR$\zeta_{A63\text{-}R80}$ crystal data to the orthorhombic $P2_12_12_1$ space group, several strong molecular replacement solutions were readily found with TFZ scores 6.1-9.2, using a consensus model derived from unliganded HIV-1 Nef_{core} crystal structures. In principle, molecular replacement solutions corresponding to both twin orientations and non-crystallographically related molecules are expected. Transformations among these solutions were examined to assign each to a twin or NCS domain (Figure III-5). All solutions could be accounted for using a single NCS transformation, the (*k*,*h*,-*l*) twinning operator, and the $P2_12_12_1$ space group symmetry. Two nearby molecules (A, B) in the same twin domain related by an approximate 90^o rotation were selected to comprise the asymmetric unit.

Once the twinning arrangement was properly understood and taken into account, model building and refinement in the $P2_12_12_1$ space group with 2 molecules per asymmetric unit was relatively straightforward. The twin operation (*k*,*h*,-*l*) was factored into each round of twinned refinement in *phenix.refine* that included three cycles of individual atomic displacement parameter (B factor) and energy minimization refinement. The twin fraction α was also refined in each round and used to detwin the

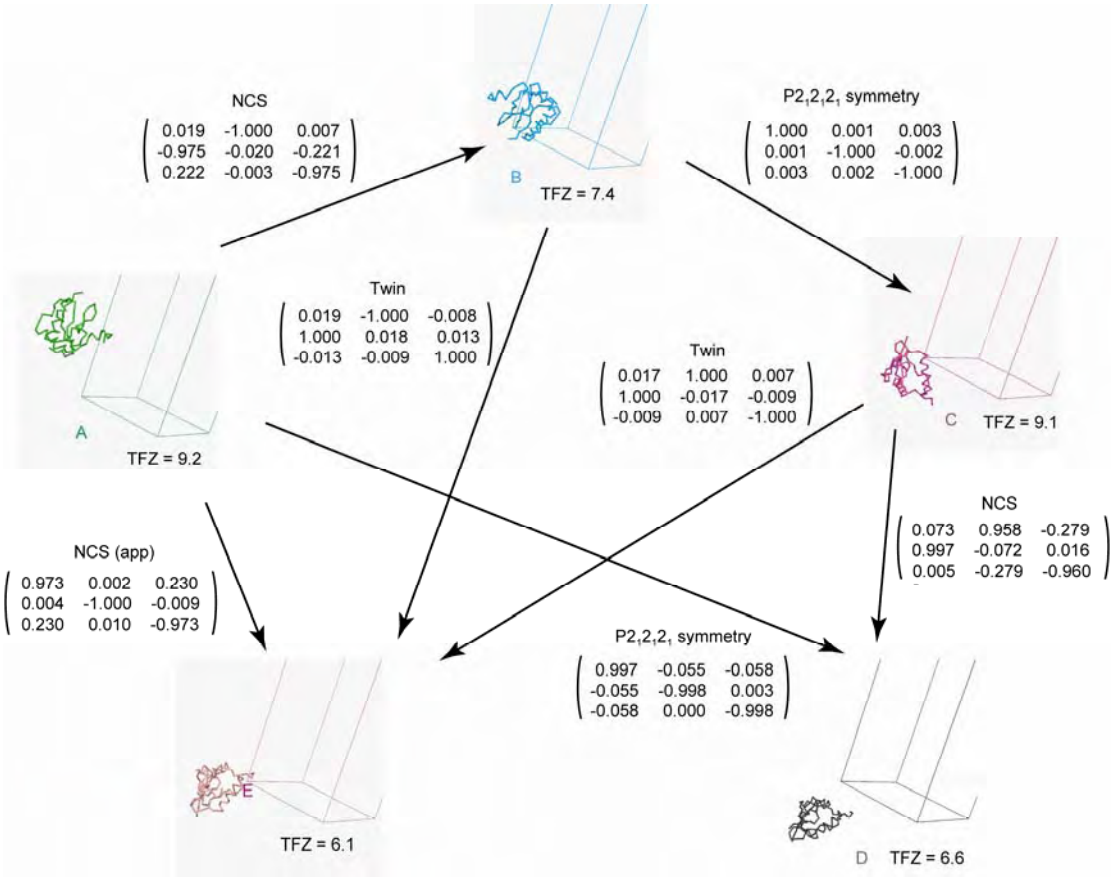

Figure III-5. Molecular replacement solutions. Five molecular replacement solutions (A-E) are shown with their translation function Z (TFZ) scores denoted. The relationship and rotation matrix relating each molecular replacement solution is shown.

intensity data in order to generate interpretable $2F_o - F_c$ and $F_o - F_c$ omit electron density maps suitable for manual model building. However, during the first round of refinement, the twin fraction converged to 0.5 for crystal 1 and 0.426 for crystal 2. The calculated $2F_o – F_c$ electron density maps generated by *phenix.refine* were noticeably less interpretable for crystal 1 than for crystal 2. Therefore, structure determination proceeded with crystal 2 through iterative cycles of twinned refinement interspersed with rounds of model inspection and building. As the model and twin fraction continued to refine, there was marked improvement in the quality of the electron density maps that allowed for the building of 5 additional residues at the N-terminus (V98-V102), 1 residue at the C-terminus (G234) and 11 residues in the internal disordered loop (P197-W207) on Nef; the starting model generated from the published crystal structures of HIV-1 Nef was missing 9 residues at the N-terminus, 2 residues at the C-terminus and 29 residues in the disordered loop. Clear density for the $TCR\zeta_{A63\text{-}R80}$ polypeptide ligand was observed, and this region also was built into the structure with 13 of the 16 resolved residues comprising a canonical alpha helix (Figure III-6A). Water molecules were added to the model using the automated water-picking functions in *phenix.refine* and Coot. The final structure (crystal 2) contained 120 residues on SIVmac239 Nef, 16 residues on TCRζ, 116 ordered water molecules and had R_{work} and R_{free} values of 17.0 and 18.4%, respectively (Table III-1).

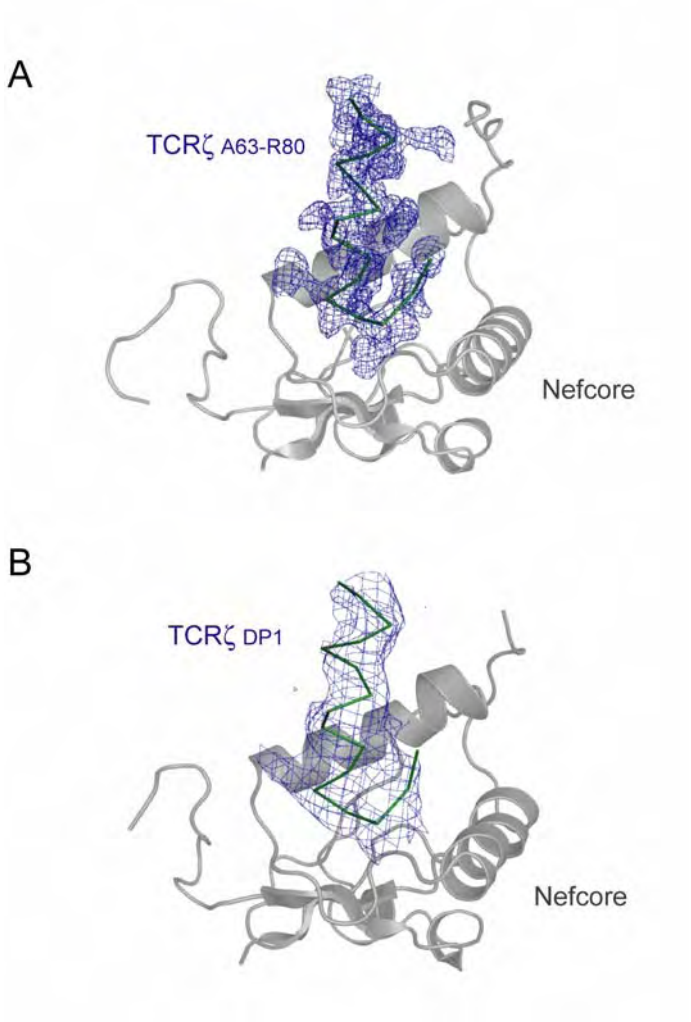

Figure III-6. 2 $F_o - F_c$ electron density maps of the TCRζ polypeptide. $2F_o - F_c$ electron density maps contoured at 1σ calculated from the detwinned $P2_12_12_1$ data of the SIVmac239 Nef_{core} –$TCR\zeta_{A63\text{-}R80}$ crystal (A) and $P4_32_12$ data of the SIVmac239 Nef_{core} – $TCR\zeta_{L51\text{-}D93}$ crystal (B) are shown for the region encompassing the TCR ζpolypeptide.

III.C.6. Structure determination and refinement of SIVmac239 Nef$_{core}$-TCRζ_{DP1}

With a high-resolution structure for SIVmac239 Nef$_{core}$-TCR$\zeta_{A63\text{-}R80}$ structure in hand, we returned to the low resolution, non-twinned SIVmac239 Nef$_{core}$-TCRζ_{DP1} $P4_32_12$ dataset. In order to determine the structure of the low resolution SIVmac239 Nef$_{core}$-TCRζ_{DP1}, the high resolution SIVmac239 Nef$_{core}$-TCR$\zeta_{A63\text{-}R80}$ structure was used as the starting model for refinement and building. Structure determination by molecular replacement was repeated for the non-twinned SIVmac239 Nef$_{core}$-TCRζ_{DP1} data. A stronger molecular replacement solution was found (TFZ = 10.5, LLG = 266) but in the same general orientation as that described previously. Refinement of atomic positions and individual b-factor was performed in *phenix.refine*, as described above for the twinned crystal, although without twin refinement and detwinning steps. The TCRζ_{DP1} peptide extends 12 residues futher at the N-terminus and 14 residues further at the C-terminus as compared to the TCR$\zeta_{A63\text{-}R80}$ polypeptide, but no additional electron density was observed beyond that seen in the SIVmac239 Nef$_{core}$-TCR$\zeta_{A63\text{-}R80}$ complex, (Figure III-6B), suggesting that both the N- and C-termini of the -TCR$\zeta_{L51\text{-}D93}$ fragment were disordered, and that no additional Nef contacts were present. The final structure of the SIVmac239 Nef$_{core}$-TCRζ_{DP1} complex contained 111 residues on Nef, 16 residues on TCRζ and had R_{work} and R_{free} values of 0.287 and 0.332, respectively (Table III-1).

III.C.7. Analysis of the $P2_12_12_1$ and $P4_32_12$ crystal forms of the SIVmac239 Nef_{core}-TCRζ polypeptide complex

As described above, the SIVmac239 Nef_{core}-TCRζ polypeptide complex crystallized in two related but different crystal lattices depending on the length of the TCRζ ligand. In the presence of the longer 43-residue $TCR\zeta_{DP1}$ polypeptide, SIVmac239 Nef_{core} crystallized in the tetragonal $P4_32_12$ space group with one SIVmac239 Nef_{core}-$TCR\zeta_{DP1}$ heterodimer comprising the asymmetric unit. In the presence of the shorter 18 residue $TCR\zeta_{A63\text{-}R80}$ polypeptide, the complex unexpectedly crystallized in the $P2_12_12_1$ space group with severe pseudo-hemihedral twinning. In this crystal form, a rotation axis parallel to c exhibited pseudo-fourfold symmetry that deviated slightly from the crystallographic fourfold screw axis observed in the $P4_32_12$ crystal form (Figure III-7). The overall packing of the unit cell was also condensed in orthorhombic crystal form as evidenced by a ~4Å (~8%) reduction in the a and b axes and a ~6Å (~3%) shortening of the c axis.

The transformation from the tetragonal to orthorhombic crystal system was caused by the introduction of non-crystallographic symmetry (NCS) and the rearrangement of the hydrogen bonding network at the crystal contact sites. The $P4_32_12$ crystal form contained one molecule per asymmetric unit. The $P2_12_12_1$ crystal form contained two molecules per asymmetric unit which were no longer related by a crystallographic twofold symmetry operation (*y*,*x*,-*l*) but instead by a twofold NCS operation.

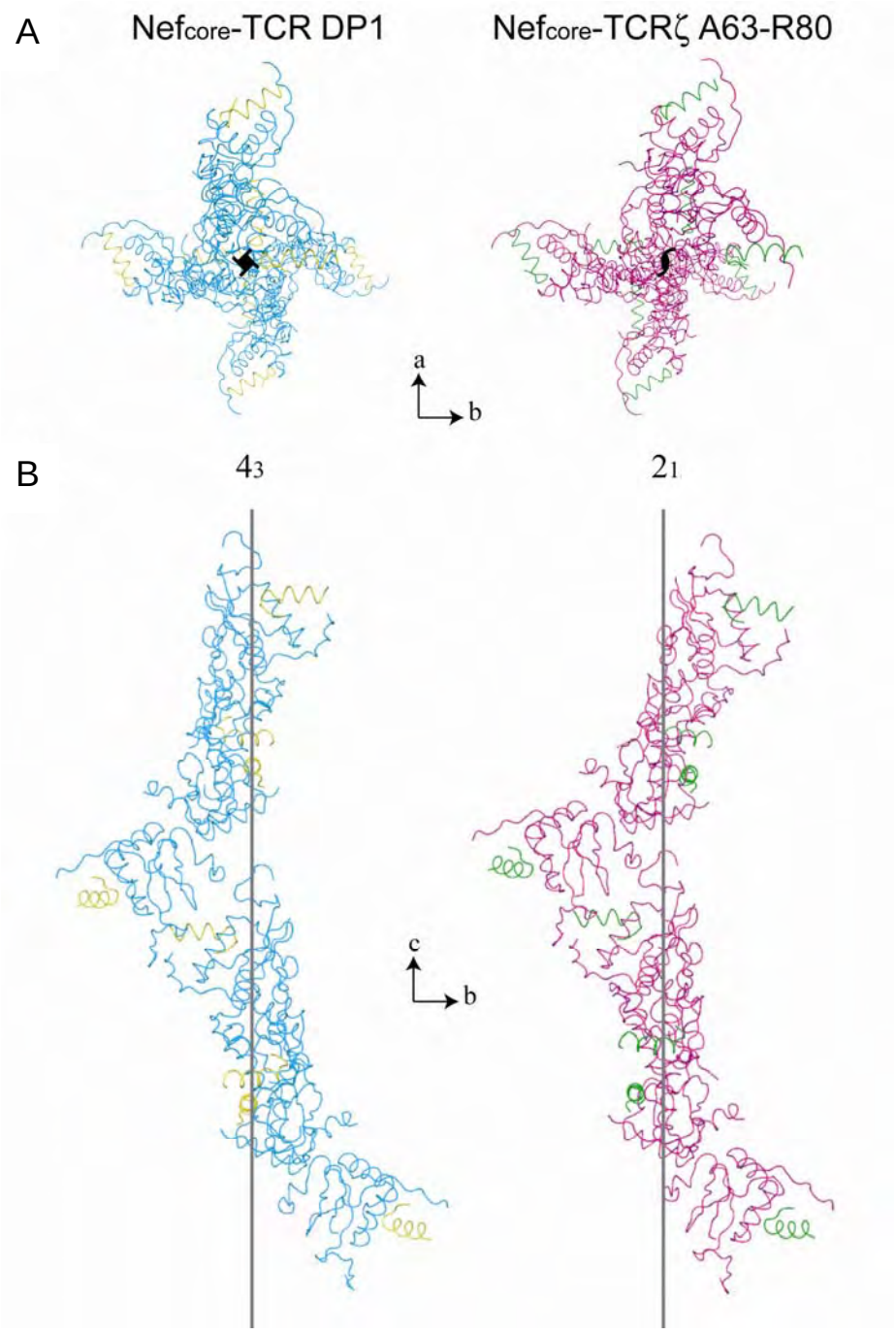

Figure III-7. Crystal packing of the $P4_32_12$ and $P2_12_12_1$ crystal forms. A. The crystal symmetry organization of the $P4_32_12$ crystal form (left) and the $P2_12_12_1$ crystal form (right) is shown viewed down the four-fold symmetry axis and corresponding two fold symmetry axis for the two SIVmac239 Nef_{core}-TCRζ polypeptide complexes. In B, the crystal packing along the c axis is shown for both crystal forms. SIVmac239 Nef_{core}/TCRζ are colored cyan/yellow (left) and magenta/green (right).

$$\begin{pmatrix} 0.000 & 1.000 & 0.000 \\ 1.000 & 0.000 & 0.000 \\ 0.000 & 0.000 & -1.000 \end{pmatrix} + \begin{pmatrix} 0.000 \\ 0.000 \\ 0.000 \end{pmatrix} \rightarrow \begin{pmatrix} 0.036 & 0.999 & -0.027 \\ 0.981 & -0.030 & 0.194 \\ 0.193 & -0.033 & -0.981 \end{pmatrix} + \begin{pmatrix} 1.382 \\ 1.844 \\ 2.435 \end{pmatrix}$$

In the tetragonal crystal form, the SIVmac239 Nef_{core}-TCRζ_{DP1} complex and its symmetry-related partner (*y,x,-z*) form an anti-parallel dimer similar to the crystallographic dimer described previously for HIV-1 Nef_{core} (Arold et al., 1997). Structural alignment of one SIVmac239 Nef_{core}-TCR$\zeta_{A63\text{-}R80}$ complex from the $P2_12_12_1$ crystal form with its corresponding molecule in the $P4_32_12$ crystallographic dimer reveals that the NCS-related molecule in the orthorhombic crystal form is rotated ~10^o from its corresponding molecule in $P4_32_12$ crystal form (Figure III-8A). The interface between the two molecules involves the C-terminus of SIVmac239 Nef_{core} and is predominantly occupied by aromatic residues (Y113, Y221, F171, Y223, Y226). Shown in Figure III-8B, SIVmac239 Nef_{core} is rotated as a single rigid body in the orthorhombic crystal form with no significant changes in either main chain or side chain geometry, suggesting that the crystallographic Nef_{core} dimer interface is flexible and permissible to variations in crystal packing.

Alternate crystal packing was also observed at the crystal contact of two asymmetric units in the orthorhombic crystal form and the corresponding symmetry-related molecules (*y,x,-z*) and (*1/2+y,1/2-x,1/4+z*) in the tetragonal crystal form. The interface involves three proteins: SIVmac239 Nef_{core} and its bound TCRζ polypeptide ligand from the symmetry-related molecule (*1/2+y,1/2-x,1/4+z*) and SIVmac239 Nef_{core} from the symmetry-related molecule (*y,x,-z*) (Figure 3-7 A). Interestingly, the N-terminus of the TCRζ polypeptide abuts the neighboring SIVmac239 Nef_{core} protein, suggesting

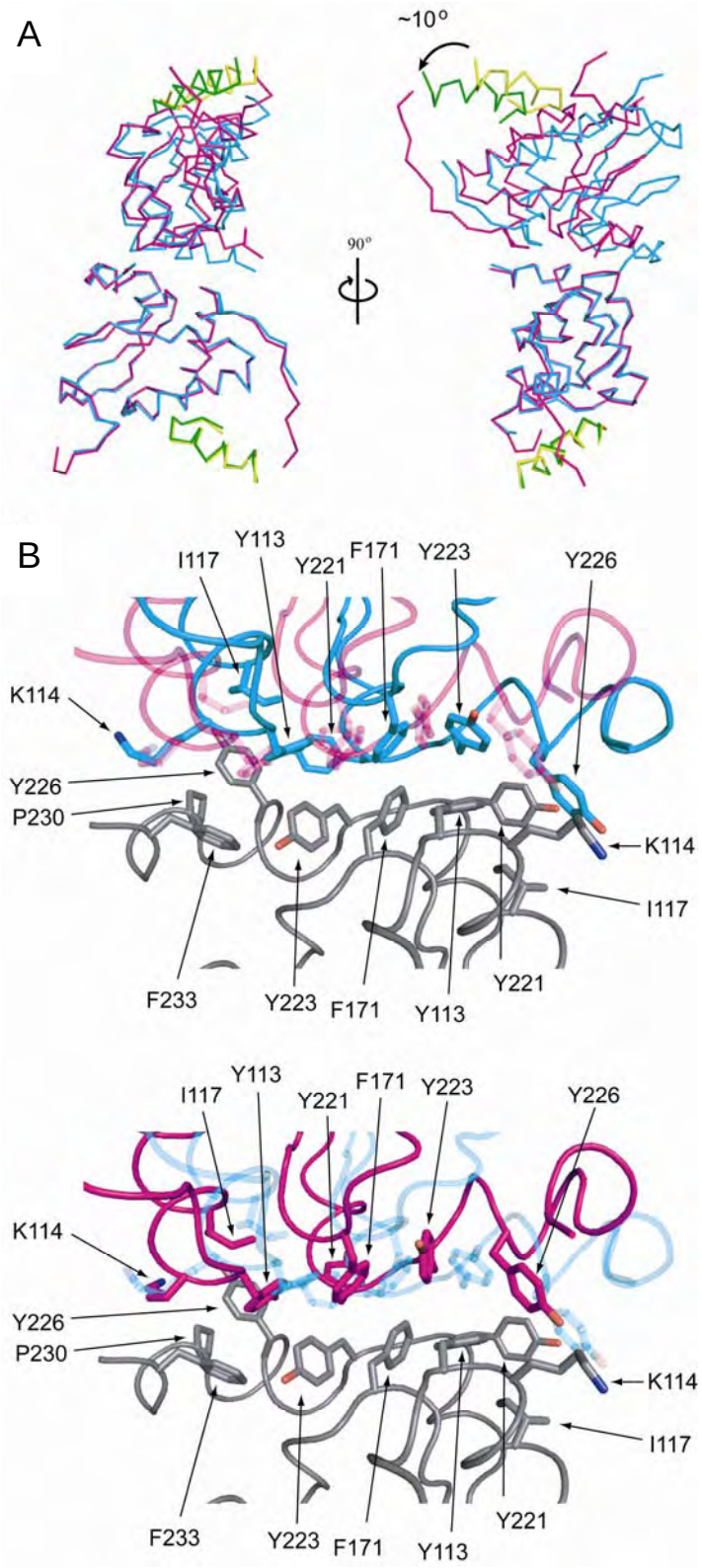
A
~10°
90°
B
I117
Y113
Y221
F171
Y223
Y226
K114
Y226
P230
K114
I117
F233
Y223
F171
Y113
Y221
I117
Y113
Y221
F171
Y223
Y226
K114
Y226
P230
K114
I117
F233
Y223
F171
Y113
Y221

Figure III-8. SIVmac239 Nef_{core} dimer interface in the $P4_32_12$ and $P2_12_12_1$ crystal forms. A. Overlay of the two molecules in the asymmetric unit of the $P2_12_12_1$ crystal (magenta/green) and two symmetry-related molecules [(*x*,*y*,*z*), (*y*,*x*,-*z*) in the $P4_32_12$ crystal (cyan/yellow). SIVmac239 Nef_{core} is colored magenta ($P2_12_12_1$ crystal) or cyan ($P4_32_12$ crystal) and the TCRζ polypeptide is colored green ($P2_12_12_1$ crystal) or yellow ($P4_32_12$ crystal). The structures of the lower SIVmac239 Nef_{core}-TCRζ polypeptide complex were aligned by least-squared methods. The relative 10^o counter-clockwise rotation of the top $P2_12_12_1$ crystal SIVmac239 Nef_{core}-TCRζ polypeptide complex is depicted. B. Detailed view of the SIVmac239 Nef_{core} dimer interface in the $P2_12_12_1$ (magenta) and $P4_32_12$ (blue) crystal. The aligned lower SIVmac239 Nef_{core}-TCRζ polypeptide complex is colored grey and the side chains of residues involved in the interface are shown in stick models.

that the length of the N-terminal sequence of the TCRζ polypeptide ligand directs the space group in which the SIVmac239 Nef_{core}-TCRζ polypeptide complex crystals grow. Superimposition of the TCRζ polypeptide helix from the symmetry-related molecule (*1/2+y,1/2-x,1/4+z*) with its corresponding partner in the $P2_12_12_1$ crystal form reveals that the neighboring SIVmac239 Nef_{core} protein is rotated ~4.5^o inward towards the pseudo-fourfold symmetry axis in the $P2_12_12_1$ crystal form (Figure III-9A).

Accompanying the transformation is a possible reorganization of the hydrogen bonding network at the crystal contact site. In the orthorhombic crystal form, the $TCR\zeta_{A63\text{-}R80}$ polypeptide forms a main-chain hydrogen bond with the neighboring SIVmac239 Nef_{core} protein between the main-chain amide of TCRζ Y64 and the side-chain carbonyl of Nef Q202 (Figure III-8B). TCRζ residue Q65 additionally participates in hydrogen bonding with the main chain amide and carbonyl of residues R103 and V102, respectively, on its bound SIVmac239 Nef_{core} partner. Interestingly, this interaction orders the proline-rich region in the N-terminus of the bound SIVmac239 Nef_{core} into a polyproline type II (PPII) helix as evidenced by the clearly resolved electron density maps calculated from the $P2_12_12_1$ crystal data for that region. This carries significant functional importance due to the regulatory role the PPII helix on HIV-1 Nef has been suggested to play in modulating kinase activity through its interaction with the SH3 domain of the kinase (Chapter IV, (Arold et al., 1997; Lee et al., 1996)). The PPII helix was found to be disordered in the unliganded HIV-1 Nef_{core} crystals and was only ordered in crystals containing the Fyn SH3 domain. Surprisingly, the hydrogen bonding network between the TCRζ polypeptide and its bound SIVmac239 Nef_{core} partner is

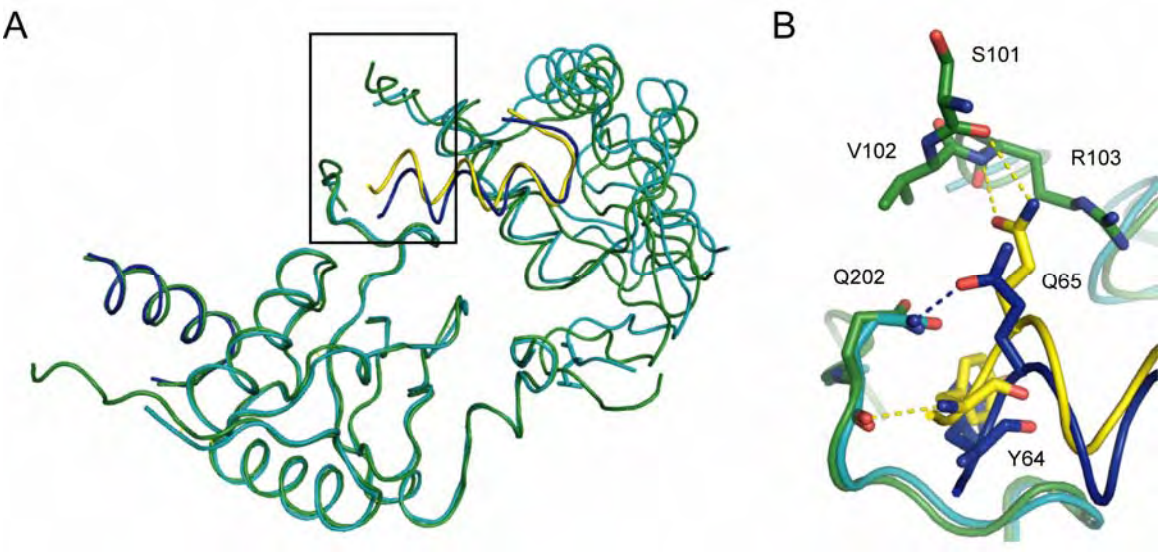

Figure III-9. Variation in the crystal contact hydrogen bond network. Overlay of the crystal packing interface between two asymmetric units of the $P2_12_12_1$ crystal lattice (SIVmac239 Nef is green and TCRζ is yellow) and two symmetry-related molecules (*y,x,-z*) and (*1/2+y,1/2-x,1/4+z*) of the $P4_32_12$ crystal lattice (SIVmac239 Nef is cyan and TCRζ is blue). Alignment was performed by least-squares methods of one SIVmac239 Nef-TCRζ polypeptide complex (at bottom of panel A). Hydrogen bonds present in the crystal lattices are represented by dashed lines and are colored yellow and blue for the $P2_12_12_1$ and $P4_32_12$ crystal forms, respectively.

seemingly absent in the tetragonal crystal form; this explains the lack of electron density calculated from the $P4_32_12$ data for the N-terminus of SIVmac239 Nef_{core} since the PPII helix would no longer be expected to be ordered. Instead of participating in a side chain main-chain hydrogen bond with its bound partner, residue Q65 on TCRζ is translocated in the tetragonal crystal form, bringing it in close enough proximity to residue Q202 on the neighboring SIVmac239 Nef_{core} protein to participate in a side chain-side chain hydrogen bond. The main chain-main chain hydrogen bond between the TCRζ polypeptide and the neighboring SIVmac239 Nef_{core} protein is also lost in the rearranged $P4_32_12$ crystal contact interface.

Since the proposed hydrogen bond between Q65 on TCRζ and Q202 on SIVmac239 was formed by TCRζ and an adjacent SIVmac239 Nef_{core} protein in the crystal lattice and not its interacting SIVmac239 Nef_{core} partner, it would likely be an artifact of crystallization that was necessary for the proper lattice packing in the tetragonal crystal form. Curiously, the more physiologically relevant interaction of Q65 on TCRζ to its bound SIVmac239 Nef_{core} partner was restored when the TCRζ polypeptide was truncated. The loss of the crystal contact hydrogen bond reduced the crystal symmetry to an orthorhombic crystal lattice that was subsequently prone to twinning. This was unexpected due to the inclusion of a more complete TCRζ sequence in the tetragonal crystal and represents an interesting scenario where a protein-ligand interaction was disrupted by a crystal contact interaction that permitted higher order crystal packing.

IV. Conclusions

Crystal twinning can be induced by a number of perturbations, including heavy-metal soaking, ligand binding, selenomethionine substitution, flash-freezing and the introduction of point mutations (Helliwell et al., 2006; Parsons, 2003). The structure determination of the two SIVmac239 Nef_{core}-TCRζ polypeptide complexes provides a unique example of crystal twinning caused by the modification of peptide ligand size. Truncation of the TCRζ polypeptide reduced the crystal symmetry from a tetragonal crystal system to an orthorhombic crystal system and introduced an NCS operation that only deviated slightly from the true fourfold symmetry axis. The pseudo-symmetry in the $P2_12_12_1$ crystal made crystal growth highly susceptible to crystal twinning but serendipitously restored a physiologically relevant protein-ligand interaction at the crystal contact interface.

Table III-1. Data collection and refinement statistics (molecular replacement)

	Nef_{core}-TCRζ_{DP1}	Nef_{core}-TCR$\zeta_{A63\text{-}R80}$ Crystal 1	Nef_{core}-TCR$\zeta_{A63\text{-}R80}$ Crystal 2
Data Collection			
Space Group	$P4_32_12$	$P2_12_12_1$	$P2_12_12_1$
Cell dimensions			
a, *b*, *c* (Å)	51.638, 51.638, 189.449	47.190, 47.236, 182.989	47.417, 47.421, 183.519
. α, β, γ(°)	90, 90, 90	90, 90, 90	90, 90, 90
Resolution* (Å)	50-3.70 (3.83-3.70)*	50-1.93 (2.02-1.93)	30-2.05 (2.12-2.05)
R_{merge}*[a]	0.051 (0.393)	0.083 (0.513)	0.084 (0.498)
I/σI*	12.8	9.7 (2.4)	9.6 (2.5)
Completeness* (%)	99.4 (100.0)	99.5 (98.8)	99.1 (96.5)
Redundancy*	12.6 (12.7)	6.9 (5.9)	6.8 (5.2)
Refinement			
Resolution (Å)	36-3.70		27-2.05
Total Reflections	2,923		25,896
R_{work} / R_{free}	0.287 / 0.332		0.170 / 0.184
Twin fraction (*k,h,-l*)	N/A		0.424
Number of atoms			
Protein	1054		2223
Water	N/A		116
NCS deviations (Å)	N/A		0.326
Average *B*-factor, Å^2			
SIVmac239Nef_{core}			46.0
TCRζ polypeptide			49.2
Waters	N/A		45.2
RMS deviations			
Bond lengths (Å)	0.011		0.003
Bond angles (°)	1.326		0.564
PDB ID code	3IOZ		3IK5

* highest resolution shell in parentheses

CHAPTER IV: Structure of the Nef-TCRζ complex and its role in modulation of Src family protein tyrosine kinase activity

Abstract

The HIV/SIV accessory factor Nef is known to target several cell surface receptors in an infected T cell and to alter receptor-mediated signaling pathways, but the structural basis for these interactions and their functional consequences are not well understood. Here we report the crystal structure of the complex of the conserved core domain of Nef from SIVmac239 bound to a polypeptide from the T cell receptor zeta subunit cytoplasmic domain and the effect of Nef-TCR zeta complex formation on Src family protein tyrosine kinase activity. The SIV Nef core domain adopts a three-dimensional fold similar to that previously reported for HIV-1 Nef, but the T cell receptor polypeptide adopts a previously unobserved alpha-helical conformation. The dominant features of the binding interface on Nef include a basic patch and hydrophobic pocket, forming a novel interaction helping to explain the observed specificity for particular immunoreceptor tyrosine-based activation motifs.. The interaction with TCR zeta stabilizes the polyproline type II helix on Nef, disordered in the unliganded HIV-1 Nef structure, which previously has been implicated in interactions with the SH3 domain of the protein tyrosine kinase Fyn. In vitro phosphorylation of TCR zeta by Lck, Fyn and Src is enhanced in the presence of HIV-1 and SIV Nef, suggesting a functional role for the Nef-TCR zeta interaction in modulation of T cell signaling pathways.

IV.A. Introduction

Nef is a 27-35 kDa myristylated viral accessory protein unique to HIV and SIV that plays a significant role in the pathogenesis of HIV and SIV infection. Although it lacks enzymatic function, Nef engages in a number of functions through protein-protein interactions that collectively enhance viral infectivity, viral replication and modulate immune activation (reviewed in (Arien and Verhasselt, 2008; Foster and Garcia, 2008; Kirchhoff et al., 2008). Notable among Nef's functions is its association with the signaling components of the T cell signaling pathway, including the signaling ζ subunit the T cell receptor (TCRζ) and Src family protein tyrosine kinases (PTKs). Nef has also been reported to localize to the immunological synapse (IS) during T cell activation (Fenard et al., 2005; Thoulouze et al., 2006), suggesting that it may affect T cell activation at a very early step in the signaling pathway. However, the effect of Nef on TCR-mediated T cell activation has been a source of controversy with some studies reporting an enhancement of activation (Baur et al., 1994; Djordjevic et al., 2004; Fenard et al., 2005; Skowronski et al., 1993; Wang et al., 2000; Xu et al., 1999) while others demonstrate an inhibitory effect (Collette et al., 1996; Niederman et al., 1992; Niederman et al., 1993).

T cell activation is initiated by the ligation of T cell receptors by MHC-peptide complexes on antigen presenting cells. Upon binding of surface TCR molecules at the IS, intracellular Src family PTKs such as Lck and Fyn phosphorylate tyrosine residues located within the immunoreceptor tyrosine-based activation motifs (ITAMs) found on the cytoplasmic domains of the of TCR signaling subunits γ, δ, ε, ζ. ITAMs have a

consensus sequence Yxx(L/I)X_{6-8}Yxx(L/I) of which TCRζ, the primary signaling subunit of the TCR, contains three (ITAM 1,2,3). Phosphorylation of both tyrosines in each of the individual ITAMs on TCRζ results in the recruitment of the cellular kinase ZAP-70 and initiation of a phosphorylation cascade that culminates in full T cell activation [reviewed in (Smith-Garvin et al., 2009)].

Previous studies have demonstrated that SIV Nef binds TCRζ at two unique sites that include the YxxL/I motifs in ITAMs 1 an 2 (Schaefer et al., 2000) and that HIV-1 Nef only shares the ITAM 1-binding region (Chapter II). However, the functional consequences of complex formation in T cell activation are undescribed. In addition, the structural features on Nef that determine its specificity for TCRζ remain unknown. In this work, we performed a detailed analysis of the crystal structure of the core domain of SIVmac239 Nef in complex with a TCRζ polypeptide that contains the Yxx(L/I) motif from ITAM 1 and investigated the role of complex formation in modulation of Src PTK activity. Our results reveal a novel interaction interface on Nef specific to TCRζ that is not shared by any of Nef's reported binding partners. In addition, the TCRζ orders the N-terminus of Nef into a polyproline type II helix that we postulate mediates the enhancement of TCRζ-specific activity of Src PTKs.

IV.B. Materials and Methods

IV.B.1. Protein expression and purification

The cytoplasmic domain of TCRζ (residues L51-R164) and the core domain of Nef from SIVmac239 (residues D98-S235), HIV-1 laboratory strain NL4-3 (A56-N206) were expressed in *E. coli* and purified to >95% purity as described (Chapter II). Briefly, $TCR\zeta_{cyt}$ and all of the Nef_{core} variants were expressed as thioredoxin fusion proteins and purified under denaturing conditions by Ni-NTA affinity chromatography. The proteins were then dialyzed against non-denaturing conditions and cleaved with thrombin (MP Biochemicals) to remove the N-terminal tag sequence. The cleaved proteins were purified by anion exchange (POROS HQ) and size exclusion chromatography (Superdex S-200). Nef_{core} and $TCR\zeta_{cyt}$ proteins were concentrated to 700μM in PBS, pH 7.4. The TCRζ polypeptide $TCR\zeta_{A63\text{-}R80}$ was synthesized (21^{st} Century Biochemicals), validated by mass spectrometry, and concentrated to 700μM in 20mM Tris, pH 8.0. The TCRζ polypeptide $TCR\zeta_{L71\text{-}D87}$ was synthesized (Sigma) with an N-terminal biotin affinity tag in unmodified, mono-phosphorylated (pY72 or pY83) or bi-phosphorylated (pY2, pY83) forms and validated by mass spectrometry. The FHIT peptide used in in vitro kinase experiments was purchased (Cell Signaling Technology) and validated by mass spectrometry.

IV.B.2. Crystallization and data collection

Crystals of SIVmac239 Nef_{core} in complex with $TCR\zeta_{A63\text{-}R80}$ were grown and optimized as described (Chapter III). Briefly, crystals of the SIVmac239 Nef_{core}-$TCR\zeta_{A63\text{-}R80}$

complex were grown over 3-7 days (approximate dimensions 400 x 150 x 150 μm) using the vapor diffusion method in hanging drops; 2μl of a 1:1 molar ratio of SIVmac239 Nef_{core} and $TCR\zeta_{A63\text{-}R80}$ were mixed with 1μl reservoir solution (10-14% PEG 3,350, 200mM NH_4F, 100mM HEPES, pH 7.4-7.5) over a 1ml volume of reservoir solution. The single flash-frozen SIVmac239 Nef_{core}-$TCR\zeta_{A63\text{-}R80}$ crystal used for structure determination was orthorhombic ($P2_12_12_1$; a = 47.417, b = 47.421, c =183.519) and nearly perfectly pseudo-merohedrally twinned with a twin fraction $\alpha = 0.424$ (Chapter III). Data was collected to 2.05 Å resolution at beamline X29 at the National Synchrotron Light Source (NSLS) at Brookhaven National Laboratories (BNL) on a CCD detector at $\lambda = 1.003$ Å. The x-ray diffraction images were processed in HKL-2000 (Otwinowski and Minor, 1997) and assessed for quality and twinning in *phenix.xtriage* of the PHENIX software package (Adams et al., 2002).

IV.2.C. Model building and refinement

Structure determination of the SIVmac239 Nef_{core}-$TCR\zeta_{A63\text{-}R80}$ complex was performed by molecular replacement in the orthorhombic space group $P2_12_12_1$ and is described extensively in Chapter III. Briefly, an ensemble of structures of the core domain of HIV-1 Nef was used a search model to find a molecular replacement solution. Two molecules of Nef_{core} comprised the asymmetric unit and were related by non-crystallographic symmetry. Each molecule was refined individually in *phenix.refine* (Laskowski et al., 1993); each round of refinement included three cycles of bulk solvent correction, atomic positional refinement and individual b-factor refinement. Following each round of

refinement, the data was detwinned in *phenix.refine* to calculate $2F_o - F_c$ and $F_o - F_c$ electron density maps that were used to inspect and build into the model of the Nef_{core}-$TCR\zeta_{A63\text{-}R80}$ complex in Coot. The $TCR\zeta_{A63\text{-}R80}$ polypeptide was built manually as an alpha helix with 16 of 18 residues clearly resolved in the electron density maps. Water molecules were added to the refined model using automated water picking procedures in *phenix.refine*. The stereochemistry of the final refined model was monitored with *PROCHECK* (Laskowski et al., 1993).

IV.B.3. Surface plasmon resonance (SPR)

SPR spectroscopy experiments were performed at 25^{o}C on a Biacore 3000 system (GE Healthcare). 5000-8000 resonance units (RU) of neutravidin were coupled to a CM5 sensor chip (GE Healthcare) in 10mM acetate buffer (pH 5.0) using standard amine coupling protocols as described previously (Chapter II). 25 RU of unmodified $TCR\zeta_{L71\text{-}D87}$, mono-phosphorylated $TCR\zeta_{L71\text{-}D87}$ (pY72), mono-phosphorylated $TCR\zeta_{L71\text{-}D87}$ (pY83) and bi-phosphorylated $TCR\zeta_{L71\text{-}D87}$ (pY72, pY83) were captured in different neutravidin-coupled experimental flow cells leaving one flow cell unbound as a control surface. Each immobilized TCRζ polypeptide was directed uniformly in an N-terminal to C-terminal orientation away from the neutravidin-CM5 surface due to placement of the biotin tag at the N-terminus. SIVmac239 Nef_{core} was injected at a flow rate of 30μl/min over each experimental flow cell and the control flow cell, generating SPR sensorgrams. The sensorgram from the control neutravidin-only flow cell was subtracted from the experimental neutravidin-bio-TCRζ polypeptide flow cell sensorgram (reference

subtraction), generating a resultant Nef binding sensorgram that described the specific binding of Nef for the captured TCRζ polypeptide and removed any nonspecific interaction with the CM5 or neutravidin surface.

IV.B.4. In vitro kinase assay

Phosphorylation of the biotinylated FHIT substrate peptide (Cell Signaling Technology) (Pekarsky et al., 2004) by Src family protein tyrosine kinases (PTK) was assessed in the absence and presence of HIV-1 NL4-3 and SIVmac239 Nef_{core} using a modified protocol of the HTScan Lck Kinase Assay Kit (Cell Signaling Technology). FHIT peptide (1.5μM) was pre-incubated in an equimolar ratio with either HIV-1 NL4-3 Nef_{core} or SIVmac239 Nef_{core} in the kinase assay buffer (60mM HEPES, 5mM $MgCl_2$, 5mM $MnCl_2$, 3μM Na_3VO_4, 1.25mM DTT, 20μM ATP, pH 7.5) for 30 minutes at 25^oC. Following the pre-incubation period, Lck (Cell Signaling Technology), Fyn (Invitrogen) or c-Src (Invitrogen) was added to each reaction volume (25μl) to a final concentration of 12nM; each reaction mixture was immediately incubated for 0, 15, 30, 60 or 120 minutes at 37^oC. The reaction mixtures were quenched by the addition of 25μl of 50mM EDTA, transferred to 96-well streptavidin-coated black plates (Pierce) and incubated at room temperature for 1 hour. Each well was washed three times with PBS + 0.05% Tween-20 (PBS-T) and then incubated with a mouse anti-phosphotyrosine monoclonal antibody (Cell Signaling Technology) for 1 hour at room temperature. Following triplicate washes with PBS-T, each well was incubated with FITC-conjugated goat anti-mouse antibody

(BD Biosciences) for 30 minutes at room temperature. After triplicate washes in PBS-T, FITC fluoresence was measured on a FLUOstar OPTIMA (BMG) microplate reader.

IV.B.4. In vitro TCRζ phosphorylation assay

Phosphorylation of the cytoplasmic domain of TCRζ by Src family PTKs was assessed in the absence and presence of Nef_{core} proteins from HIV-1 NL4-3 and SIVmac239 by SDS-PAGE. $TCR\zeta_{cyt}$ (7.5μM) was pre-incubated alone and with each Nef_{core} protein for 30 minutes at 4°C in the kinase assay buffer (60mM HEPES, 5mM $MgCl_2$, 5mM $MnCl_2$, 3μM Na_3VO_4, 1.25mM DTT, 20μM ATP, pH 7.5). Lck (Cell Signaling Technology), Fyn (Invitrogen) or c-Src (Invitrogen) was added to each reaction volume (25μl) to a final concentration of 12nM; each reaction mixture was immediately incubated for 0, 15, 30, 60 or 120 minutes at 37°C and quenched with 25μl 50mM EDTA. $TCR\zeta_{cyt}$ phosphorylation was analyzed by SDS-PAGE and gel band analysis was performed in Quantity One (Bio-Rad).

IV.C. Results

IV.C.1. Overall structure of the SIVmac239 Nef_{core}-TCR$\zeta_{A63\text{-}R80}$ complex

The structure of SIVmac239 Nef_{core} bound to TCR$\zeta_{A63\text{-}R80}$ was determined to 2.05 Å by molecular replacement and twinned refinement procedures. The overall structure of the SIVmac239 Nef_{core}-TCR$\zeta_{A63\text{-}R80}$ complex (Figure IV-1A) exhibits significant structural conservation in the Nef_{core} protein and novel structural features on the TCRζ polypeptide. SIVmac239 Nef_{core} adopts a similar α/β fold to the core domain of HIV-1 Nef as previously observed in the crystal structures of HIV-1 isolate LAI Nef_{core} (L58-C206), SH3 domain-bound HIV-1 isolate LAI Nef_{core} (Arold et al., 1997) and SH3 domain-bound HIV-1 laboratory strain NL4-3 Nef_{core} (A54-N205) (Lee et al., 1996) (Figure 1C) as well as the NMR solution structure of HIV-1 isolate BH10 (Δ2-39, Δ159-173, T71R) Nef (Grzesiek et al., 1996a). The structural similarity is expected considering the significant sequence conservation observed for this region on Nef (Figure IV-1C). Superimposition of the SIVmac239 Nef_{core} structure with the crystal structures of HIV-1 Nef (Figure IV-1B) results in a only small deviation in Cα coordinate position with an overall root mean square deviation (r.m.s.d.) of 0.65 - 0.89 Å.

The N-terminal region (R103-R109) is ordered in a left-handed polyproline type II (PPII) helical conformation as observed in the SH3 domain-bound forms of HIV-1 Nef (Arold et al., 1997; Lee et al., 1996). The PPII helix is followed by two large anti-parallel α-helices (α1, Y113-E125; α2 A136-E150) connected by a 10 residue loop (K126-S135) that collectively form the TCRζ-interacting region on Nef. The remainder of the core

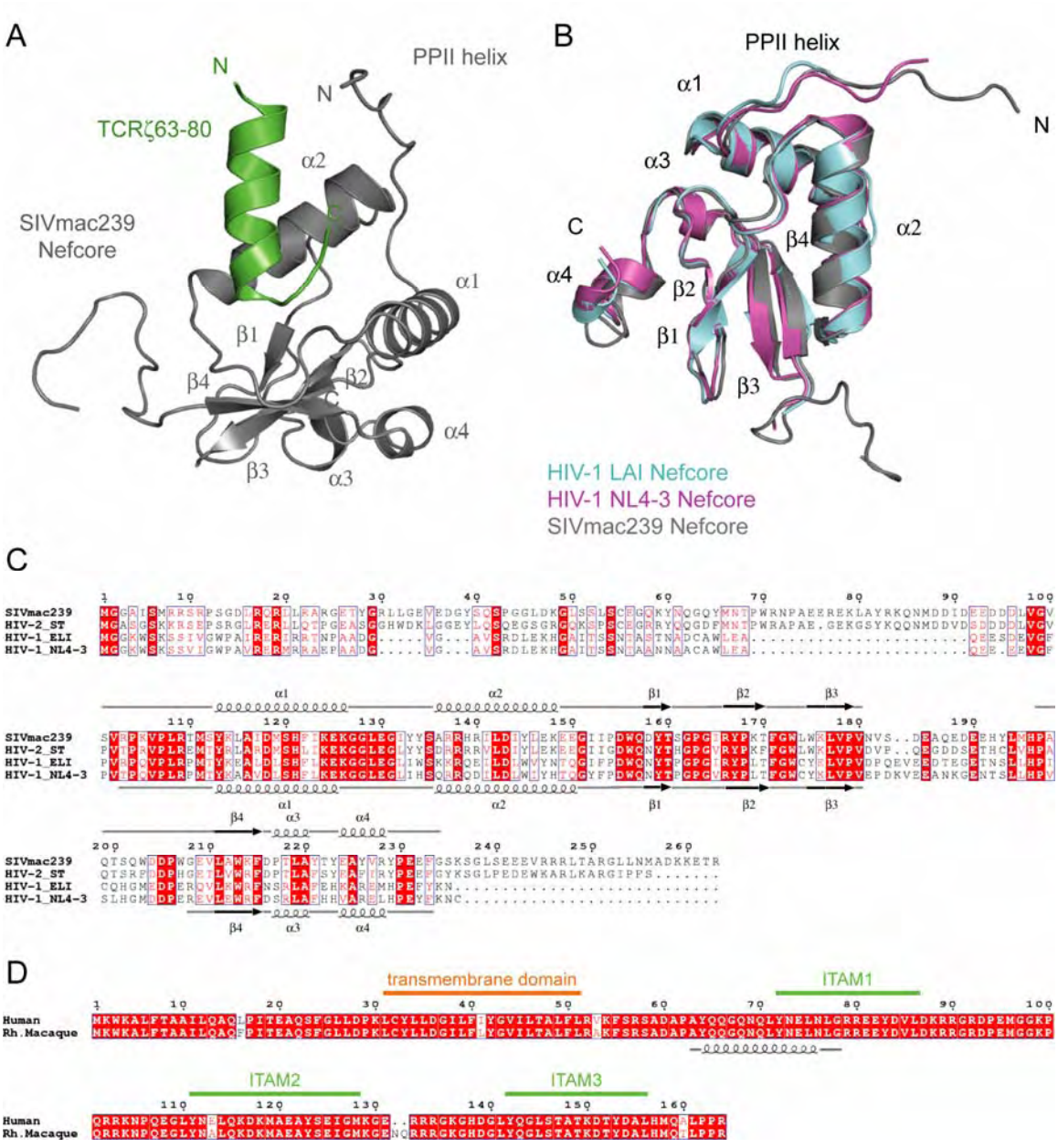

Figure IV-1. Structure of the SIVmac239 Nef$_{core}$-TCRζ$_{63-80}$ complex. A. Ribbon diagram of SIVmac239 Nef$_{core}$ in complex with TCRζ$_{63-80}$ polypeptide. B. Secondary structure alignment of Nef. Crystal structures of Nef$_{core}$ were superimposed by least-squares fitting of the folded core (V103-V181 for SIVmac239 Nef). Unliganded HIV-1 LAI Nef$_{core}$ (PDB code 1AVV) is colored cyan, SH3 domain-bound HIV-1 NL4-3 Nef$_{core}$ (PDB code 1EFN) is purple and TCRζ$_{63-80}$-bound SIVmac239 Nef$_{core}$ is grey. C. Primary structure alignment of Nef. Residue numbering corresponds to SIVmac239 Nef. Identical residues are boxed and shaded in red and partially conserved residues are boxed and in pink. Secondary structure elements observed in SIVmac239 Nef$_{core}$ (above sequence) and

HIV-1 NL4-3 Nef_{core} (below sequence) are denoted by curls for alpha helices (α1-α4) and arrows for beta strands (β1-β2) with loop regions denoted by gray lines. D. Primary structure alignment of TCRζ. The full length sequence of human and rhesus macaque TCRζ are shown with transmembrane region and ITAMs denoted in orange and green, respectively. Secondary structure elements observed for human TCRζ are denoted by curls for alpha helices and grey lines for loops.

domain consists of a pair of anti-parallel β strands (β1, W175-P180; β2, L211-F215) that form the bulk of the hydrophobic core of the protein and a pair of smaller α-helices (α3, P217-A220; α4, E224-R228) found near the C-terminus. The β strands do not form a contiguous β-sheet due to the structural distortion caused by two well conserved proline residues (P168, P179) in addition to the limited number of residues that participate in hydrogen bonding; a similar distortion of β-sheet topology is observed in the structures of HIV-1 Nef (Arold et al., 1997; Lee et al., 1996). A large loop (N181-H196) between β1 and β2 is absent in the crystal structure due to significant disorder in that region as previously described for HIV-1 Nef (Arold et al., 1997; Grzesiek et al., 1997; Lee et al., 1996). Although there are 11 extra residues built into the disordered region compared to the HIV-1 Nef structures, they are likely ordered due to crystallization artifact and therefore do not represent physiologically relevant structure (Chapter III).

The majority of the TCRζ polypeptide adopts alpha helical structure. Of the 16 residues (A63-G78) resolved in the calculated electron density (Figure IV-2B), 13 residues (A63 - L75) comprise the alpha helix and 3 residues (N76-G78) form a loop at the C-terminus. The N-terminus of the alpha helix lies proximal to the N-terminus of Nef, suggesting that the TCRζ polypeptide is oriented in a physiologically relevant direction in the crystal structure. The alpha helical conformation of the TCRζ polypeptide is striking considering the largely disordered nature of the cytoplasmic domain of TCRζ (Duchardt et al., 2007; Laczko et al., 1998; Sigalov et al., 2004) and the lack of secondary structure observed previously for the ITAM 1 region (69-86) (Laczko et al., 1998).

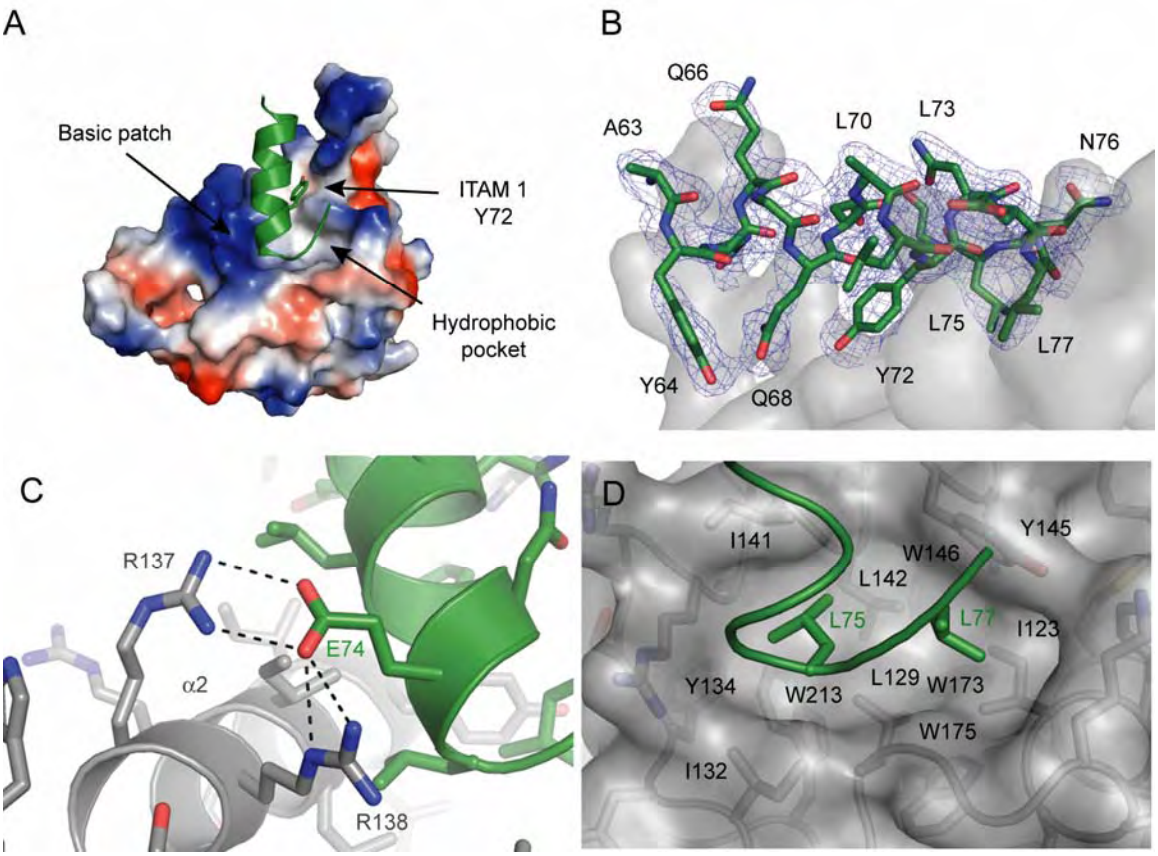

Figure IV-2. Interaction between SIVmac239 Nef_{core} and TCR$\zeta_{63\text{-}80}$. A. Electrostatic surface representation of Nef with bound TCR$\zeta_{A63\text{-}80}$. Positively charged regions are colored blue, negatively charged are colored red and neutral regions are colored white. ITAM 1 residue Y72 and the basic patch and hydrophobic pocket on Nef are indicated by arrow. The TCRζ polypeptide is drawn in ribbon diagram (green). B $2F_o$-F_c electron density map of TCR$\zeta_{63\text{-}80}$ countered at α=1.0. Surface representation of Nef is shown in grey. B. Salt bridge between SIVmac239 Nef_{core} (grey) and TCR$\zeta_{63\text{-}80}$ (green). The possible hydrogen bonds between residue E74 on Nef and residues R137 and R138 on TCRζ are denoted by black dashed lines. C. TCR$\zeta_{63\text{-}80}$ binds to a hydrophobic pocket on SIVmac239 Nef. Residues L75 and L77 on TCRζ (green) are buried in a hydrophobic pocket on Nef. Residues lining the pocket are labeled in grey.

Therefore, the TCR$\zeta_{A63\text{-}R80}$ polypeptide seems to undergo a disorder-to-order transition upon binding its Nef_{core} interaction partner.

The accessible surface area of the unbound forms of SIVmac239 Nef_{core} and TCR$\zeta_{A63\text{-}R80}$ are 7655.9 $Å^2$ and 1672.7 $Å^2$, respectively. In the bound complex, the TCR$\zeta_{A63\text{-}R80}$ polypeptide occupies a hydrophobic crevice on Nef bordered by alpha helices $\alpha1$ and $\alpha2$. This results in a total buried surface area at the binding interface of 1313.9 Å, with 595.6 $Å^2$ and 718.3 $Å^2$ contributed by Nef_{core} and TCRζ, respectively.

IV.C.2. Specificity of the Nef-TCRζ interaction

The specificity of the TCR$\zeta_{A63\text{-}R80}$ polypeptide for Nef_{core} is conferred through a novel set of electrostatic and hydrophobic interactions (Figure IV-2). At the N-terminus of the $\alpha2$ alpha helix on Nef_{core}, a glutamic acid on TCRζ (E74) forms a salt bridge with a positively charged patch on Nef consisting of two adjacent arginine residues (R137, R138) (Figure IV-2C). The di-arginine motif is highly conserved among the different Nef variants from HIV-1, HIV-2 and SIV and has been suggested to be important for affecting PAK1/2 function (Fackler et al., 2000; Sawai et al., 1995). However, a direct protein-protein interaction mediated by the diarginine motif on Nef has not been described previously.

The TCR$\zeta_{A63\text{-}R80}$ polypeptide also binds to an extensive hydrophobic surface on Nef_{core} formed by the C-terminus of $\alpha1$, the N-terminus of $\alpha2$ and the $\alpha1$-$\alpha2$ loop. Residues L75 and L77 on TCRζ are buried in a deep hydrophobic pocket lined by

residues I123, L129, L132, I141, L142, W173, W213 on Nef (Figure IV-2C). In addition, the first ITAM 1 YxxI/L tyrosine (Y72) rests on a cleft contiguous with the hydrophobic pocket that almost completely buries the hydroxyl group (Figure IV-2A). Summarized in Table IV-1 are the residues present at the Nef-TCRζ interface.

The electrostatic and hydrophobic contacts collectively explain the observed specificity of Nef for TCRζ among ITAM-containing proteins and specifically for the A61-R80 and E121-G140 regions on TCRζ observed to bind SIV Nef (Chapter II). The only two ITAM regions that satisfy the binding requirement for a tyrosine, negatively charged residue and two neutral residues (i.e. YxELxL) are the regions described previously to comprise SNID-1 (72-YNELNL-77) and SNID-2 (123-YSEIGM-128) (Schaefer et al., 2000). Therefore, it is likely that SIV Nef binds to the SNID-2 binding site in the same manner observed for SNID-1 binding in the crystal structure.

We demonstrated in Chapter II that HIV-1 Nef additionally bound TCRζ but only at the ITAM 1 region. Curiously, the only significant differences in the two binding sequences on TCRζ are the substitutions of two leucines (L75, L77) with an isoleucine (I126) and a methionine (M128) in the ITAM 2 binding site. Although the majority of residues on Nef surrounding L75 and L77 on TCRζ are highly conserved in HIV-1 Nef (Table IV-1), the isoleucine at residue position 123 in SIV Nef is substituted by a leucine (L92) in HIV-1 Nef which may serve as a determinant of TCRζ specificity. However, the precise mechanism by which the isoleucine-leucine substitution may reduce HIV-1 Nef's interaction with the second ITAM binding region is unclear and will require further investigation.

IV.C.3. Phosphorylation of ITAM 1 residue Y72 abrogrates Nef binding

In the structure of the Nef_{core}-$TCR\zeta_{A63-R80}$ complex, the first YxxI/L motif tyrosine (Y72) in ITAM 1on TCRζ is partially buried on Nef. The close proximity of the hydroxyl group of Y72 on TCRζ and the interfacing side chain of residue E149 on Nef suggests that Nef (Figure IV-3A) would not be able to spatially nor electrostatically accommodate a negatively charged phosphorylation modification on Y72. Alternatively, phosphorylation of Y72 would not be expected to permit binding of Nef. In order to determine the effect of phosphorylation on Nef binding, SPR binding studies were performed using differentially phosphorylated TCRζ ITAM 1 peptides. Following immobilization of unphosphorylated (Y72, Y83), mono-phosphorylated (pY72 or pY83) and bi-phosphorylated (pY72, pY83) forms of the ITAM 1 TCRζ polypeptide (L710-D87), SIVmac239 Nef_{core} was injected and binding sensorgrams were recorded. Shown in Figure IV-3B, the interaction of SIVmac239 Nef with ITAM 1 on TCRζ is abrogated when Y72 is phosphorylated, either alone or in combination with pY83. However, since phosphorylation of Y83 alone had no effect on Nef binding, phosphorylation of Y72 was the primary cause for disruption of Nef binding.

IV.C.4. Interaction with TCRζ orders the SH3 binding motif on Nef

Nef contains several structurally disordered regions, including the N-terminus, C-terminus and internal β1-β2 loop, that are not observed in the crystal (Arold et al., 1997) and NMR solution (Grzesiek et al., 1996a; Grzesiek et al., 1997) structures of HIV-1 Nef.

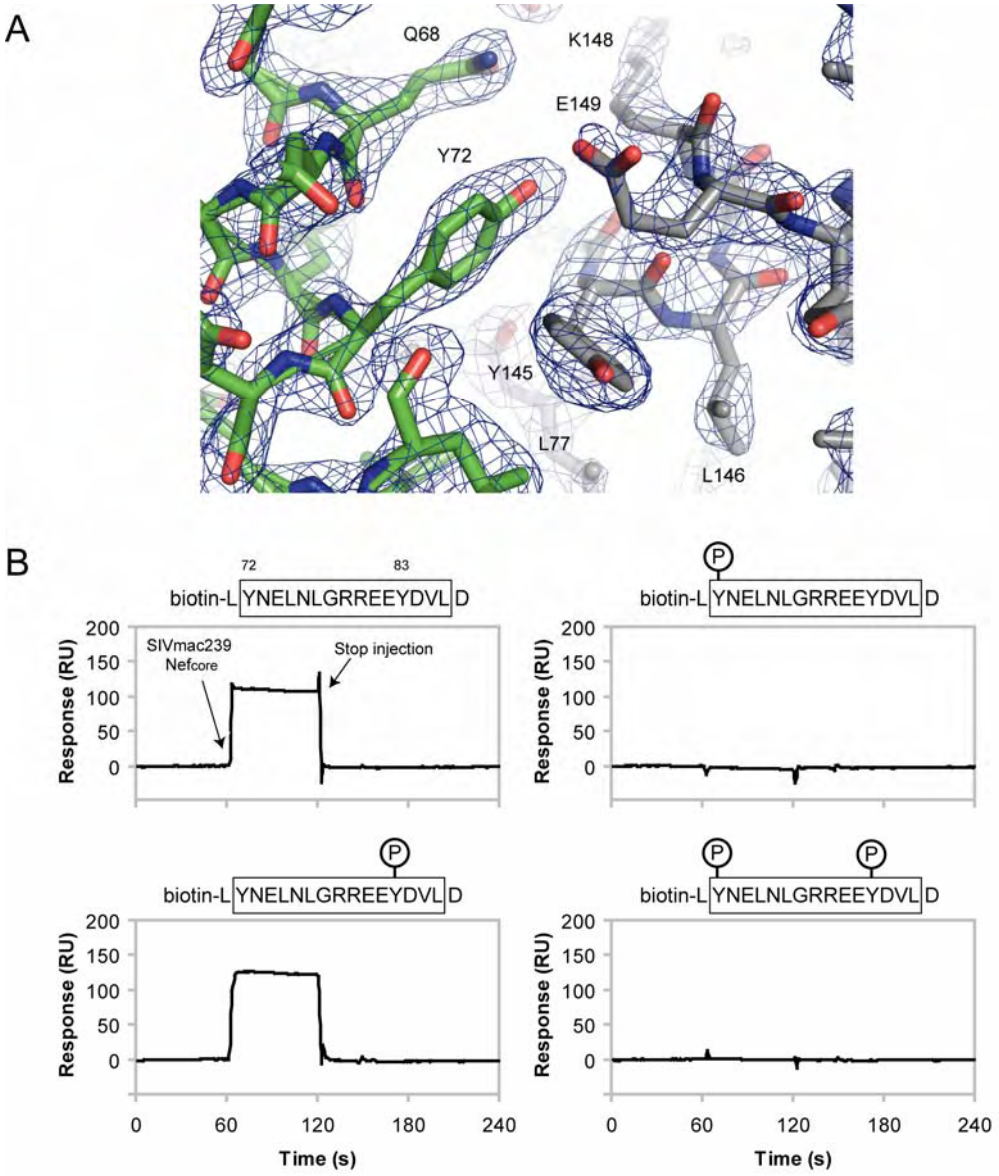

Figure IV-3. Phosphorylation of ITAM1 residue Y72 disrupts Nef binding. A. $2F_o$-F_c electron density map at α=1.0 for the Nef-TCRζ interface region at residue Y72 on TCRζ is shown. TCRζ is depicted in green and SIVmac239 Nef_{core} is depicted in grey. B. SPR sensorgrams of the interaction of SIVmac239 Nef_{core} and differentially-phosphorylated ITAM 1 peptides. ITAM1 (Y72-L86) is denoted by a boxed outline and phosphorylation modification on residues Y72 and Y83 are marked with an encircled "P".

One such region near the N-terminus of the core domain includes a PxxP motif (P104-P107) that is disordered in the unliganded HIV-1 Nef structure but folds into a well ordered left-handed polyproline type II helix in SIV Nef when bound to $TCR\zeta_{A63\text{-}R80}$. Interestingly, the PPII helix is ordered by the bidentate hydrogen bonding of the terminal amide residues on Q65 of TCRζ with the main chain amide atoms on S103-R103 (Figure IV-4). A similar main chain torsional restraint resulting in induced PPII helix comformation has been observed previously for peptides bound to MHC molecules (Jardetzky et al., 1996). The homologous region on HIV-1 has also been observed to dopt a near identical PPII helix conformation when bound to the SH3 domain of Fyn (Arold et al., 1997; Lee et al., 1996). The PPII helix on Nef has been suggested to enhance the activity of Src PTKs by displacing the SH3 domain thus relieving the auto-inhibitory intramolecular constraints in the PTK (Lee et al., 1996; Moarefi et al., 1997).

IV.C.5. Enhancement of TCRζ phosphorylation by Nef

In order to investigate the potential role of Nef-TCRζ complex formation on modulation of Src PTK activity, *in vitro* phosphorylation studies were performed. First, the effect of Nef on Src PTK activity was studied with the core domains of HIV-1 NL4-3 and SIVmac239 Nef and a Src substrate peptide from FHIT (Pekarsky et al., 2004) that contains a single tyrosine susceptible to modification byt phosphorylation by Src PTKs. By observing the effect of Nef on the phosphorylation of a random Src PTK substrate not observed to interact with Nef (data not shown), the effect of Nef on Src PTK activity

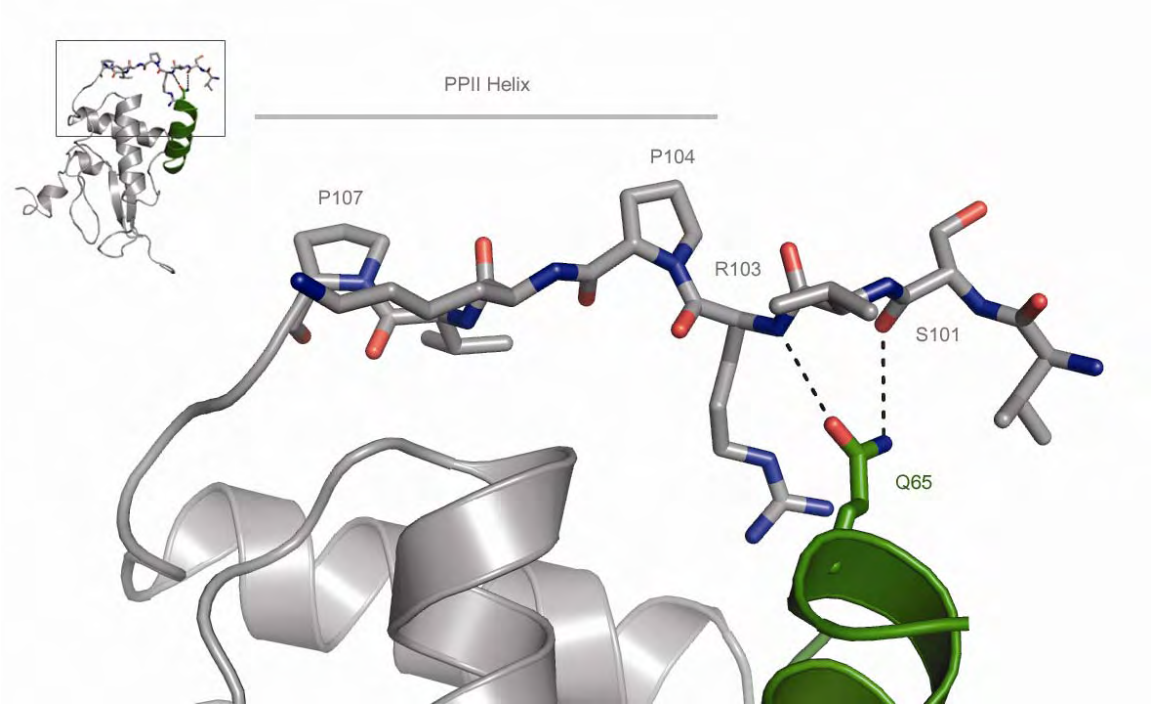

Figure IV-4. TCRζ orders a PPII helix at the N-terminus of Nef. SIVmac239 Nefcore (grey) and TCRζ (green) are shown in ribbon diagram. The side chain-main chain hydrogen bonding network between Q65 (TCRζ) and S101, R103 (Nef) is illustrated by dashed black lines.

could be determined in a substrate-independent manner. HIV-1 NL4-3 and SIVmac239 Nef_{core} were pre-incubated with the test FHIT peptide for 30 minutes after which the Src PTKs Lck, Fyn and Src were added independently. Shown in Figure IV-5, both HIV-1 and SIV Nef_{core} significantly increased the amount of detected phosphorylated peptide at earlier time points for Lck as compared to Lck alone. In addition, HIV-1 NL4-3 Nef_{core} exhibited an enhancing effect on Src activity that exceeded SIVmac239 Nef_{core} effects. In contrast, Nef_{core} had either no effect (SIVmac239) or a small inhibitory effect (HIV-1 NL4-3) on Fyn activity, respectively. Therefore, Nef appears to be capable of modulating Src PTK activity but exerts different effects specific to each kinase and Nef type. Furthermore, HIV-1 Nef is observed to enhance activity of Lck, contrary to a previous report (Greenway et al., 1996).

In order to explore the effect of Nef on TCRζ-specific Src PTK activity, the test peptide was replaced with purified $TCR\zeta_{cyt}$ in the phosphorylation experiments. Due to the presence of six possible phosphorylation sites on $TCR\zeta_{cyt}$, and high percentage SDS-PAGE gel mobility assay was used to evaluate the initiation and extent of phosphorylation on $TCR\zeta_{cyt}$. Previous studies have demonstrated that the mobility of $TCR\zeta_{cyt}$ is reduced upon phosphorylation at each tyrosine due to the addition of negative charge on the protein by the phosphate modification and that all phosphorylated states (P1-P6) of $TCR\zeta_{cyt}$ can be visualized by gel electrophoresis (Weissenhorn et al., 1996). However, due to the multiple phosphorylated states $TCR\zeta_{cyt}$, quantitative analysis of the unphosphorylated $TCR\zeta_{cyt}$ protein gel band was performed to assess initiation of kinase

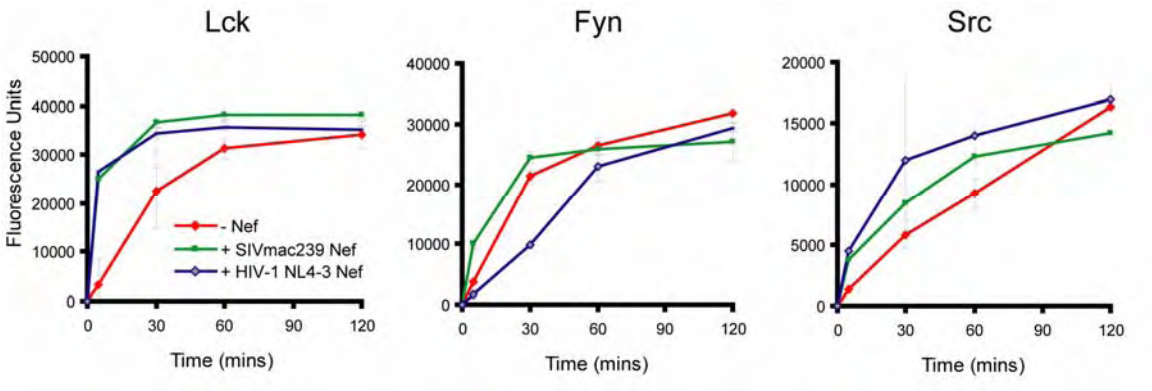

Figure IV-5. Modulation of *in vitro* Src PTK activity by Nef$_{core}$. Biotinylated FHIT peptide was incubated with or without SIVmac239 Nefcore or HIV-1 NL403 Nefcore for varying times in the presence of Lck, Fyn and Src. The phosphorylation reaction was quenched with 50mM EDTA. Quantity of phosphorylated peptide was detected by anti-phosphotyrosine antibody ELISA.

activity; as TCRζ_{cyt} becomes phosphorylated, the amount of unmodified protein will decrease.

In the absence of Nef, TCRζ_{cyt} was readily phosphorylated by Lck into multiple phosphorylated species early in the time course (Figure IV-6). By two hours, over 40% of the TCRζ_{cyt} protein was phosphorylated. In contrast, more mild activity was observed by Fyn and Src (Figure IV-6 A); at two hours, ~30% of the TCRζ_{cyt} protein was phosphorylated. However, in the presence of SIVmac239 Nef$_{core}$, TCRζ_{cyt} was more rapidly phosphorylated and to higher phosphorylated species by all of the Src PTKs and especially by Fyn and Src, leaving less than 30% unmodified TCRζ_{cyt} after two hours. HIV-1 NL4-3 Nef$_{core}$ also augmented phosphorylation of TCRζ_{cyt} by all of the Src PTKs but to a lesser extent than that observed for SIVmac239 Nef$_{core}$ with the exception of Lck.

SIVmac239 Nef$_{core}$ was also observed to migrate to a higher gel band indicating that the Src PTKs additionally phosphorylated Nef$_{core}$. In contrast, HIV-1 NL4-3 was not observed to become phosphorylated in the presence of Src PTKs, confirming a previous report demonstrating that SIV Nef and not HIV-1 Nef was susceptible to modification by Lck (Cheng et al., 1999). Surprisingly, phosphorylation of SIVmac239 Nef$_{core}$ in the reaction mixture including TCRζ_{cyt} was markedly increased as compared to when SIVmac239 Nef$_{core}$ was incubated with Lck or Fyn alone (Figure IV-7). Incubation of SIVmac239 Nef$_{core}$ with Src resulted in the generation of multiple differentially migrating gel bands suggesting multiple phosphorylated forms. In the reaction mixtures including TCRζ_{cyt}, these multiply phosphorylated Nef gel bands reduced to one, suggesting that the

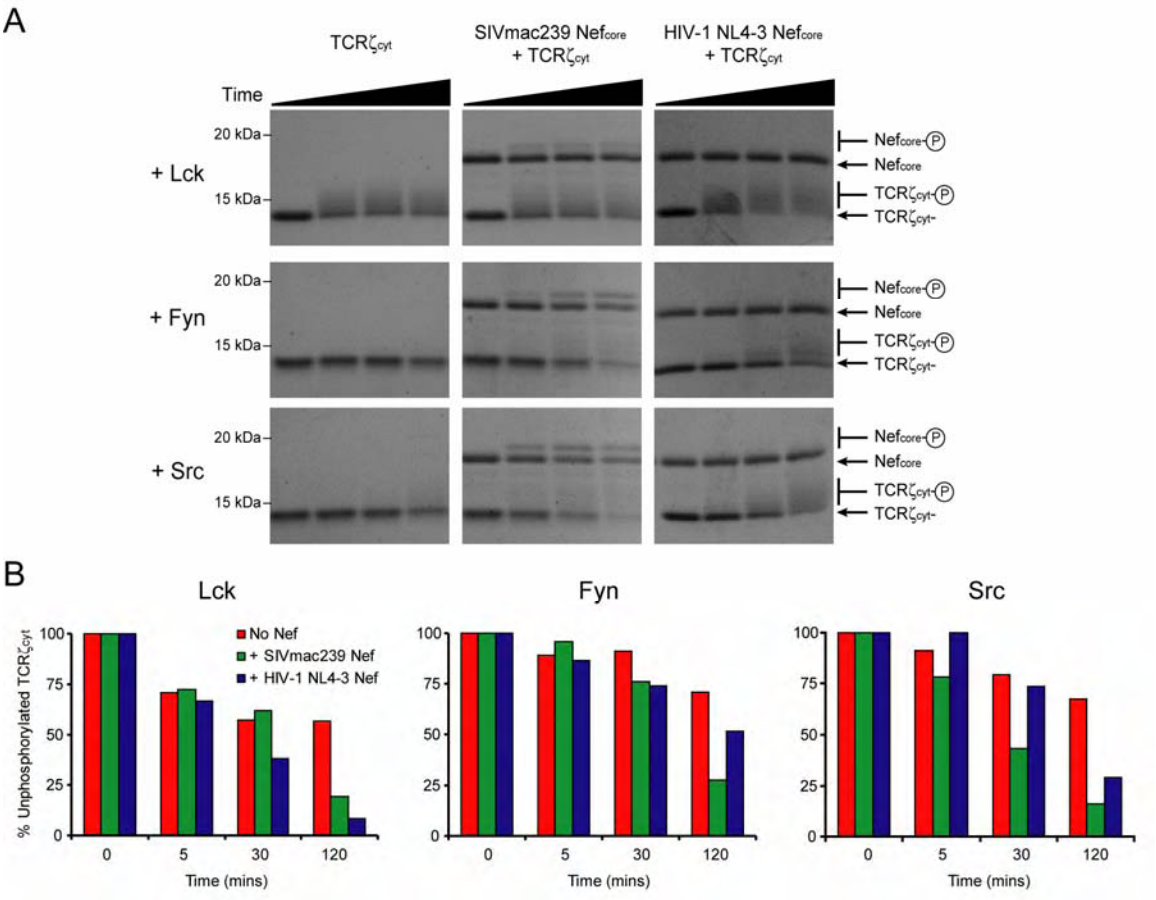

Figure IV-6. Modulation of TCRζ$_{cyt}$ phosphorylation. A. SDS-PAGE analysis of TCRζ$_{cyt}$ phosphorylation by Src PTKs. TCR $_{cyt}$ was incubated with Src PTKs in the absence or presence of SIVmac239 Nefcore and HIV-1 NL4-3core for 0, 5, 30 and 120 minutes and then analyzed by 16% SDS-PAGE. Molecular weight positions are denoted on left and gel migration levels correlating to phosphorylated (TCRζ$_{cyt}$-P, Nef$_{core}$-P) and unphosphorylated (TCRζ$_{cyt}$, Nef$_{core}$) proteins are shown on right. B. Quantitaive analysis of unphosphorylated TCRζ$_{cyt}$. The gel band corresponding to the unphosphorylated TCRζ$_{cyt}$ protein was intergrated for each reaction time point in Quantity One (Bio-Rad) and divided by the zero time point gel band generate the % unphosphorylated TCRζ$_{cyt}$ values plotted.

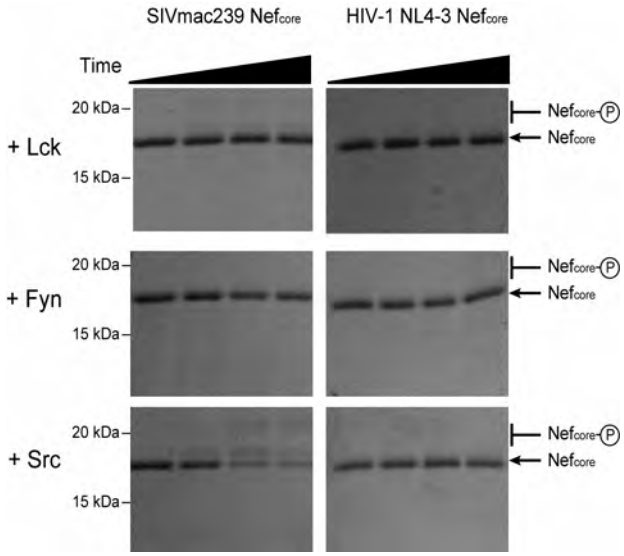

Figure IV-7. Phosphorylation of HIV-1 and SIV Nef_{core} by Src PTKs. SDS-PAGE analysis of Nef_{core} phosphorylation by Src PTKs. Nefcore from HIV-1 NL4-3 and SIVmac239 were ncubated with Src PTKs for 0, 5, 30 and 120 minutes and then analyzed by 16% SDS-PAGE. Molecular weight positions are denoted on left and gel migration levels correlating to phosphorylated (Nef_{core}-P) and unphosphorylated (Nef_{core}) Nef_{core} are shown on right.

Nef-TCRζ complex directed the phosphorylation of SIVmac239 to a single phosphorylated start species.

IV.D. Discussion

Here we report the high resolution crystal structure of SIVmac239 Nef_{core} in complex with a TCRζ polypeptide and the investigation of the potential role of Nef-TCRζ complex formation in the modulation of TCRζ-specific phosphorylation by Src PTKs. The structure of the Nef_{core}-TCRζ complex reveals that the core domain of SIVmac239 Nef adopts a similar fold to that observed for HIV-1 Nef (Arold et al., 1997; Grzesiek et al., 1997; Lee et al., 1996). Strikingly, the TCRζ polypeptide, which contains the N-terminal YxxL/I motif in ITAM 1, adopts an alpha helix in the Nef-bound form that partially buries the first tyrosine in ITAM 1 (Y72) in Nef. The presence of secondary structure in the Nef-bound TCRζ polypeptide refutes our previous assertation that $TCR\zeta_{cyt}$ does not undergo a disorder-to-order transition upon binding SIVmac239 Nef_{core},. This conclusion was based on the lack of observed chemical shift changes and changes in cross-peak intensity between the HSQC spectra of $TCR\zeta_{cyt}$ alone and in the presence of SIVmac239 Nef_{core} (Sigalov et al., 2008). However, no chemical shift changes were observed, including those that should have corresponded to the known binding sites on TCRζ. We therefore suggested that the observed lack of changes in the HSQC spectra of TCRζ in its free and Nef-bound state could be explained by the multivalency of TCRζ for Nef where each binding site could be bound or unbound at any point in the experiment (Sigalov et al., 2008). While this possibility may explain the discrepancy in the NMR and crystallography findings, a more detailed investigation will need to be performed.

Crystal structures of TCRζ peptides in complex with other binding partners have been described previously (Hatada et al., 1995; Nam et al., 2005). However, none of the crystallized TCRζ peptides adopt significant secondary structure in their bound states, including the ZAP-70-bound ITAM 1 polypeptide (Q69-D87, pY72, pY83) that contains an overlapping sequence (D69-R80) with the $TCR\zeta_{A63\text{-}R80}$ polypeptide used in our studies. Therefore, the induction of secondary structure in TCRζ by Nef represents a novel mechanism by which TCRζ binds to a protein interaction partner.

The structural features on Nef that determine its specificity for the TCRζ form a novel interaction surface that includes a highly conserved diarginine motif (R137, R138) and a hydrophobic pocket that accommodates residues L75 and L77 on TCRζ. The diarginine motif has been suggested to be important for affecting PAK1/2 function (Fackler et al., 2000; Sawai et al., 1995), however direct bimolecular binding studies have not been performed. PAK1/2 may therefore share specificity to the diarginine motif with TCRζ or may alternatively cooperatively participate in the formation of a ternary complex with Nef and TCRζ. HIV-1 Nef's interaction with PAK1/2 has been associated with the recruitment of PAK1/2 to lipid rafts (Krautkramer et al., 2004) where Nef is suggested to prime the T cell for activation (Wang et al., 2000). Interestingly, HIV-1 Nef has also been demonstrated recently to increase the association of TCRζ with lipid rafts (Djordjevic et al., 2004) further suggesting that Nef may be serving as an adaptor protein between PAK1/2 and TCRζ.

In the crystal structures of the complex of HIV-1 Nef_{core} with the SH3 domain of Fyn (Arold et al., 1997; Lee et al., 1996), the N-terminus of Nef is ordered in a left-handed polyproline helix that is otherwise disordered in the unliganded Nef protein. The ordered PPII helix has been suggested to play a vital role in binding SH3 domains but more importantly, in activating Src PTKs (Moarefi et al., 1997). In the structure of the SIVmac239 Nef_{core}-TCRζ complex, the N-terminus is strikingly ordered in the same PPII conformation observed for SH3 domain-bound HIV-1. Therefore, we postulate that binding of TCRζ to Nef facilitates the formation of a ternary complex with Src PTKs that is mediated by TCRζ-induced ordering of the PPII helix on Nef. In turn, binding of Src PTKs with Nef would be expected to enhance the binding of TCRζ. The functional outcome would be expected to be enhanced kinase activity specific to TCRζ. A similar cooperative model has been proposed for the association of HIV-1 Nef, the cytoplasmic tail of CD4 and Hck but the functional effects of complex formation is unknown (Grzesiek et al., 1996b).

Our results demonstrate that TCRζ phosphorylation is significantly enhanced in the presence of HIV-1 and SIV Nef_{core}. The effect was most significant with the Src PTKs Fyn and Src and less with Lck which exhibited inherent elevated activity on TCRζ. The hyperactivation of Fyn is of particular importance considering its reduced functional role in T cells. Although both present in T cells and capable of phosphorylating TCRζ, Lck and Fyn differ in the kinetics of their activity where Lck activity peaks early following TCR stimulation and Fyn activity lags behind [(Filipp et al., 2003), reviewed in (Palacios and Weiss, 2004)]. In addition, Fyn was found to be either inactive (Filipp et

al., 2003) or to induce dysregulated T cell signaling patterns that led to markedly reduced Il-2 secretion (Denny et al., 2000) in Lck-deficient T cells. Therefore, hyperactivation of Fyn by the Nef-TCRζ complex may restore functionally competent kinase activity. Surprisingly, increased basal Fyn activity has been closely linked to its increased localization to lipid rafts (Filipp et al., 2004) where HIV-1 Nef has been demonstrated to also localize to affect T cell activation (Djordjevic et al., 2004; Fenard et al., 2005; Krautkramer et al., 2004).

The functional outcome of increased TCRζ phosphorylation mediated by the enhancement of Src PTK activity by the Nef-TCRζ complex would be expected to be an increase in T cell activation. However, studies of Nef-transfected cells and Nef-transgenic mice have demonstrated that Nef can induce both hyperactivation and inhibition of T cell activation (Table I-2). Although this is likely the result of Nef's many other effects in T cells, it may also come from Nef's effect on TCRζ phosphorylation. Phosphorylation of the six ITAM tyrosines results in full activation of a T cell following stimulus through the TCR. However, partial phosphorylation of the TCRζ ITAMs has been demonstrated to not only reduce T cell signaling but to additionally suppress T cell activation (Kersh et al., 1999). The primary mediator of the suppressive outcome was the phosphorylated state of the N-terminal ITAM 1 YxxL/I motif tyrosine (Y72). In studies where each successive ITAM tyrosine was mutated to a phenylalanine, the mutation observed to have a functional effect was Y72 which when mutated, resulted in significantly reduced IL-2 secretion. In the Nef-bound state, Y72 on TCRζ is partially buried and likely inaccessible to free kinases. In addition, when Y72 is phosphorylated,

Nef binding activity was abolished. However, the accessibility of Y72 in a ternary complex including Lck, Fyn or Src is unknown. Therefore, depending on the bound state of Nef on TCRζ and the accessibility of Y72 to Src PTKs, Nef could potentially have an enhancing or suppressive effect on T cell activation. However, more detailed characterization of the effect of Nef-TCRζ complex formation on T cell activation will need to be pursued to clarify the discrepancy in Nef's reported effects on T cell activation.

Table IV-1. Residues involved in the Nef-TCRζ_{63-80} interaction

TCRζ	SIVmac239 Nef	HIV-1 ELI Nef*	HIV-2 ST Nef*
Y64	K148	N117	K147
Q65	S101	P70	P100
	V102	V71	V101
	R103	R72	T102
Q68	K148	N117	K147
L71	I141	L110	V140
	I144	L113	L141
Y72	I141	L110	V140
	I144	L113	L143
	Y145	W114	W144
	E149	T118	E148
E74	R137	K106	R136
	R138	R107	R137
L75	L129	L98	I129
	I141	I110	V140
	L142	L111	L141
	W213	W182	W212
L77	I123	L92	I122
	L129	L98	I128
	I132	L101	L131
	L142	L111	L141
	W173	W142	W172

* Residues are listed based on sequence homology to SIVmac239 Nef

CHAPTER V: Discussion

HIV and its orthologous counterpart SIV encode a limited number of proteins but it is becoming more apparent that each protein engages in a number of activities that collectively enhance viral fitness in the infected host. For naturally infected nonhuman primates, viral fitness equates to commensal survival whereas in human hosts it leads to rampant viral production and increased susceptibility to fatal outcome. Recently, Schindler et al. suggested that downregulation of the T cell receptor was a prominent feature of nonpathogenic SIV infection and that the capability of the viral accessory protein Nef to suppress T cell activation was lost during the zoonotic transfer of SIV to HIV-1 (Schindler et al., 2006). This thesis was directed towards enhancing our knowledge of the interaction of Nef with the T cell receptor ζ subunit, elucidating the lentiviral type-dependency on the interaction and to exploring its potential effects on T cell activation.

Conservation of TCRζ binding

Stimulation through the T cell receptor by exogenous stimuli results in TCR downregulation as part of the normal T cell response. SIV hijacked this feature of the T cell activation pathway through the viral accessory protein Nef that catalyzes TCR downregulation through the cooperative binding of the clathrin associated protein AP-2 and TCRζ, a function not shared by HIV-1 Nef. Chapter II demonstrated that HIV-1 Nef binds to the cytoplasmic domain of TCRζ despite its inability to downregulate TCR

surface expression in T cells and that the binding activity was mediated by the core domain that is highly conserved among HIV-1, HIV-2 and SIV isolates. However, HIV-1 Nef_{core} only bound an ITAM 1 region on TCRζ and with the lowest calculated affinity among the Nef proteins. HIV-2 and SIV Nef bound to the same ITAM 1 region but also bound a second site on TCRζ containing elements of ITAM 2. Chapter IV reported the structure of the core domain of SIV Nef bound to a polypeptide spanning the shared ITAM 1-binding site on TCRζ and revealed that the binding interface on Nef specific to TCRζ lies on a well-conserved face of the Nef protein (Figure V-1). This provides the structural basis for the conservation of TCRζ-binding by HIV-1, HIV-2 and SIV Nef. Furthermore the structural features on Nef and TCRζ revealed to form a novel interaction surface not shared by Nef's other binding partners. Therefore, guided by the structure, mutagenesis experiments can now be performed to further understand the fine details of the Nef-TCRζ interaction and to provide further insight into the observed differences in affinity and specificity observed for HIV-1 and SIV Nef.

The retention of TCRζ-binding ability by HIV-1 Nef, despite its lost ability to downregulate the TCR, suggests that Nef likely mediates other functions at the TCR outside its downregulation. The most attractive activity would be modulation of TCR-mediated T cell activation which HIV-1 Nef has been reported to have varying effects on (Table I-2). In addition, highly pathogenic variants of SIV Nef carrying ITAM-like sequences have been demonstrated to have significant effects on T cell activation and virulence presumably through its association with components of the T cell signaling

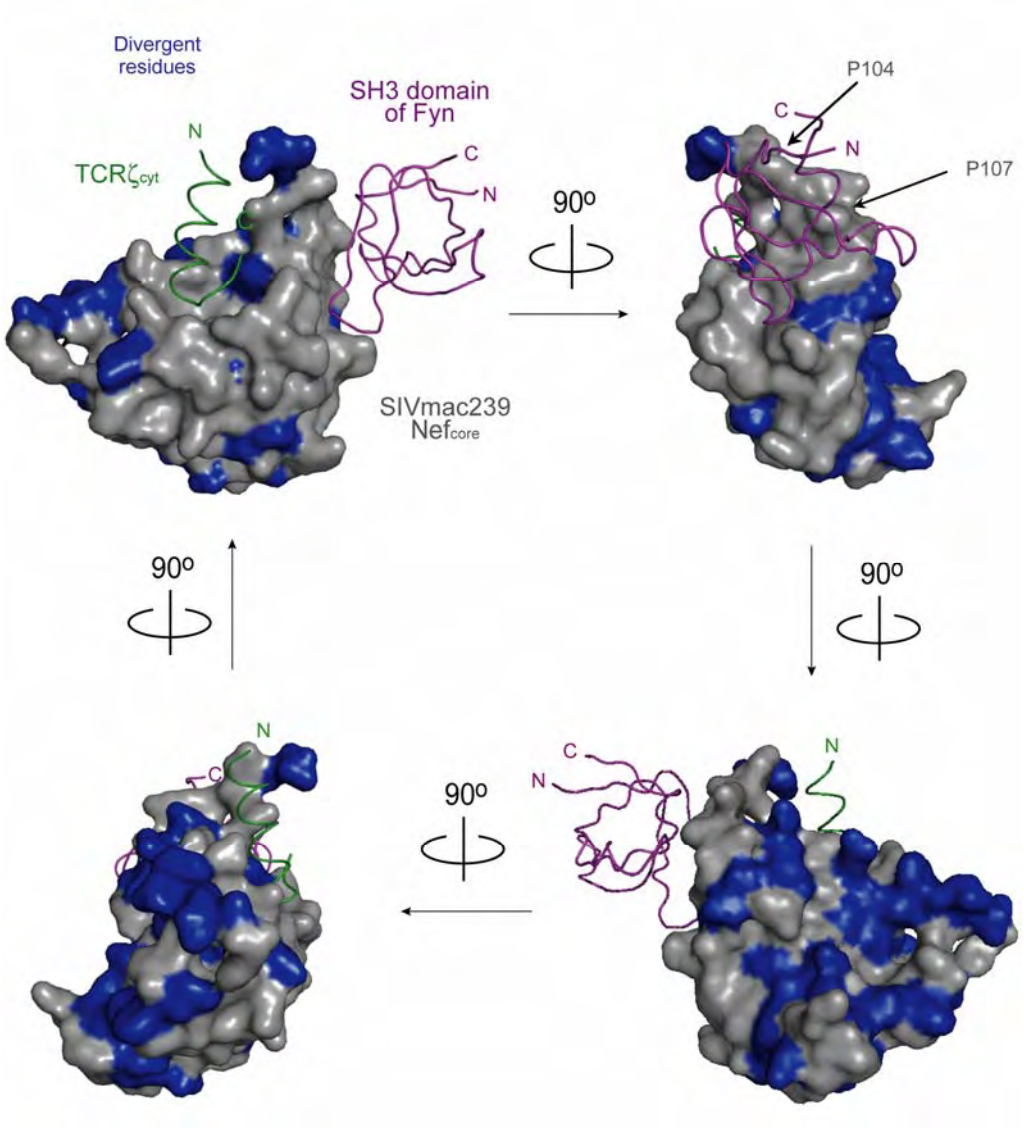

Figure V-1. Conservation in the TCRζ and SH3 domain binding interface on Nef. Surface representation of SIVmac239 Nef_{core}. Divergent residues not conserved among HIV-1, HIV-2 and SIV Nef are shaded blue. TCRζ (green) and the SH3 domain of Fyn (purple) are shown in ribbon diagram. Residues P104 and P107 (of the PxxP motif) are denoted by arrow.

machinery (Dehghani et al., 2002; Hodge et al., 1998; Lafont et al., 2003; Luo and Peterlin, 1997; Xu et al., 1999).Whether HIV-1 Nef may also affect T cell signaling in a similar role is unclear but it is evident that SIV and HIV-1 Nef not only share sequence conservation, but more structural and functional conservation than previously thought.

Crystal Twinning and Structure Determination

Structure determination of protein-protein complexes provides unique insight into the fine details that determine the specificity of an interaction. However, complications with crystallization and structure determination can occur and are often detrimental. In Chapter III, the methods employed to determine the high and low resolution structures of the core domain of SIVmac239 Nef in complex with two different length TCRζ polypeptides are described. The structure determination of the high resolution structure was complicated by the presence of twinning in the crystal that was likely caused by the use of a truncated polypeptide ligand. However, systematic analysis of the x-ray diffraction data and identification of pseudo-merohedral twinning allowed for the determination of the structure of the SIVmac239 Nef_{core}-$TCR\zeta_{cyt}$ complex to 2.05 Å resolution. Although crystal twinning has generally been considered a crystal pathology, the twinning caused by the fortuitous reduction in symmetry of tetragonal crystal form to an orthorhombic form likely played a role in the significantly enhanced resolution of the diffraction data as has been suggested for other cases (Yeates, 1997). Therefore, crystal twinning can be of benefit towards structure determination and should not be equated

with poor data quality. This work highlights the significant advances in crystallographic structure determination methods and provides a unique case of “twinning gone good”.

The role of Nef-TCRζ complex formation on Src PTK activiity

The ζ subunit of T cell receptor serves as the primary mediator of signal propagation at the cell membrane. Therefore, the formation of a Nef-TCRζ complex has multiple implications ranging from activating the T cell signaling pathway through the recruitment Src PTKs to inhibiting the T signaling pathway by sequestering ITAM tyrosines important for activation. The structure of SIVmac239 Nef_{core} in complex with the ITAM 1 YxxL/I motif-containing TCRζ polypeptide described in Chapter IV suggests that both scenarios are conceivable and could lead to differential modulation of T cell activation. Based on the surprising ordering of the N-terminus of Nef into a PPII helix known to confer specificity to SH3 domains found in Src family kinases, a model for the ternary complex of Nef, TCRζ and a Src family kinase (i.e. Lck) as it exists at the cell membrane is presented (Figure V-2). The binding interface on Nef for TCRζ and the SH3 domain do not overlap and are accommodated by a single Nef molecule. In addition, the binding surfaces for TCRζ and the SH3 domain are well conserved among the Nef proteins from HIV-1, HIV-2 and SIV (Figure V-1) suggesting that the formation of a Nef-TCRζ-Src PTK complex is expected to be a conserved property of Nef proteins from all lentiviral subtypes. However, the order and kinetics of complex formation exhibited by Nef from HIV-1, HIV-2 and SIV both *in vitro* and in T cells is unknown. A simplified model of Nef’s activity on TCRζ is presented Figure V-3.

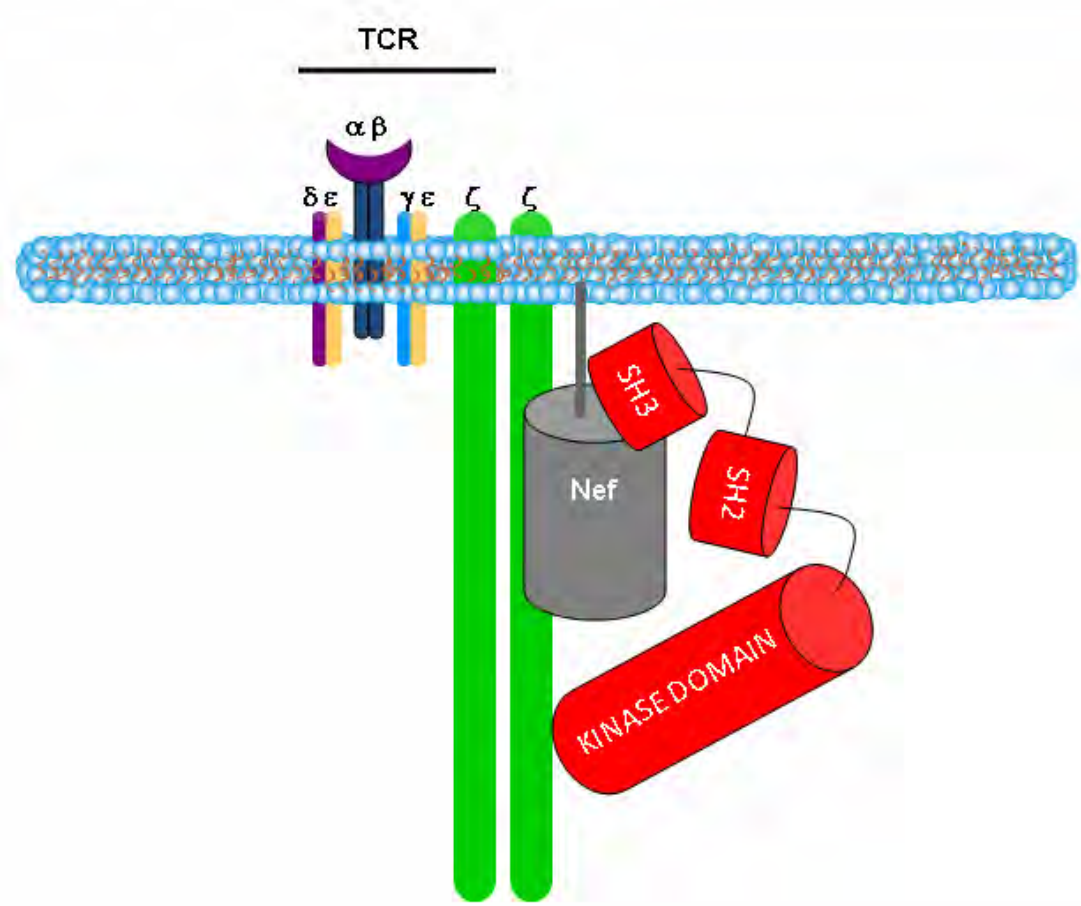

Figure V-2. Model of the Nef-TCRζ-Src PTK ternary complex at the cell membrane. Nef (grey), TCRζ polypeptide (green) and Src PTK (red) are represented in cartoon format oriented with their N-termini facing the inner leaflet of the cell membrane.

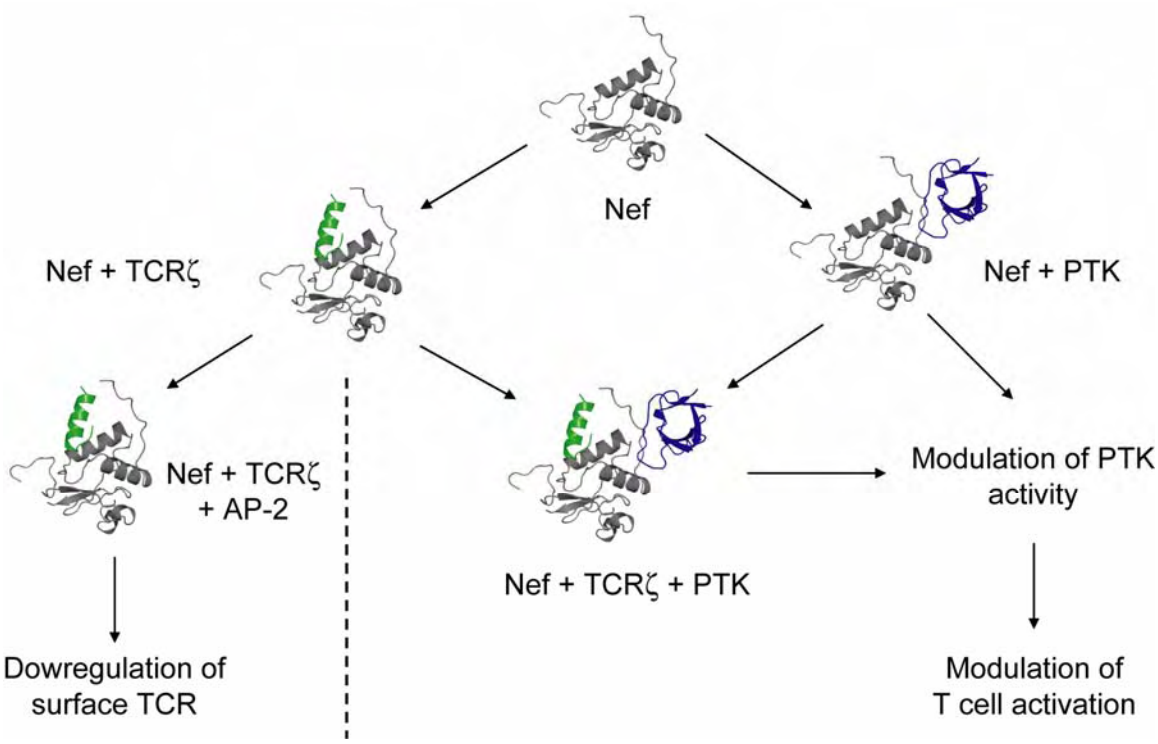

Figure V-3. Model of Nef activity on TCRζ. Successive steps in complex formation leading to downregulation and modulation of T cell activation are shown. All of the binding events occur at the cell membrane. Nef (grey), TCRζ (green) and Src PTK SH3 domain (blue) are represented in ribbon diagram.

In the model, Nef is able to first bind the SH3 domain of Src PTKs or TCRζ. By binding Src PTKs, Nef may either have a direct effect on PTK activity (right) a substrate other than TCRζ. Alternatively, binding of Src PTKs may order the N-terminal PxxP loop into a PPII helix thus ordering the Nef-PTK complex into a TCRζ-receptive conformation. This results in the cooperative binding of TCRζ and ternary complex formation. Rapid phosphorylation of TCRζ ensues leading to modulation of T cell activation. Depending on the phosphorylated state of TCRζ, T cell activation could be enhanced or inhibited.

Alternatively, Nef could start the binding cascade by binding TCRζ. TCRζ would then order the PxxP motif on Nef into a PPII helix. The now PTK-receptive form of the Nef-TCRζ complex would bind a Src PTK in a cooperative manner (middle), release the kinase domain from its auto-inhibited state and induce phosphorylation of the bound TCRζ. As with the previously described binding cascade, T cell activation could be augmented or suppressed. For SIV and HIV-2 Nef, binding of TCRζ can also lead to the formation for an AP-2 binding surface that recruits AP-2 for downregulation of the TCR (left).

This model provides the foundation for a new avenue of investigation into Nef's effect on T cell activation. In this model, the formation of the Nef-TCRζ-PTK ternary complex is essential to Nef's function. By selectively investigating each component of the complex and the interactions that mediate complex formation, we can begin to elucidate the functional importance of the Nef-TCRζ-PTK complex. Furthermore, by

understanding the mechanisms of complex formation, comparative studies of SIV, HIV-2 and HIV-1 Nef can be performed to gain insight into the host effect that may influence Nef's TCRζ-specific and Src PTK-specific effects.

Nef has been demonstrated to participate in a number of activities that may not be easily dissected. However, the ability of Nef to impart a number of mechanistic perturbations in an infected cell may comprise its overall regulatory function. Through the enchancement or suppression of specific signaling pathways in a T cell, Nef may shift the homeostatic balance from with the T cell intracellular environment from one that is deleterious to viral infection to one that is permissible to enhanced viral replication. For example, the enhancement of Fyn activity on TCRζ by Nef may result in the augmentation of Fyn-mediated T cell signaling pathways that are distinct from Lck-mediated pathways (reviewed in (Palacios and Weiss, 2004; Salmond et al., 2009)) and may provide an "active" environment for viral fitness but not necessarily for T cell function. Clearly, Nef's effects in a T cell are multifaceted and collectively participate in viral survival. Therefore, continued detailed investigation of the molecular mechanisms of Nef activity such as that presented here for the Nef-TCRζ interaction will need to be performed. In addition, by understanding Nef's perturbation of normal T cell activity, insight into normal T cell processes will be gained.

Future Directions

The in vitro evidence of the ability of select HIV-1 Nef variants to bind TCRζ and in a specificity/affinity profile unique to the HIV-1 Nef variants studied raises the question of

whether Nef proteins from all HIV-1 clades are able to bind TCRζ in a specific manner. Preliminary sequence analysis of Nef proteins from various HIV-1 clades suggests that the binding determinants on Nef are highly conserved, but detailed biochemical studies should be pursued with both full-length and core domain Nef proteins to confirm the universal specificity of the Nef-TCRζ interaction and more importantly, correlate those binding results with functional outcome. Furthermore, the binding experiments described here were predominately performed with core domain protein constructs. Therefore, these experiments should be extended to the full length proteins to determine if there are any effects of the N-terminal domain on binding activity.

The crystal structure of the complex of the core domain of SIVmac239 Nef with the first YxxL motif in ITAM1 of TCRζ revealed that a salt bridge and hydrophobic pocket were the primary structural determinants that mediated the interaction of Nef with TCRζ. In order to confirm these findings, mutational analyses should be performed by substituting the residues on Nef involved in the salt bridge (R137, R138) to either non-charged (A137, A138) or negatively charged residues (E137, E138) and observe the effects on binding. In addition, point mutations could be introduced in the hydrophobic pocket as well as the YxxL motif tyrosine residue in ITAM 1 to determine the functional significance of those interacting residues. Furthermore, the residues involved in the interaction of Nef with TCRζ that are not conserved among SIV and HIV-1 could be re-introduced into the lower-affinity HIV-1 Nef protein to identify the primary residues that determine SIV Nef's higher affinity for TCRζ. One other major feature of the interaction of SIV and HIV-2 Nef with TCRζ is the dual site specificity that was not observed for

HIV-1 Nef. Therefore, as an extension of the mutagenesis studies in HIV-1 Nef, the residues that confer dual site-specificity in HIV-2 and SIV Nef may be identified. Collectively, these mutation studies would 1) confirm the relevance of the residues involved in the SIV Nef-TCRζ interaction, 2) determine the residues that confer increased affinity for TCRζ and 3) identify the residues that determine Nef's ability to bind to two unique YxxL motifs on TCRζ.

Since the structure of the Nef-TCRζ polypeptide complex only involved the first ITAM YxxL motif where SIV Nef was shown to bind to two unique regions, little is known about whether the same binding site on Nef is shared by the two regions on TCRζ. Based on sequence analysis, we have extrapolated that Nef shares the same binding site for TCRζ's two binding regions, but this has not been experimentally explored. Therefore, simple mutagenesis/binding studies can be performed to determine the specificity of Nef for each region. However, the crystal structure of the complex of SIV Nef with the second binding site found on ITAM 2 should be determined to confirm that one binding site on Nef binds to both TCRζ binding regions but to also identify if the alpha helix is also present in the second ITAM region. These results would not only highlight the significance of the TCRζ-binding site on Nef, but additionally provide insight into TCRζ's structural components.

The primary focus of these studies has been to explore the interaction of Nef with TCRζ and determine its functional role during infection. Comments on the functional outcome of the interaction have been primarily a literature survey and require further

attention. With the determined binding parameters and structure of the Nef-TCRζ complex, a number of experiments can be performed in T cells to determine if this specific interaction is vital to viral fitness and more importantly, if we are more enabled to perturb its enhancement of viral survival. In the preliminary experiments, the effect of the Nef proteins used in this studiy on T cell activation should be explored through transfection experiments of Nef constructs and observation of Nef's effects on TCR downregulation as well as T-cell activation in the presence of an exogenous stimulus. Introduction of the mutated proteins described above should further determine the functional importance of the interaction and if abrogation of binding has a negative impact on viral replication. Functional outcomes, including membrane-proximal T cell signaling events (i.e. TCRζ, Lck, Fyn, ERK, PLC-γ phosphorylation) and late activation markers (i.e. IL-2 transcription, secretion), should be monitored to determine Nef's effects early and late in the signaling pathway. Another approach to determine the functional importance of the Nef- TCRζ interaction is to develop novel chemical inhibitors that exploit the structural determinants of the Nef-TCRζ interaction. As observed the crystal structure, the primary binding motifs include a salt bridge and hydrophobic pocket on Nef. Therefore, chemical libraries and rational drug design efforts could be applied to invent inhibitors that could be used in binding studies, functional studies in cells as well as potential therapeutics in animal models and human trials. Nef's effect on T cell activation is expected to be complicated by its numerous effects on its various binding partners, however careful analysis and segregation of the TCRζ-specific effects will provide invaluable insight.

APPENDIX

A.1. Protein sequence inventory

A.2. DNA sequence inventory

A.3. Primer inventory

A.1. Protein Sequence Inventory

Nef (HIV-1; ARV2/SF2; Accession# P03407) fl [M1-C210]

MGGKWSKRSMGGWSAIRERMRRAEPRAEPAADGVGAVSRDLEKHGAITSSNTAATNADCAWLEAQEEEEVG
FPVRPQVPLRPMTYKAALDISHFLKEKGGLEGLIWSQRRQEILDLWIYHTQGYFPDWQNYTPGPGIRYPLT
FGWCFKLVPVEPEKVEEANEGENNSLLHPMSLHGMEDAEKEVLVWRFDSKLAFHHMARELHPEYYKDC

Nef (HIV-1; ARV2/SF2; Accession# P03407) AL [K4-C210]

GSKWSKRSMGGWSAIRERMRRAEPRAEPAADGVGAVSRDLEKHGAITSSNTAATNADCAWLEAQEEEEVGF
PVRPQVPLRPMTYKAALDISHFLKEKGGLEGLIWSQRRQEILDLWIYHTQGYFPDWQNYTPGPGIRYPLTF
GWCFKLVPVEPEKVEEANEGENNSLLHPMSLHGMEDAEKEVLVWRFDSKLAFHHMARELHPEYYKDC

Nef (HIV-1; ARV2/SF2; Accession# P03407) AS [A60-C210]

GSAWLEAQEEEEVGFPVRPQVPLRPMTYKAALDISHFLKEKGGLEGLIWSQRRQEILDLWIYHTQGYFPDW
QNYTPGPGIRYPLTFGWCFKLVPVEPEKVEEANEGENNSLLHPMSLHGMEDAEKEVLVWRFDSKLAFHHMA
RELHPEYYKDC

Nef (HIV-1; Consensus; Accession# AAA03700) fl [M1-C206]

MGGKWSKRSVSGWPAVRERMRRAEPAAEGVGAVSRDLEKHGAITSSNTAATNAACAWLEAQEEEEVGFPVR
PQVPLRPMTYKAAVDLSHFLKEKGGLEGLIYSQKRQDILDLWVYHTQGYFPDWQNYTPGPGIRYPLTFGWC
FKLVPVEPEKVEEANEGENNCLLHPMSQHGMDDPEKEVLVWKFDSKLAFHHMARELHPEYYKDC

Nef (HIV-1; Consensus; Accession# AAA03700) CL [K4-C206]

GSKWSKRSVSGWPAVRERMRRAEPAAEGVGAVSRDLEKHGAITSSNTAATNAACAWLEAQEEEEVGFPVRP
QVPLRPMTYKAAVDLSHFLKEKGGLEGLIYSQKRQDILDLWVYHTQGYFPDWQNYTPGPGIRYPLTFGWCF
KLVPVEPEKVEEANEGENNCLLHPMSQHGMDDPEKEVLVWKFDSKLAFHHMARELHPEYYKDC

Nef (HIV-1; Consensus; Accession# AAA03700) CS [A56-C206]

GSAWLEAQEEEEVGFPVRPQVPLRPMTYKAAVDLSHFLKEKGGLEGLIYSQKRQDILDLWVYHTQGYFPDW
QNYTPGPGIRYPLTFGWCFKLVPVEPEKVEEANEGENNCLLHPMSQHGMDDPEKEVLVWKFDSKLAFHHMA
RELHPEYYKDC

Nef (HIV-1; ELI; Accession# P04604) fl [M1-N206]

MGGKWSKSSIVGWPAIRERIRRTNPAADGVGAVSRDLEKHGAITSSNTASTNADCAWLEAQEESDEVGFPV
RPQVPLRPMTYKEALDLSHFLKEKGGLEGLIWSKKRQEILDLWVYNTQGIFPDWQNYTPGPGIRYPLTFGW
CYELVPVDPQEVEEDTEGETNSLLHPICQHGMEDPERQVLKWRFNSRLAFEHKAREMHPEFYKN

Nef (HIV-1; ELI; Accession# P04604) EL [K4-N206]

GSKWSKSSIVGWPAIRERIRRTNPAADGVGAVSRDLEKHGAITSSNTASTNADCAWLEAQEESDEVGFPVR
PQVPLRPMTYKEALDLSHFLKEKGGLEGLIWSKKRQEILDLWVYNTQGIFPDWQNYTPGPGIRYPLTFGWC
YELVPVDPQEVEEDTEGETNSLLHPICQHGMEDPERQVLKWRFNSRLAFEHKAREMHPEFYKN

Nef (HIV-1; ELI; Accession# P04604) ES [A56-N206]

GSAWLEAQEESDEVGFPVRPQVPLRPMTYKEALDLSHFLKEKGGLEGLIWSKKRQEILDLWVYNTQGIFPD
WQNYTPGPGIRYPLTFGWCYELVPVDPQEVEEDTEGETNSLLHPICQHGMEDPERQVLKWRFNSRLAFEHK
AREMHPEFYKN

Nef (HIV-1; LAI; Accession# Q9QPN3) fl [M1-C206]

MGGKWSKSSVVGWPTVRERMRRAEPAADGVGAASRDLEKHGAITSSNTAATNAACAWLEAQEEEEVGFPVT
PQVPLRPMTYKAAVDLSHFLKEKGGLEGLIHSQRRQDILDLWIYHTQGYFPDWQNYTPGPGVRYPLTFGWC
YKLVPVEPDKVEEANKGENTSLLHPVSLHGMDDPEREVLEWRFDSRLAFHHVARELHPEYFKNC

Nef (HIV-1; LAI; Accession# Q9QPN3) LL [K4-C206]

GSKWSKSSVVGWPTVRERMRRAEPAADGVGAASRDLEKHGAITSSNTAATNAACAWLEAQEEEEVGFPVTP
QVPLRPMTYKAAVDLSHFLKEKGGLEGLIHSQRRQDILDLWIYHTQGYFPDWQNYTPGPGVRYPLTFGWCY
KLVPVEPDKVEEANKGENTSLLHPVSLHGMDDPEREVLEWRFDSRLAFHHVARELHPEYFKNC

Nef (HIV-1; LAI; Accession# Q9QPN3) LS [A56-C206]

GSAWLEAQEEEEVGFPVTPQVPLRPMTYKAAVDLSHFLKEKGGLEGLIHSQRRQDILDLWIYHTQGYFPDW
QNYTPGPGVRYPLTFGWCYKLVPVEPDKVEEANKGENTSLLHPVSLHGMDDPEREVLEWRFDSRLAFHHVA
RELHPEYFKNC

Nef (HIV-1; NL4-3; Accession# AAK08490) fl [M1-C206]

MGGKWSKSSVIGWPAVRERMRRAEPAADGVGAVSRDLEKHGAITSSNTAANNAACAWLEAQEEEEVGFPVT
PQVPLRPMTYKAAVDLSHFLKEKGGLEGLIHSQRRQDILDLWIYHTQGYFPDWQNYTPGPGVRYPLTFGWC
YKLVPVEPDKVEEANKGENTSLLHPVSLHGMDDPEREVLEWRFDSRLAFHHVARELHPEYFKNC

Nef (HIV-1; NL4-3; Accession# AAK08490) NL [K4-C206]

GSKWSKSSVIGWPAVRERMRRAEPAADGVGAVSRDLEKHGAITSSNTAANNAACAWLEAQEEEEVGFPVTP
QVPLRPMTYKAAVDLSHFLKEKGGLEGLIHSQRRQDILDLWIYHTQGYFPDWQNYTPGPGVRYPLTFGWCY
KLVPVEPDKVEEANKGENTSLLHPVSLHGMDDPEREVLEWRFDSRLAFHHVARELHPEYFKNC

Nef (HIV-1; NL4-3; Accession# AAK08490) NS [A56-C206]

GSAWLEAQEEEEVGFPVTPQVPLRPMTYKAAVDLSHFLKEKGGLEGLIHSQRRQDILDLWIYHTQGYFPDW
QNYTPGPGVRYPLTFGWCYKLVPVEPDKVEEANKGENTSLLHPVSLHGMDDPEREVLEWRFDSRLAFHHVA
RELHPEYFKNC

Nef (HIV-2; ST; Accession# AAB01359) fl [M1-S255]

MGASGSKKRSEPSRGLRERLLQTPGEASGGHWDKLGGEYLQSQEGSGRGQKSPSCEGRRYQQGDFMNTPWR
APAEGEKGSYKQQNMDDVDSDDDDLVGVPVTPRVPLREMTYRLARDMSHLIKEKGGLEGLYYSDRRRRVLD
IYLEKEEGIIGDWQNYTHGPGVRYPKFFGWLWKLVPVDVPQEGDDSETHCLVHPAQTSRFDDPHGETLVWR
FDPTLAFSYEAFIRYPEEFGYKSGLPEDEWKARLKARGIPFS

Nef (HIV-2; ST; Accession# AAB01359) HL [S4-S255]

GSSGSKKRSEPSRGLRERLLQTPGEASGGHWDKLGGEYLQSQEGSGRGQKSPSCEGRRYQQGDFMNTPWRA
PAEGEKGSYKQQNMDDVDSDDDDLVGVPVTPRVPLREMTYRLARDMSHLIKEKGGLEGLYYSDRRRRVLDI
YLEKEEGIIGDWQNYTHGPGVRYPKFFGWLWKLVPVDVPQEGDDSETHCLVHPAQTSRFDDPHGETLVWRF
DPTLAFSYEAFIRYPEEFGYKSGLPEDEWKARLKARGIPFS

Nef (HIV-2; ST; Accession# AAB01359) HS [D94-Y234]

GSDDLVGVPVTPRVPLREMTYRLARDMSHLIKEKGGLEGLYYSDRRRRVLDIYLEKEEGIIGDWQNYTHGP
GVRYPKFFGWLWKLVPVDVPQEGDDSETHCLVHPAQTSRFDDPHGETLVWRFDPTLAFSYEAFIRYPEEFG
Y

Nef (SIV; mac239; Accession# AAU14056) fl [M1-R263]

MGGAISMRRSRPSGDLRQRLLRARGETYGRLLGEVEDGYSQSPGGLDKGLSSLSCEGQKYNQGQYMNTPWR
NPAEEREKLAYRKQNMDDIDEEDDDLVGVSVRPKVPLRTMSYKLAIDMSHFIKEKGGLEGIYYSARRHRIL
DIYLEKEEGIIPDWQDYTSGPGIRYPKTFGWLWKLVPVNVSDEAQEDEEHYLMHPAQTSQWDDPWGEVLAW
KFDPTLAYTYEAYVRYPEEFGSKSGLSEEEVRRRLTARGLLNMADKKETR

Nef (SIV; mac239; Accession# AAU14056) SL [A4-R263]

GSAISMRRSRPSGDLRQRLLRARGETYGRLLGEVEDGYSQSPGGLDKGLSSLSCEGQKYNQGQYMNTPWRN
PAEEREKLAYRKQNMDDIDEEDDDLVGVSVRPKVPLRTMSYKLAIDMSHFIKEKGGLEGIYYSARRHRILD
IYLEKEEGIIPDWQDYTSGPGIRYPKTFGWLWKLVPVNVSDEAQEDEEHYLMHPAQTSQWDDPWGEVLAWK
FDPTLAYTYEAYVRYPEEFGSKSGLSEEEVRRRLTARGLLNMADKKETR

Nef (SIV; mac239; Accession# AAU14056) SS [D95-S235]

GSDDLVGVSVRPKVPLRTMSYKLAIDMSHFIKEKGGLEGIYYSARRHRILDIYLEKEEGIIPDWQDYTSGP
GIRYPKTFGWLWKLVPVNVSDEAQEDEEHYLMHPAQTSQWDDPWGEVLAWKFDPTLAYTYEAYVRYPEEFG
S

A.2. DNA Inventory

A. pEGFP-N1

GAATTC *(EcoRI)*
GGATCC *(BamHI)*

TAGTTATTAA TAGTAATCAA TTACGGGGTC ATTAGTTCAT AGCCCATATA TGGAGTTCCG
CGTTACATAA CTTACGGTAA ATGGCCCGCC TGGCTGACCG CCCAACGACC CCCGCCCATT
GACGTCAATA ATGACGTATG TTCCCATAGT AACGCCAATA GGGACTTTCC ATTGACGTCA
ATGGGTGGAG TATTTACGGT AAACTGCCCA CTTGGCAGTA CATCAAGTGT ATCATATGCC
AAGTACGCCC CCTATTGACG TCAATGACGG TAAATGGCCC GCCTGGCATT ATGCCCAGTA
CATGACCTTA TGGGACTTTC CTACTTGGCA GTACATCTAC GTATTAGTCA TCGCTATTAC
CATGGTGATG CGGTTTTGGC AGTACATCAA TGGGCGTGGA TAGCGGTTTG ACTCACGGGG
ATTTCCAAGT CTCCACCCCA TTGACGTCAA TGGGAGTTTG TTTTGGCACC AAAATCAACG
GGACTTTCCA AAATGTCGTA ACAACTCCGC CCCATTGACG CAAATGGGCG GTAGGCGTGT
ACGGTGGGAG GTCTATATAA GCAGAGCTGG TTTAGTGAAC CGTCAGATCC GCTAGCGCTA WMK55
CCGGACTCAG ATCTCGAGCT CAAGCTTCG

AATTCTGCAGTCGACGGTACCGCGGGCCCGG

GATCCACCGG TCGCCACCAT GGTGAGCAAG GGCGAGGAGC TGTTCACCGG GGTGGTGCCC WMK56
ATCCTGGTCG AGCTGGACGG CGACGTAAAC GGCCACAAGT TCAGCGTGTC CGGCGAGGGC
GAGGGCGATG CCACCTACGG CAAGCTGACC CTGAAGTTCA TCTGCACCAC CGGCAAGCTG
CCCGTGCCCT GGCCCACCCT CGTGACCACC CTGACCTACG GCGTGCAGTG CTTCAGCCGC
TACCCCGACC ACATGAAGCA GCACGACTTC TTCAAGTCCG CCATGCCCGA AGGCTACGTC
CAGGAGCGCA CCATCTTCTT CAAGGACGAC GGCAACTACA AGACCCGCGC CGAGGTGAAG
TTCGAGGGCG ACACCCTGGT GAACCGCATC GAGCTGAAGG GCATCGACTT CAAGGAGGAC
GGCAACATCC TGGGGCACAA GCTGGAGTAC AACTACAACA GCCACAACGT CTATATCATG
GCCGACAAGC AGAAGAACGG CATCAAGGTG AACTTCAAGA TCCGCCACAA CATCGAGGAC
GGCAGCGTGC AGCTCGCCGA CCACTACCAG CAGAACACCC CCATCGGCGA CGGCCCCGTG
CTGCTGCCCG ACAACCACTA CCTGAGCACC CAGTCCGCCC TGAGCAAAGA CCCCAACGAG
AAGCGCGATC ACATGGTCCT GCTGGAGTTC GTGACCGCCG CCGGGATCAC TCTCGGCATG
GACGAGCTGT ACAAGTAAAG CGGCCGCGAC TCTAGATCAT AATCAGCCAT ACCACATTTG
TAGAGGTTTT ACTTGCTTTA AAAAACCTCC CACACCTCCC CCTGAACCTG AAACATAAAA
TGAATGCAAT TGTTGTTGTT AACTTGTTTA TTGCAGCTTA TAATGGTTAC AAATAAAGCA
ATAGCATCAC AAATTTCACA AATAAAGCAT TTTTTTCACT GCATTCTAGT TGTGGTTTGT
CCAAACTCAT CAATGTATCT TAAGGCGTAA ATTGTAAGCG TTAATATTTT GTTAAAATTC
GCGTTAAATT TTTGTTAAAT CAGCTCATTT TTTAACCAAT AGGCCGAAAT CGGCAAAATC
CCTTATAAAT CAAAAGAATA GACCGAGATA GGGTTGAGTG TTGTTCCAGT TTGGAACAAG
AGTCCACTAT TAAAGAACGT GGACTCCAAC GTCAAAGGGC GAAAAACCGT CTATCAGGGC
GATGGCCCAC TACGTGAACC ATCACCCTAA TCAAGTTTTT TGGGGTCGAG GTGCCGTAAA
GCACTAAATC GGAACCCTAA AGGGAGCCCC CGATTTAGAG CTTGACGGGG AAAGCCGGCG
AACGTGGCGA GAAAGGAAGG GAAGAAAGCG AAAGGAGCGG GCGCTAGGGC GCTGGCAAGT
GTAGCGGTCA CGCTGCGCGT AACCACCACA CCCGCCGCGC TTAATGCGCC GCTACAGGGC
GCGTCAGGTG GCACTTTTCG GGGAAATGTG CGCGGAACCC CTATTTGTTT ATTTTTCTAA
ATACATTCAA ATATGTATCC GCTCATGAGA CAATAACCCT GATAAATGCT TCAATAATAT
TGAAAAAGGA AGAGTCCTGA GGCGGAAAGA ACCAGCTGTG GAATGTGTGT CAGTTAGGGT
GTGGAAAGTC CCCAGGCTCC CCAGCAGGCA GAAGTATGCA AAGCATGCAT CTCAATTAGT
CAGCAACCAG GTGTGGAAAG TCCCCAGGCT CCCCAGCAGG CAGAAGTATG CAAAGCATGC
ATCTCAATTA GTCAGCAACC ATAGTCCCGC CCCTAACTCC GCCCATCCCG CCCCTAACTC
CGCCCAGTTC CGCCCATTCT CCGCCCCATG GCTGACTAAT TTTTTTTATT TATGCAGAGG
CCGAGGCCGC CTCGGCCTCT GAGCTATTCC AGAAGTAGTG AGGAGGCTTT TTTGGAGGCC

TAGGCTTTTG CAAAGATCGA TCAAGAGACA GGATGAGGAT CGTTTCGCAT GATTGAACAA
GATGGATTGC ACGCAGGTTC TCCGGCCGCT TGGGTGGAGA GGCTATTCGG CTATGACTGG
GCACAACAGA CAATCGGCTG CTCTGATGCC GCCGTGTTCC GGCTGTCAGC GCAGGGGCGC
CCGGTTCTTT TTGTCAAGAC CGACCTGTCC GGTGCCCTGA ATGAACTGCA AGACGAGGCA
GCGCGGCTAT CGTGGCTGGC CACGACGGGC GTTCCTTGCG CAGCTGTGCT CGACGTTGTC
ACTGAAGCGG GAAGGGACTG GCTGCTATTG GGCGAAGTGC CGGGGCAGGA TCTCCTGTCA
TCTCACCTTG CTCCTGCCGA GAAAGTATCC ATCATGGCTG ATGCAATGCG GCGGCTGCAT
ACGCTTGATC CGGCTACCTG CCCATTCGAC CACCAAGCGA AACATCGCAT CGAGCGAGCA
CGTACTCGGA TGGAAGCCGG TCTTGTCGAT CAGGATGATC TGGACGAAGA GCATCAGGGG
CTCGCGCCAG CCGAACTGTT CGCCAGGCTC AAGGCGAGCA TGCCCGACGG CGAGGATCTC
GTCGTGACCC ATGGCGATGC CTGCTTGCCG AATATCATGG TGGAAAATGG CCGCTTTTCT
GGATTCATCG ACTGTGGCCG GCTGGGTGTG GCGGACCGCT ATCAGGACAT AGCGTTGGCT
ACCCGTGATA TTGCTGAAGA GCTTGGCGGC GAATGGGCTG ACCGCTTCCT CGTGCTTTAC
GGTATCGCCG CTCCCGATTC GCAGCGCATC GCCTTCTATC GCCTTCTTGA CGAGTTCTTC
TGAGCGGGAC TCTGGGGTTC GAAATGACCG ACCAAGCGAC GCCCAACCTG CCATCACGAG
ATTTCGATTC CACCGCCGCC TTCTATGAAA GGTTGGGCTT CGGAATCGTT TTCCGGGACG
CCGGCTGGAT GATCCTCCAG CGCGGGGATC TCATGCTGGA GTTCTTCGCC CACCCTAGGG
GGAGGCTAAC TGAAACACGG AAGGAGACAA TACCGGAAGG AACCCGCGCT ATGACGGCAA
TAAAAAGACA GAATAAAACG CACGGTGTTG GGTCGTTTGT TCATAAACGC GGGGTTCGGT
CCCAGGGCTG GCACTCTGTC GATACCCCAC CGAGACCCCA TTGGGGCCAA TACGCCCGCG
TTTCTTCCTT TTCCCCACCC CACCCCCCAA GTTCGGGTGA AGGCCCAGGG CTCGCAGCCA
ACGTCGGGGC GGCAGGCCCT GCCATAGCCT CAGGTTACTC ATATATACTT TAGATTGATT
TAAAACTTCA TTTTTAATTT AAAAGGATCT AGGTGAAGAT CCTTTTTGAT AATCTCATGA
CCAAAATCCC TTAACGTGAG TTTTCGTTCC ACTGAGCGTC AGACCCCGTA GAAAAGATCA
AAGGATCTTC TTGAGATCCT TTTTTTCTGC GCGTAATCTG CTGCTTGCAA ACAAAAAAAC
CACCGCTACC AGCGGTGGTT TGTTTGCCGG ATCAAGAGCT ACCAACTCTT TTTCCGAAGG
TAACTGGCTT CAGCAGAGCG CAGATACCAA ATACTGTCCT TCTAGTGTAG CCGTAGTTAG
GCCACCACTT CAAGAACTCT GTAGCACCGC CTACATACCT CGCTCTGCTA ATCCTGTTAC
CAGTGGCTGC TGCCAGTGGC GATAAGTCGT GTCTTACCGG GTTGGACTCA AGACGATAGT
TACCGGATAA GGCGCAGCGG TCGGGCTGAA CGGGGGGTTC GTGCACACAG CCCAGCTTGG
AGCGAACGAC CTACACCGAA CTGAGATACC TACAGCGTGA GCTATGAGAA AGCGCCACGC
TTCCCGAAGG GAGAAAGGCG GACAGGTATC CGGTAAGCGG CAGGGTCGGA ACAGGAGAGC
GCACGAGGGA GCTTCCAGGG GGAAACGCCT GGTATCTTTA TAGTCCTGTC GGGTTTCGCC
ACCTCTGACT TGAGCGTCGA TTTTTGTGAT GCTCGTCAGG GGGGCGGAGC CTATGGAAAA
ACGCCAGCAA CGCGGCCTTT TTACGGTTCC TGGCCTTTTG CTGGCCTTTT GCTCACATGT
TCTTTCCTGC GTTATCCCCT GATTCTGTGG ATAACCGTAT TACCGCCATG CAT

B. Nef (Full Length) / No GFP Fusion (-G)

ELI (M1-N206)

AATTCCTGGTTCCTCGTGGCAGCATGGGTGGCAAATGGTCAAAAAGTAGTATAGTGGGATGGCCTGCTATA
AGGGAAAGAATAAGAAGAACTAATCCAGCAGCAGATGGGGTAGGAGCAGTATCTCGAGACCTGGAAAAACA
TGGGGCAATCACAAGTAGCAATACAGCAAGTACTAATGCTGACTGTGCCTGGCTAGAAGCACAAGAAGAGA
GCGACGAGGTGGGCTTTCCAGTCAGACCCCAGGTACCTTTAAGACCAATGACTTACAAAGAAGCTCTAGAT
CTCAGCCACTTTTTAAAAGAAAAGGGGGGACTGGAAGGGCTAATTTGGTCCAAAAAGAGACAAGAGATCCT
TGATCTTTGGGTCTACAACACACAAGGCATCTTCCCTGATTGGCAAAACTACACACCAGGGCCAGGGATCA
GATATCCACTAACCTTTGGATGGTGCTACGAGCTAGTACCAGTTGATCCACAGGAGGTAGAAGAAGACACT
GAAGGAGAGACCAACAGCTTGTTACACCCTATATGCCAGCATGGAATGGAGGACCCGGAGAGACAAGTGTT
AAAATGGAGATTTAACAGCAGACTAGCATTTGAGCACAAGGCCCGAGAGATGCATCCGGAGTTCTACAAAA
ACTAATGAG

NL4-3 (M1-C206)

AATTCCTGGTTCCTCGTGGCAGCATGGGTGGCAAGTGGTCAAAAAGTAGTGTGATTGGATGGCCTGCTGTA
AGGGAAAGAATGAGACGAGCTGAGCCAGCAGCAGATGGGGTGGGAGCAGTATCTCGAGACCTAGAAAAACA
TGGAGCAATCACAAGTAGCAATACAGCAGCTAACAATGCTGCTTGTGCCTGGCTAGAAGCACAAGAGGAGG
AAGAGGTGGGTTTTCCAGTCACACCTCAGGTACCTTTAAGACCAATGACTTACAAGGCAGCTGTAGATCTT
AGCCACTTTTTAAAAGAAAAGGGGGGACTGGAAGGGCTAATTCACTCCCAAAGAAGACAAGATATCCTTGA
TCTGTGGATCTACCACACACAAGGCTACTTCCCTGATTGGCAGAACTACACACCAGGGCCAGGGGTCAGAT
ATCCACTGACCTTTGGATGGTGCTACAAGCTAGTACCAGTTGAGCCAGATAAGGTAGAAGAGGCCAATAAA
GGAGAGAACACCAGCTTGTTACACCCTGTGAGCCTGCATGGAATGGATGACCCTGAGAGAGAAGTGTTAGA
GTGGAGGTTTGACAGCCGCCTAGCATTTCATCACGTGGCCCGAGAGCTGCATCCGGAGTACTTCAAGAACT
GCTAATGAG

HIV-2 (M1-S255)

AATTCATGGGCGCCAGTGGCTCCAAGAAGCGTTCCGAGCCTTCGCGAGGGCTACGGGAGAGACTCTTACAA
ACGCCTGGAGAGGCTTCTGGGGGACACTGGGACAAATTGGGAGGGGAATACTTGCAGTCCCAAGAAGGATC
AGGCAGGGGGCAGAAATCACCCTCCTGTGAGGGACGGCGGTATCAACAGGGAGATTTTATGAATACCCCAT
GGAGAGCCCCAGCAGAAGGGGAGAAAGGCTCGTACAAGCAACAAAATATGGATGATGTAGATTCAGATGAT
GATGACCTAGTAGGGGTCCCTGTCACACCAAGAGTACCATTAAGAGAAATGACATATCGTTTGGCAAGAGA
TATGTCACATTTGATAAAAGAAAAGGGGGGACTGGAAGGGCTGTATTACAGTGATAGAAGACGTAGAGTGC
TAGACATATACTTAGAAAAGGAAGAGGGAATAATTGGAGACTGGCAGAACTATACTCATGGACCAGGAGTA
AGGTATCCAAAGTTCTTTGGGTGGTTATGGAAGCTAGTACCAGTAGATGTCCCACAAGAGGGAGATGACAG
TGAGACTCACTGCTTAGTGCATCCAGCACAAACAAGCAGGTTTGATGACCCGCATGGAGAAACATTAGTTT
GGAGGTTTGACCCCACGCTAGCTTTTAGCTACGAGGCCTTTATTCGATACCCAGAGGAGTTTGGGTACAAG
TCAGGCCTGCCAGAGGATGAATGGAAGGCAAGACTGAAAGCAAGAGGGATACCGTTTAGCTAATGAG

SIV (M1-R263)

AATTCATGGGCGGCGCTATTTCCATGAGGCGGTCCAGGCCGTCTGGAGATCTGCGACAGAGACTCTTGCGG
GCGCGTGGGGAGACTTATGGGAGACTCTTAGGAGAGGTGGAAGATGGATACTCGCAATCCCCAGGAGGATT
AGACAAGGGCTTGAGCTCACTCTCTTGTGAGGGACAGAAATACAATCAGGGACAGTATATGAATACTCCAT
GGAGAAACCCAGCTGAAGAGAGAGAAAAATTAGCATACAGAAAACAAAATATGGATGATATAGATGAGGAA
GATGATGACTTGGTAGGGGTATCAGTGAGGCCAAAAGTTCCCCTAAGAACAATGAGTTACAAATTGGCAAT
AGACATGTCTCATTTTATAAAAGAAAAGGGGGGACTGGAAGGGATTTATTACAGTGCAAGAAGACATAGAA
TCTTAGACATATACTTAGAAAAGGAAGAAGGCATCATACCAGATTGGCAGGATTACACCTCAGGACCAGGA
ATTAGATACCCAAAGACATTTGGCTGGCTATGGAAATTAGTCCCTGTAAATGTATCAGATGAGGCACAGGA
GGATGAGGAGCATTATTTAATGCATCCAGCTCAAACTTCCCAGTGGGATGACCCTTGGGGAGAGGTTCTAG
CATGGAAGTTTGATCCAACTCTGGCCTACACTTATGAGGCATATGTTAGATACCCAGAAGAGTTTGGAAGC
AAGTCAGGCCTGTCAGAGGAAGAGGTTAGAAGAAGGCTAACCGCAAGAGGCCTTCTTAACATGGCTGACAA
GAAGGAAACTCGCTAATGAG

C. Nef (Full Length) / GFP Fusion (+G)

ELI (M1-N206)

AATTCCTGGTTCCTCGTGGCAGCATGGGTGGCAAATGGTCAAAAAGTAGTATAGTGGGATGGCCTGCTATA
AGGGAAAGAATAAGAAGAACTAATCCAGCAGCAGATGGGGTAGGAGCAGTATCTCGAGACCTGGAAAAACA
TGGGGCAATCACAAGTAGCAATACAGCAAGTACTAATGCTGACTGTGCCTGGCTAGAAGCACAAGAAGAGA
GCGACGAGGTGGGCTTTCCAGTCAGACCCCAGGTACCTTTAAGACCAATGACTTACAAAGAAGCTCTAGAT
CTCAGCCACTTTTTAAAAGAAAAGGGGGGACTGGAAGGGCTAATTTGGTCCAAAAAGAGACAAGAGATCCT
TGATCTTTGGGTCTACAACACACAAGGCATCTTCCCTGATTGGCAAAACTACACACCAGGGCCAGGGATCA
GATATCCACTAACCTTTGGATGGTGCTACGAGCTAGTACCAGTTGATCCACAGGAGGTAGAAGAAGACACT
GAAGGAGAGACCAACAGCTTGTTACACCCTATATGCCAGCATGGAATGGAGGACCCGGAGAGACAAGTGTT
AAAATGGAGATTTAACAGCAGACTAGCATTTGAGCACAAGGCCCGAGAGATGCATCCGGAGTTCTACAAAA
AC

NL4-3 (M1-C206)

AATTCCTGGTTCCTCGTGGCAGCATGGGTGGCAAGTGGTCAAAAAGTAGTGTGATTGGATGGCCTGCTGTA
AGGGAAAGAATGAGACGAGCTGAGCCAGCAGCAGATGGGGTGGGAGCAGTATCTCGAGACCTAGAAAAACA
TGGAGCAATCACAAGTAGCAATACAGCAGCTAACAATGCTGCTTGTGCCTGGCTAGAAGCACAAGAGGAGG
AAGAGGTGGGTTTTCCAGTCACACCTCAGGTACCTTTAAGACCAATGACTTACAAGGCAGCTGTAGATCTT
AGCCACTTTTTAAAAGAAAAGGGGGGACTGGAAGGGCTAATTCACTCCCAAAGAAGACAAGATATCCTTGA
TCTGTGGATCTACCACACACAAGGCTACTTCCCTGATTGGCAGAACTACACACCAGGGCCAGGGGTCAGAT
ATCCACTGACCTTTGGATGGTGCTACAAGCTAGTACCAGTTGAGCCAGATAAGGTAGAAGAGGCCAATAAA
GGAGAGAACACCAGCTTGTTACACCCTGTGAGCCTGCATGGAATGGATGACCCTGAGAGAGAAGTGTTAGA
GTGGAGGTTTGACAGCCGCCTAGCATTTCATCACGTGGCCCGAGAGCTGCATCCGGAGTACTTCAAGAACT
GC

HIV-2 (M1-S255)

AATTCATGGGCGCCAGTGGCTCCAAGAAGCGTTCCGAGCCTTCGCGAGGGCTACGGGAGAGACTCTTACAA
ACGCCTGGAGAGGCTTCTGGGGGACACTGGGACAAATTGGGAGGGGAATACTTGCAGTCCCAAGAAGGATC
AGGCAGGGGGCAGAAATCACCCTCCTGTGAGGGACGGCGGTATCAACAGGGAGATTTTATGAATACCCCAT
GGAGAGCCCCAGCAGAAGGGGAGAAAGGCTCGTACAAGCAACAAAATATGGATGATGTAGATTCAGATGAT
GATGACCTAGTAGGGGTCCCTGTCACACCAAGAGTACCATTAAGAGAAATGACATATCGTTTGGCAAGAGA
TATGTCACATTTGATAAAAGAAAAGGGGGGACTGGAAGGGCTGTATTACAGTGATAGAAGACGTAGAGTGC
TAGACATATACTTAGAAAAGGAAGAGGGAATAATTGGAGACTGGCAGAACTATACTCATGGACCAGGAGTA
AGGTATCCAAAGTTCTTTGGGTGGTTATGGAAGCTAGTACCAGTAGATGTCCCACAAGAGGGAGATGACAG
TGAGACTCACTGCTTAGTGCATCCAGCACAAACAAGCAGGTTTGATGACCCGCATGGAGAAACATTAGTTT
GGAGGTTTGACCCCACGCTAGCTTTTAGCTACGAGGCCTTTATTCGATACCCAGAGGAGTTTGGGTACAAG
TCAGGCCTGCCAGAGGATGAATGGAAGGCAAGACTGAAAGCAAGAGGGATACCGTTTAGC

SIV (M1-R263)

AATTCATGGGCGGCGCTATTTCCATGAGGCGGTCCAGGCCGTCTGGAGATCTGCGACAGAGACTCTTGCGG
GCGCGTGGGGAGACTTATGGGAGACTCTTAGGAGAGGTGGAAGATGGATACTCGCAATCCCCAGGAGGATT
AGACAAGGGCTTGAGCTCACTCTCTTGTGAGGGACAGAAATACAATCAGGGACAGTATATGAATACTCCAT
GGAGAAACCCAGCTGAAGAGAGAGAAAAATTAGCATACAGAAAACAAAATATGGATGATATAGATGAGGAA
GATGATGACTTGGTAGGGGTATCAGTGAGGCCAAAAGTTCCCCTAAGAACAATGAGTTACAAATTGGCAAT
AGACATGTCTCATTTTATAAAAGAAAAGGGGGGACTGGAAGGGATTTATTACAGTGCAAGAAGACATAGAA
TCTTAGACATATACTTAGAAAAGGAAGAAGGCATCATACCAGATTGGCAGGATTACACCTCAGGACCAGGA
ATTAGATACCCAAAGACATTTGGCTGGCTATGGAAATTAGTCCCTGTAAATGTATCAGATGAGGCACAGGA
GGATGAGGAGCATTATTTAATGCATCCAGCTCAAACTTCCCAGTGGGATGACCCTTGGGGAGAGGTTCTAG
CATGGAAGTTTGATCCAACTCTGGCCTACACTTATGAGGCATATGTTAGATACCCAGAAGAGTTTGGAAGC
AAGTCAGGCCTGTCAGAGGAAGAGGTTAGAAGAAGGCTAACCGCAAGAGGCCTTCTTAACATGGCTGACAA
GAAGGAAACTCGC

D. Nef (Full Length) / GFP Fusion (+G) / Internal BamHI site

ELI (M1-W57.BamHI.L58-N206)

AATTCCTGGTTCCTCGTGGCAGCATGGGTGGCAAATGGTCAAAAAGTAGTATAGTGGGATGGCCTGCTATA
AGGGAAAGAATAAGAAGAACTAATCCAGCAGCAGATGGGGTAGGAGCAGTATCTCGAGACCTGGAAAAACA
TGGGGCAATCACAAGTAGCAATACAGCAAGTACTAATGCTGACTGTGCCTGGGGATCCCTAGAAGCACAAG
AAGAGAGCGACGAGGTGGGCTTTCCAGTCAGACCCCAGGTACCTTTAAGACCAATGACTTACAAAGAAGCT
CTAGATCTCAGCCACTTTTTAAAAGAAAAGGGGGGACTGGAAGGGCTAATTTGGTCCAAAAAGAGACAAGA
GATCCTTGATCTTTGGGTCTACAACACACAAGGCATCTTCCCTGATTGGCAAAACTACACACCAGGGCCAG
GGATCAGATATCCACTAACCTTTGGATGGTGCTACGAGCTAGTACCAGTTGATCCACAGGAGGTAGAAGAA
GACACTGAAGGAGAGACCAACAGCTTGTTACACCCTATATGCCAGCATGGAATGGAGGACCCGGAGAGACA
AGTGTTAAAATGGAGATTTAACAGCAGACTAGCATTTGAGCACAAGGCCCGAGAGATGCATCCGGAGTTCT
ACAAAAAC

NL4-3 (M1-W57.BamHI.L58-C206)

AATTCCTGGTTCCTCGTGGCAGCATGGGTGGCAAGTGGTCAAAAAGTAGTGTGATTGGATGGCCTGCTGTA
AGGGAAAGAATGAGACGAGCTGAGCCAGCAGCAGATGGGGTGGGAGCAGTATCTCGAGACCTAGAAAAACA
TGGAGCAATCACAAGTAGCAATACAGCAGCTAACAATGCTGCTTGTGCCTGGGGATCCCTAGAAGCACAAG
AGGAGGAAGAGGTGGGTTTTCCAGTCACACCTCAGGTACCTTTAAGACCAATGACTTACAAGGCAGCTGTA
GATCTTAGCCACTTTTTAAAAGAAAAGGGGGGACTGGAAGGGCTAATTCACTCCCAAAGAAGACAAGATAT
CCTTGATCTGTGGATCTACCACACACAAGGCTACTTCCCTGATTGGCAGAACTACACACCAGGGCCAGGGG
TCAGATATCCACTGACCTTTGGATGGTGCTACAAGCTAGTACCAGTTGAGCCAGATAAGGTAGAAGAGGCC
AATAAAGGAGAGAACACCAGCTTGTTACACCCTGTGAGCCTGCATGGAATGGATGACCCTGAGAGAGAAGT
GTTAGAGTGGAGGTTTGACAGCCGCCTAGCATTTCATCACGTGGCCCGAGAGCTGCATCCGGAGTACTTCA
AGAACTGC

HIV-2 (M1-D88.BamHI.V89-S255)

AATTCATGGGCGCCAGTGGCTCCAAGAAGCGTTCCGAGCCTTCGCGAGGGCTACGGGAGAGACTCTTACAA
ACGCCTGGAGAGGCTTCTGGGGGACACTGGGACAAATTGGGAGGGGAATACTTGCAGTCCCAAGAAGGATC
AGGCAGGGGGCAGAAATCACCCTCCTGTGAGGGACGGCGGTATCAACAGGGAGATTTTATGAATACCCCAT
GGAGAGCCCCAGCAGAAGGGGAGAAAGGCTCGTACAAGCAACAAAATATGGATGATGGATCCGTAGATTCA
GATGATGATGACCTAGTAGGGGTCCCTGTCACACCAAGAGTACCATTAAGAGAAATGACATATCGTTTGGC
AAGAGATATGTCACATTTGATAAAAGAAAAGGGGGGACTGGAAGGGCTGTATTACAGTGATAGAAGACGTA
GAGTGCTAGACATATACTTAGAAAAGGAAGAGGGAATAATTGGAGACTGGCAGAACTATACTCATGGACCA
GGAGTAAGGTATCCAAAGTTCTTTGGGTGGTTATGGAAGCTAGTACCAGTAGATGTCCCACAAGAGGGAGA
TGACAGTGAGACTCACTGCTTAGTGCATCCAGCACAAACAAGCAGGTTTGATGACCCGCATGGAGAAACAT
TAGTTTGGAGGTTTGACCCCACGCTAGCTTTTAGCTACGAGGCCTTTATTCGATACCCAGAGGAGTTTGGG
TACAAGTCAGGCCTGCCAGAGGATGAATGGAAGGCAAGACTGAAAGCAAGAGGGATACCGTTTAGC

SIV (M1-D89.BamHI.V90-S263)

AATTCATGGGCGGCGCTATTTCCATGAGGCGGTCCAGGCCGTCTGGAGATCTGCGACAGAGACTCTTGCGG
GCGCGTGGGGAGACTTATGGGAGACTCTTAGGAGAGGTGGAAGATGGATACTCGCAATCCCCAGGAGGATT
AGACAAGGGCTTGAGCTCACTCTCTTGTGAGGGACAGAAATACAATCAGGGACAGTATATGAATACTCCAT
GGAGAAACCCAGCTGAAGAGAGAGAAAAATTAGCATACAGAAAACAAAATATGGATGATGGATCCATAGAT
GAGGAAGATGATGACTTGGTAGGGGTATCAGTGAGGCCAAAAGTTCCCCTAAGAACAATGAGTTACAAATT
GGCAATAGACATGTCTCATTTTATAAAAGAAAAGGGGGGACTGGAAGGGATTTATTACAGTGCAAGAAGAC
ATAGAATCTTAGACATATACTTAGAAAAGGAAGAAGGCATCATACCAGATTGGCAGGATTACACCTCAGGA
CCAGGAATTAGATACCCAAAGACATTTGGCTGGCTATGGAAATTAGTCCCTGTAAATGTATCAGATGAGGC
ACAGGAGGATGAGGAGCATTATTTAATGCATCCAGCTCAAACTTCCCAGTGGGATGACCCTTGGGGAGAGG
TTCTAGCATGGAAGTTTGATCCAACTCTGGCCTACACTTATGAGGCATATGTTAGATACCCAGAAGAGTTT
GGAAGCAAGTCAGGCCTGTCAGAGGAAGAGGTTAGAAGAAGGCTAACCGCAAGAGGCCTTCTTAACATGGC
TGACAAGAAGGAAACTCGC

E. Nef (Full Length) / GFP Fusion (+G) / Internal BamHI site / Chimera

ELI-SIV (M1-W57.BamHI.V90-S263)

AATTCCTGGTTCCTCGTGGCAGCATGGGTGGCAAATGGTCAAAAAGTAGTATAGTGGGATGGCCTGCTATA
AGGGAAAGAATAAGAAGAACTAATCCAGCAGCAGATGGGGTAGGAGCAGTATCTCGAGACCTGGAAAAACA
TGGGGCAATCACAAGTAGCAATACAGCAAGTACTAATGCTGACTGTGCCTGGGGATCCATAGATGAGGAAG
ATGATGACTTGGTAGGGGTATCAGTGAGGCCAAAAGTTCCCCTAAGAACAATGAGTTACAAATTGGCAATA
GACATGTCTCATTTTATAAAAGAAAAGGGGGGACTGGAAGGGATTTATTACAGTGCAAGAAGACATAGAAT
CTTAGACATATACTTAGAAAAGGAAGAAGGCATCATACCAGATTGGCAGGATTACACCTCAGGACCAGGAA
TTAGATACCCAAAGACATTTGGCTGGCTATGGAAATTAGTCCCTGTAAATGTATCAGATGAGGCACAGGAG
GATGAGGAGCATTATTTAATGCATCCAGCTCAAACTTCCCAGTGGGATGACCCTTGGGGAGAGGTTCTAGC
ATGGAAGTTTGATCCAACTCTGGCCTACACTTATGAGGCATATGTTAGATACCCAGAAGAGTTTGGAAGCA
AGTCAGGCCTGTCAGAGGAAGAGGTTAGAAGAAGGCTAACCGCAAGAGGCCTTCTTAACATGGCTGACAAG
AAGGAAACTCGC

NL4-3-SIV (M1-W57.BamHI.V90-S263)

AATTCCTGGTTCCTCGTGGCAGCATGGGTGGCAAGTGGTCAAAAAGTAGTGTGATTGGATGGCCTGCTGTA
AGGGAAAGAATGAGACGAGCTGAGCCAGCAGCAGATGGGGTGGGAGCAGTATCTCGAGACCTAGAAAAACA
TGGAGCAATCACAAGTAGCAATACAGCAGCTAACAATGCTGCTTGTGCCTGGGGATCCATAGATGAGGAAG
ATGATGACTTGGTAGGGGTATCAGTGAGGCCAAAAGTTCCCCTAAGAACAATGAGTTACAAATTGGCAATA
GACATGTCTCATTTTATAAAAGAAAAGGGGGGACTGGAAGGGATTTATTACAGTGCAAGAAGACATAGAAT
CTTAGACATATACTTAGAAAAGGAAGAAGGCATCATACCAGATTGGCAGGATTACACCTCAGGACCAGGAA
TTAGATACCCAAAGACATTTGGCTGGCTATGGAAATTAGTCCCTGTAAATGTATCAGATGAGGCACAGGAG
GATGAGGAGCATTATTTAATGCATCCAGCTCAAACTTCCCAGTGGGATGACCCTTGGGGAGAGGTTCTAGC
ATGGAAGTTTGATCCAACTCTGGCCTACACTTATGAGGCATATGTTAGATACCCAGAAGAGTTTGGAAGCA
AGTCAGGCCTGTCAGAGGAAGAGGTTAGAAGAAGGCTAACCGCAAGAGGCCTTCTTAACATGGCTGACAAG
AAGGAAACTCGC

SIV-ELI (M1-D89.BamHI.L58-N206)

AATTCATGGGCGGCGCTATTTCCATGAGGCGGTCCAGGCCGTCTGGAGATCTGCGACAGAGACTCTTGCGG
GCGCGTGGGGAGACTTATGGGAGACTCTTAGGAGAGGTGGAAGATGGATACTCGCAATCCCCAGGAGGATT
AGACAAGGGCTTGAGCTCACTCTCTTGTGAGGGACAGAAATACAATCAGGGACAGTATATGAATACTCCAT
GGAGAAACCCAGCTGAAGAGAGAGAAAAATTAGCATACAGAAAACAAAATATGGATGATGGATCCCTAGAA
GCACAAGAAGAGAGCGACGAGGTGGGCTTTCCAGTCAGACCCCAGGTACCTTTAAGACCAATGACTTACAA
AGAAGCTCTAGATCTCAGCCACTTTTTAAAAGAAAAGGGGGGACTGGAAGGGCTAATTTGGTCCAAAAAGA
GACAAGAGATCCTTGATCTTTGGGTCTACAACACACAAGGCATCTTCCCTGATTGGCAAAACTACACACCA
GGGCCAGGGATCAGATATCCACTAACCTTTGGATGGTGCTACGAGCTAGTACCAGTTGATCCACAGGAGGT
AGAAGAAGACACTGAAGGAGAGACCAACAGCTTGTTACACCCTATATGCCAGCATGGAATGGAGGACCCGG
AGAGACAAGTGTTAAAATGGAGATTTAACAGCAGACTAGCATTTGAGCACAAGGCCCGAGAGATGCATCCG
GAGTTCTACAAAAAC

SIV-NL4-3 (M1-D89.BamHI.L58-C206)

AATTCATGGGCGGCGCTATTTCCATGAGGCGGTCCAGGCCGTCTGGAGATCTGCGACAGAGACTCTTGCGG
GCGCGTGGGGAGACTTATGGGAGACTCTTAGGAGAGGTGGAAGATGGATACTCGCAATCCCCAGGAGGATT
AGACAAGGGCTTGAGCTCACTCTCTTGTGAGGGACAGAAATACAATCAGGGACAGTATATGAATACTCCAT
GGAGAAACCCAGCTGAAGAGAGAGAAAAATTAGCATACAGAAAACAAAATATGGATGATGGATCCCTAGAA
GCACAAGAGGAGGAAGAGGTGGGTTTTCCAGTCACACCTCAGGTACCTTTAAGACCAATGACTTACAAGGC
AGCTGTAGATCTTAGCCACTTTTTAAAAGAAAAGGGGGGACTGGAAGGGCTAATTCACTCCCAAAGAAGAC
AAGATATCCTTGATCTGTGGATCTACCACACACAAGGCTACTTCCCTGATTGGCAGAACTACACACCAGGG
CCAGGGGTCAGATATCCACTGACCTTTGGATGGTGCTACAAGCTAGTACCAGTTGAGCCAGATAAGGTAGA
AGAGGCCAATAAAGGAGAGAACACCAGCTTGTTACACCCTGTGAGCCTGCATGGAATGGATGACCCTGAGA
GAGAAGTGTTAGAGTGGAGGTTTGACAGCCGCCTAGCATTTCATCACGTGGCCCGAGAGCTGCATCCGGAG
TACTTCAAGAACTGC

F. Nef (Full Length) / GFP Fusion (+G) / Chimera

ELI-SIV (M1-W57.BamHI.V90-S263)

AATTCCTGGTTCCTCGTGGCAGCATGGGTGGCAAATGGTCAAAAAGTAGTATAGTGGGATGGCCTGCTATA
AGGGAAAGAATAAGAAGAACTAATCCAGCAGCAGATGGGGTAGGAGCAGTATCTCGAGACCTGGAAAAACA
TGGGGCAATCACAAGTAGCAATACAGCAAGTACTAATGCTGACTGTGCCTGGATAGATGAGGAAGATGATG
ACTTGGTAGGGGTATCAGTGAGGCCAAAAGTTCCCCTAAGAACAATGAGTTACAAATTGGCAATAGACATG
TCTCATTTTATAAAAGAAAAGGGGGGACTGGAAGGGATTTATTACAGTGCAAGAAGACATAGAATCTTAGA
CATATACTTAGAAAAGGAAGAAGGCATCATACCAGATTGGCAGGATTACACCTCAGGACCAGGAATTAGAT
ACCCAAAGACATTTGGCTGGCTATGGAAATTAGTCCCTGTAAATGTATCAGATGAGGCACAGGAGGATGAG
GAGCATTATTTAATGCATCCAGCTCAAACTTCCCAGTGGGATGACCCTTGGGGAGAGGTTCTAGCATGGAA
GTTTGATCCAACTCTGGCCTACACTTATGAGGCATATGTTAGATACCCAGAAGAGTTTGGAAGCAAGTCAG
GCCTGTCAGAGGAAGAGGTTAGAAGAAGGCTAACCGCAAGAGGCCTTCTTAACATGGCTGACAAGAAGGAA
ACTCGC

NL4-3-SIV (M1-W57.BamHI.V90-S263)

AATTCCTGGTTCCTCGTGGCAGCATGGGTGGCAAGTGGTCAAAAAGTAGTGTGATTGGATGGCCTGCTGTA
AGGGAAAGAATGAGACGAGCTGAGCCAGCAGCAGATGGGGTGGGAGCAGTATCTCGAGACCTAGAAAAACA
TGGAGCAATCACAAGTAGCAATACAGCAGCTAACAATGCTGCTTGTGCCTGGATAGATGAGGAAGATGATG
ACTTGGTAGGGGTATCAGTGAGGCCAAAAGTTCCCCTAAGAACAATGAGTTACAAATTGGCAATAGACATG
TCTCATTTTATAAAAGAAAAGGGGGGACTGGAAGGGATTTATTACAGTGCAAGAAGACATAGAATCTTAGA
CATATACTTAGAAAAGGAAGAAGGCATCATACCAGATTGGCAGGATTACACCTCAGGACCAGGAATTAGAT
ACCCAAAGACATTTGGCTGGCTATGGAAATTAGTCCCTGTAAATGTATCAGATGAGGCACAGGAGGATGAG
GAGCATTATTTAATGCATCCAGCTCAAACTTCCCAGTGGGATGACCCTTGGGGAGAGGTTCTAGCATGGAA
GTTTGATCCAACTCTGGCCTACACTTATGAGGCATATGTTAGATACCCAGAAGAGTTTGGAAGCAAGTCAG
GCCTGTCAGAGGAAGAGGTTAGAAGAAGGCTAACCGCAAGAGGCCTTCTTAACATGGCTGACAAGAAGGAA
ACTCGC

SIV-ELI (M1-D89.BamHI.L58-N206)

AATTCATGGGCGGCGCTATTTCCATGAGGCGGTCCAGGCCGTCTGGAGATCTGCGACAGAGACTCTTGCGG
GCGCGTGGGGAGACTTATGGGAGACTCTTAGGAGAGGTGGAAGATGGATACTCGCAATCCCCAGGAGGATT
AGACAAGGGCTTGAGCTCACTCTCTTGTGAGGGACAGAAATACAATCAGGGACAGTATATGAATACTCCAT
GGAGAAACCCAGCTGAAGAGAGAGAAAAATTAGCATACAGAAAACAAAATATGGATGATCTAGAAGCACAA
GAAGAGAGCGACGAGGTGGGCTTTCCAGTCAGACCCCAGGTACCTTTAAGACCAATGACTTACAAAGAAGC
TCTAGATCTCAGCCACTTTTTAAAAGAAAAGGGGGGACTGGAAGGGCTAATTTGGTCCAAAAAGAGACAAG
AGATCCTTGATCTTTGGGTCTACAACACACAAGGCATCTTCCCTGATTGGCAAAACTACACACCAGGGCCA
GGGATCAGATATCCACTAACCTTTGGATGGTGCTACGAGCTAGTACCAGTTGATCCACAGGAGGTAGAAGA
AGACACTGAAGGAGAGACCAACAGCTTGTTACACCCTATATGCCAGCATGGAATGGAGGACCCGGAGAGAC
AAGTGTTAAAATGGAGATTTAACAGCAGACTAGCATTTGAGCACAAGGCCCGAGAGATGCATCCGGAGTTC
TACAAAAAC

SIV-NL4-3 (M1-D89.BamHI.L58-C206)

aattcATGggcggcgctatttccatgaggcggtccaggccgtctggagatctgcgacagagactcttgcgg
gcgcgtggggagacttatgggagactcttaggagaggtggaagatggatactcgcaatccccaggaggatt
agacaagggcttgagctcactctcttgtgagggacagaaatacaatcagggacagtatatgaatactccat
ggagaaacccagctgaagagagagaaaaattagcatacagaaaacaaaatatggatgatctagaagcacaa
gaggaggaagaggtgggttttccagtcacacctcaggtacctttaagaccaatgacttacaaggcagctgt
agatcttagccacttttaaaagaaaaggggggactggaagggctaattcactcccaaagaagacaagata
tccttgatctgtggatctaccacacacaaggctacttccctgattggcagaactacacaccagggccaggg
gtcagatatccactgacctttggatggtgctacaagctagtaccagttgagccagataaggtagaagaggc
caataaaggagagaacaccagcttgttacaccctgtgagcctgcatggaatggatgaccctgagagagaag
tgttagagtggaggtttgacagccgcctagcatttcatcacgtggcccgagagctgcatccggagtacttc
aagaactgc

A.3. Primer Inventory

WMK1: 5′ mutagenesis primer for pET32a-Nef(SS;SL;HS;HL) to eliminate 1st of 2 thrombin cleavage sites. Substitution of residue 129 from R to Q (R129Q); (126)-LVPRGS-(131) to (126)-LVPQGS-(131). Non-coding strand. Bases 686-709. 24 bases. 2 mismatched bases (GC→CT). 0.1mM stock. Tm = 69.0°C.

5′-CATACCAGAACC**CT**GTGGCACCAG-3′

WMK2: 3′ mutagenesis primer (complementary to WMK1) for pET32a-Nef(SS;SL;HS;HL) to eliminate 1st of 2 thrombin cleavage sites. Substitution of residue 129 from R to Q (R129Q); (126)-LVPRGS-(131) to (126)-LVPQGS-(131). Coding strand. Bases 686-709. 24 bases. 2 mismatched bases (GC→AG). 0.1mM stock. Tm = 69.0°C.

5′-CTGGTGCCAC**AG**GGTTCTGGTATG-3′

WMK3: 5′ mutagenesis primer for pET32a-Nef(SS;SL;HS;HL) to eliminate 1st of 2 thrombin cleavage sites. Substitution of residue 129 from R to Q (R129Q); (126)-LVPRGS-(131) to (126)-LVPQGS-(131). Non-coding strand. Bases 682-717. 36 bases. 2 mismatched bases (GC→CT). 0.1mM stock. Tm = 66°C.

5′-CTTTCATACCAGAACC**CT**GTGGCACCAGACCAGAAG-3′

WMK4: 3′ mutagenesis primer (complementary to WMK3) for pET32a-Nef(SS;SL;HS;HL) to eliminate 1st of 2 thrombin cleavage sites. Substitution of residue 129 from R to Q (R129Q); (126)-LVPRGS-(131) to (126)-LVPQGS-(131). Coding strand. Bases 682-717. 36 bases. 2 mismatched bases (GC→AG). 0.1mM stock. Tm = 66°C.

5′-CTTCTGGTCTGGTGCCAC**AG**GGTTCTGGTATGAAAG-3′

WMK5: 3′ sequencing primer for pET32a. Non-coding strand. Bases 117-142. 26 bases. GC content = 53.8%. 0.1mM stock. Tm = 61.6°C.

5′-GCTTTGTTAGCAGCCGGATCTCAGTG-3′

WMK6: 5′ mutagenesis primer for pT7consnefhis6 and pUC19-ARV2/SF2 to eliminate *KpnI* restriction digestion site (5′-GGTACC-3′). Coding strand. Bases 205-239 (coding region). 35 bases. 1 mismatched bases (A→G). 0.1mM stock. Tm = 66°C.

5′-CCAGTCAGACCTCAGGT**G**CCTTTAAGACCAATGAC-3′

WMK7: 3′ mutagenesis primer for pT7consnefhis6 and pUC19-ARV2/SF2 to eliminate *KpnI* restriction digestion site (5′-GGTACC-3′). Non-coding strand. Bases 205-239 (coding region). 35 bases. 1 mismatched bases (T→C). 0.1mM stock. Tm = 66°C.

5′-GTCATTGGTCTTAAAGG**C**ACCTGAGGTCTGACTGG-3′

WMK8: 5′ subcloning primer extracting the full-length HIV-1 Nef (consensus) coding region from pT7consnefhis6. Comprised of 27 non homologous bases and 35 homologous bases (starts with ATG). Contains 5′ *KpnI* restriction site (5′-GGTACC-3′) for cloning into pET32a-Nef (SS) expression vector. Coding strand. 62 bases. 0.1mM stock. Tm = 67°C.

5′-CTGGGTACCCTGGTTCCTCGTGGCAGCATGGGTGGCAAGTGGTCAAAACGTAGTGTGAGTGG-3′

WMK9: 3′ subcloning primer extracting the full-length HIV-1 Nef (consensus) coding region from pT7consnefhis6 and HIV-1 Nef (ARV-2/SF2) coding region from HIV-1 (SF2) provirus. Comprised of 15 non homologous bases and 32 homologous bases (starts with GCA). Contains 5′ *HindIII* restriction site (5′-AAGCTT-3′) for cloning into pET32a-Nef (SS) expression vector. Non-coding strand. 47 bases. 0.1mM stock. Tm = 66°C.

5′-CGCAAGCTTTCATTAGCAGTCTTTGTAGTACTCCGGATGCAGCTCTC-3′

WMK10: 5′ subcloning primer extracting the K4-C206 HIV-1 Nef (consensus) coding region from pT7consnefhis6. Comprised of 27 non homologous bases and 35 homologous bases (starts with AAG; K4). Contains 5′ *KpnI* restriction site (5′-GGTACC-3′) for cloning into pET32a-Nef (SS) expression vector. Coding strand. 62 bases. 0.1mM stock. Tm = 67°C.

5′-CTGGGTACCCTGGTTCCTCGTGGCAGCAAGTGGTCAAAACGTAGTGTGAGTGGATGGCCTGC-3′

WMK11: 5′ subcloning primer extracting the A56-C206 HIV-1 Nef (consensus) coding region from pT7consnefhis6. Comprised of 27 non homologous bases and 35 homologous bases (starts with GCC; A56). Contains 5′ *KpnI* restriction site (5′-GGTACC-3′) for cloning into pET32a-Nef (SS) expression vector. Coding strand. 62 bases. 0.1mM stock. Tm = 67°C.

5′-CTGGGTACCCTGGTTCCTCGTGGCAGCGCCTGGCTAGAAGCACAAGAGGAGGAAGAAGTGGG-3′

WMK12: 5′ mutagenesis primer for pET32a-Nef(HS/HL) to correct errors at residues 113 and 117. Substitution at 113 (AAG→CGT; K113R) and 117 (AAT→GAT; N117D). Coding strand. 39 bases. 4 mismatched bases. 0.1mM stock. Tm = 61°C.

5′-GAAATGACATAT**CGT**TTGGCAAGA**G**ATATGTCACATTTG-3′

WMK13: 3′ mutagenesis primer for pET32a-Nef(HS/HL) to correct errors at residues 113 and 117. Substitution at 113 (AAG→CGT; K113R) and 117 (AAT→GAT; N117D). Non-Coding strand. 39 bases. 4 mismatched bases. 0.1mM stock. Tm = 61°C.

5′-CAAATGTGACATAT**C**TCTTGCCAA**ACG**ATATGTCATTTC-3′

WMK14: 5′ mutagenesis primer for pET32a-Nef(HS/HL) to correct errors at residues 138 and 140. Substitution at 138 (CAT→CGT; H138R) and 140 (ATC→GTG; I140V). Coding strand. 38 bases. 3 mismatched bases. **DILUTED TO 0.05mM stock.**Tm = 57°C.

5′-CAGTGATAGAAGAC**G**TAGA**G**T**G**CTAGACATATACTTAG-3′

WMK15: 3′ mutagenesis primer for pET32a-Nef(HS/HL) to correct errors at residues 138 and 140. Substitution at 138 (CAT→CGT; H138R) and 140 (ATC→GTG; I140V). Non-Coding strand. 38 bases. 3 mismatched bases. 0.1mM stock. Tm = 57°C.

5′-CTAAGTATATGTCTAG**C**A**C**TCTA**C**GTCTTCTATCACTG-3′

WMK16: 5′ mutagenesis primer for pET32a-Nef(SL) to correct errors at residue 64. Substitution at residue 64 (CAT→CGT; R64Q). Coding strand. 39 bases. 1 mismatched base. 0.1mM stock. Tm = 60°C.

5′-CAGAAATACAATCAGGGAC**A**GTATATGAATACTCCATGG-3′

WMK17: 5′ mutagenesis primer for pET32a-Nef(SL) to correct errors at residue 64. Substitution at residue 64 (CAT→CGT; R64Q). Non-Coding strand. 39 bases. 1 mismatched base. 0.1mM stock. Tm = 60°C.

5′-CCATGGAGTATTCATATAC**T**GTCCCTGATTGTATTTCTG-3′

WMK18: 5′ sequencing primer for pET32a. Coding strand. Bases. 21 bases. GC content = 60.4%. 0.1mM stock. Tm = 63.9°C.

5′-CGGTGAAGTGGCGGCAACCAAAG-3′

WMK19: 5′ subcloning primer extracting the K4-C210 HIV-1 Nef (ARV-2/SF2) coding region from HIV-1 (SF2) provirus. Comprised of 27 non homologous bases and 35 homologous bases (starts with AAG; K4). Contains 5′ *KpnI* restriction site (5′-GGTACC-3′) for cloning into pET32a-Nef (SS) expression vector. Coding strand. 62 bases. 0.1mM stock.

5′-CTGGGTACCCTGGTTCCTCGTGGCAGCAAGTGGTCAAAACGTAGTATGGGTGGATGGTCTGC-3′

WMK20: 5′ subcloning primer extracting the A60-C210 HIV-1 Nef (ARV-2/SF2) coding region from HIV-1 (SF2) provirus. Comprised of 27 non homologous bases and 35 homologous bases (starts with GCC; A60). Contains 5′ *KpnI* restriction site (5′-GGTACC-3′) for cloning into pET32a-Nef (SS) expression vector. Coding strand. 62 bases. 0.1mM stock.

5′-CTGGGTACCCTGGTTCCTCGTGGCAGCGCCTGGCTAGAAGCACAAGAGGAGGAAGAGGTGGG-3′

WMK21: 5′ subcloning primer extracting the K4-N206 HIV-1 Nef (ELI) coding region from HIV-1 (ELI) provirus. Comprised of 27 non homologous bases and 35 homologous bases (starts with AAA; K4). Contains 5′ *KpnI* restriction site (5′-GGTACC-3′) for cloning into pET32a-Nef (SS) expression vector. Coding strand. 62 bases. 0.1mM stock.

5′-CTGGGTACCCTGGTTCCTCGTGGCAGCAAATGGTCAAAAAGTAGTATAGTGGGATGGCCTGC-3′

WMK22: 5′ subcloning primer extracting the A56-N206 HIV-1 Nef (ELI) coding region from HIV-1 (ELI) provirus. Comprised of 27 non homologous bases and 35 homologous bases (starts with GCC; A60). Contains 5′ *KpnI* restriction site (5′-GGTACC-3′) for cloning into pET32a-Nef (SS) expression vector. Coding strand. 66 bases. 0.1mM stock.

5′CTGGGTACCCTGGTTCCTCGTGGCAGCGCCTGGCTAGAAGCACAAGAAGAGAGCGACGAGGTGGGC-3′

WMK23: 3′ subcloning primer extracting HIV-1 Nef (ELI) coding region from HIV-1 (ELI) provirus. Comprised of 15 non homologous bases and 37 homologous bases (starts with GCA). Contains 3′ *HindIII* restriction site (5′-AAGCTT-3′) for cloning into pET32a-Nef (SS) expression vector. Non-coding strand. 52 bases. 0.1mM stock.

5′-CGCAAGCTTTCATTAGTTTTTGTAGAACTCCGGATGCATCTCTCGGGCCTTG-3′

WMK24: 5′ subcloning primer extracting the K4-Y202 HIV-1 Nef (LAI) coding region from HIV-1 (LAI) provirus. Comprised of 27 non homologous bases and 35 homologous bases (starts with AAG; K4). Contains 5′ *KpnI* restriction site (5′-GGTACC-3′) for cloning into pET32a-Nef (SS) expression vector. Coding strand. 62 bases. 0.1mM stock.

5′-CTGGGTACCCTGGTTCCTCGTGGCAGCAAGTGGTCAAAAAGTAGTGTGGTTGGATGGCCTGC-3′

WMK25: 5′ subcloning primer extracting the A56-Y202 HIV-1 Nef (LAI) coding region from HIV-1 (LAI) provirus. Comprised of 27 non homologous bases and 35 homologous bases (starts with GCC; A56). Contains 5′ *KpnI* restriction site (5′-GGTACC-3′) for cloning into pET32a-Nef (SS) expression vector. Coding strand. 62 bases. 0.1mM stock.

5′-CTGGGTACCCTGGTTCCTCGTGGCAGCGCCTGGCTAGAAGCACAAGAGGAGGAGGAGGTGGG-3′

WMK26: 3′ subcloning primer extracting truncated HIV-1 Nef (LAI) coding region (M1-Y202) from HIV-1 (LAI) provirus. Comprised of 15 non homologous bases and 33 homologous bases (starts with GTA). Contains 3′ *HindIII* restriction site (5′-AAGCTT-3′) for cloning into pET32a-Nef (SS) expression vector. Non-coding strand. 48 bases. 0.1mM stock. DO NOT USE!!!!

5′-CGCAAGCTTTCATTAGTACTCCGGATGCAGCTCTCGGGCCACGTGATG-3′

WMK27: 5′ subcloning primer extracting the K4-C206 HIV-1 Nef (NL4-3) coding region from HIV-1 (NL4-3) provirus. Comprised of 27 non homologous bases and 35 homologous bases (starts with AAG; K4). Contains 5′ *KpnI* restriction site (5′-GGTACC-3′) for cloning into pET32a-Nef (SS) expression vector. Coding strand. 62 bases. 0.1mM stock.

5′-CTGGGTACCCTGGTTCCTCGTGGCAGCAAGTGGTCAAAAAGTAGTGTGATTGGATGGCCTGC-3′

WMK28: 5′ subcloning primer extracting the A56-C206 HIV-1 Nef (NL4-3) coding region from HIV-1 (NL4-3) provirus. Comprised of 27 non homologous bases and 35 homologous bases (starts with GCC; A56).

Contains 5′ *KpnI* restriction site (5′-GGTACC-3′) for cloning into pET32a-Nef (SS) expression vector. Coding strand. 62 bases. 0.1mM stock.

5′-CTGGGTACCCTGGTTCCTCGTGGCAGCGCCTGGCTAGAAGCACAAGAGGAGGAAGAGGTGGG-3′

WMK29: 3′ subcloning primer extracting HIV-1 Nef (LAI, NL4-3) coding region from HIV-1 (NL4-3) provirus. Comprised of 15 non homologous bases and 35 homologous bases (starts with GCA). Contains 3′ *HindIII* restriction site (5′-AAGCTT-3′) for cloning into pET32a-Nef (SS) expression vector. Non-coding strand. 50 bases. 0.1mM stock. Tm = ^{o}C.

5′-CGCAAGCTTTCATTAGCAGTTCTTGAAGTACTCCGGATGCAGCTCTCGGG- 3′

WMK30: 5′ subcloning primer extracting the M1-C210 HIV-1 Nef (ARV-2/SF2) coding region from HIV-1 (SF2) provirus. Comprised of 27 non homologous bases and 35 homologous bases (starts with ATG; M1). Contains 5′ *EcoRI* restriction site (5′-GAATTC-3′) for cloning into pUC19 and pEGFP-N1. Coding strand. 62 bases. 0.1mM stock.

5′-CTGGAATTCCTGGTTCCTCGTGGCAGCATGGGTGGCAAGTGGTCAAAACGTAGTATGGGTGG-3′

WMK31: 5′ subcloning primer extracting the M1-N206 HIV-1 Nef (ELI) coding region from HIV-1 (ELI) provirus. Comprised of 27 non homologous bases and 35 homologous bases (starts with ATG; M1). Contains 5′ *EcoRI* restriction site (5′-GAATTC-3′) for cloning into pUC19 and pEGFP-N1. Coding strand. 62 bases. 0.1mM stock.

5′-CTGGAATTCCTGGTTCCTCGTGGCAGCATGGGTGGCAAATGGTCAAAAAGTAGTATAGTGGG-3′

WMK32: 5′ subcloning primer extracting the M1-C206 HIV-1 Nef (LAI) coding region from HIV-1 (LAI) provirus. Comprised of 27 non homologous bases and 35 homologous bases (starts with ATG; M1). Contains 5′ *EcoRI* restriction site (5′-GAATTC-3′) for cloning into pUC19 and pEGFP-N1. Coding strand. 62 bases. 0.1mM stock.

5′-CTGGAATTCCTGGTTCCTCGTGGCAGCATGGGTGGCAAGTGGTCAAAAAGTAGTGTGGTTGG-3′

WMK33: 5′ subcloning primer extracting the M1-C206 HIV-1 Nef (NL4-3) coding region from HIV-1 (NL4-3) provirus. Comprised of 27 non homologous bases and 35 homologous bases (starts with ATG; M1). Contains 5′ *EcoRI* restriction site (5′-GAATTC-3′) for cloning into pUC19 and pEGFP-N1. Coding strand. 62 bases. 0.1mM stock.

5′-CTGGAATTCCTGGTTCCTCGTGGCAGCATGGGTGGCAAGTGGTCAAAAAGTAGTGTGATTGG-3′

WMK34: 5′ mutagenesis primer for HIV-1 (ELI) to eliminate *KpnI* restriction digestion site (5′-GGTACC-3′). Coding strand. Bases (coding region). 35 bases. 1 mismatched bases (A→G). 0.1mM stock. Tm =66^{o}C.

5′-CCAGTCAGACCCCAGGT**G**CCTTTAAGACCAATGAC-3′

WMK35: 3′ mutagenesis primer for HIV-1 (ELI) to eliminate *KpnI* restriction digestion site (5′-GGTACC-3′). Non-coding strand. Bases (coding region). 35 bases. 1 mismatched bases (T→C). 0.1mM stock. Tm =66°C.

5′-GTCATTGGTCTTAAAGG**C**ACCTGGGGTCTGACTGG-3′

WMK36: 5′ mutagenesis primer for HIV-1 (LAI, NL4-3) to eliminate *KpnI* restriction digestion site (5′-GGTACC-3′). Coding strand. Bases (coding region). 35 bases. 1 mismatched bases (A→G). 0.1mM stock. Tm =66°C.

5′-CCAGTCACACCTCAGGT**G**CCTTTAAGACCAATGAC-3′

WMK37: 3′ mutagenesis primer for HIV-1 (LAI, NL4-3) to eliminate *KpnI* restriction digestion site (5′-GGTACC-3′). Non-coding strand. Bases (coding region). 35 bases. 1 mismatched bases (T→C). 0.1mM stock. Tm =66°C.

5′-GTCATTGGTCTTAAAGG**C**ACCTGAGGTGTGACTGG-3′

WMK38: 3′ sequencing primer for pET32a. Non-coding strand. Bases. 18 bases. 0.1mM stock. Tm = °C.

5′-CCGCTGCTGCTAAATTCG-3′

WMK39: 5′ sequencing primer for pET32a. Non-coding strand. Bases. 20 bases. 0.1mM stock. Tm = °C.

5′-CGGGCTTTGTTAGCAGCCGG-3′

WMK40: 5′ subcloning primer extracting the D94-T234 HIV-2 Nef (ST) coding region from pET32a-HL. Comprised of 27 non homologous bases and 34 homologous bases (starts with GAT; D94). Contains 5′ *KpnI* restriction site (5′-GGTACC-3′) for cloning into pET32a expression vector. Coding strand. 61 bases. 0.1mM stock.

5′-CTGGGTACCCTGGTTCCTCGTGGCAGCGATGACCTAGTAGGGGTCCCTGTCACACCAAGAG-3′

WMK41: 3′ subcloning primer extracting the D94-T234 HIV-2 Nef (ST) coding region from pET32a-HL. Comprised of 15 non homologous bases and 34 homologous bases (starts with GCA). Contains 3′ *HindIII* restriction site (5′-AAGCTT-3′) for cloning into pET32a-Nef (SS) expression vector. Non-coding strand. 49 bases. 0.1mM stock.

5′-CGCAAGCTTTCATTAGTACCCAAACTCCTCTGGGTATCGAATAAAGGCC-3′

WMK42: 5′ mutagenesis primer for pUC19-ARV2/SF2, pET32a-AS to correct errors at residues 105 and 106. Substitution at 105 (**GCTG→AAGA**; L105R) and 106 (**CT**A→**AG**A; L106R). Coding strand. 40 bases. 6 mismatched bases. 0.1mM stock. Tm = 61°C.

5′-GGGCTAATTTGGTCCCA**AAGAAG**ACAAGAGATCCTTGATC-3′

WMK43: 3′ mutagenesis primer for pUC19-ARV2/SF2, pET32a-AS to correct errors at residues 105 and 106. Substitution at 105 (**GCTG→AAGA**; L105R) and 106 (**CT**A→**AG**A; L106R). Non-Coding strand. 40 bases. 6 mismatched bases. 0.1mM stock. Tm = 61^{o}C.

5′-GATCAAGGATCTCTTGT**CTTCTT**TGGGACCAAATTAGCCC-3′

WMK44: 5′ mutagenesis primer for pUC19-ARV2/SF2, pET32a-AS to correct error at residue 135 (T frameshift deletion). Insert at residue 135 (GAAT→GA**T**AT). Coding strand. 24 bases. 1 mismatched bases. 0.1mM stock. Tm = 61^{o}C.

5′-CCAGGGATCAGA**T**ATCCACTGACC-3′

WMK45: 3′ mutagenesis primer for pUC19-ARV2/SF2, pET32a-AS to correct error at residue 135 (T frameshift deletion). Insert at residue 135 (GAAT→GA**T**AT). Non-Coding strand. 24 bases. 1 mismatched bases. 0.1mM stock. Tm = 61^{o}C.

5′-GGTCAGTGGAT**A**TCTGATCCCTGG-3′

WMK46: 3′ subcloning primer extracting the full-length HIV-1 Nef (consensus) coding region from pT7consnefhis6 and pUC19-ARV-2/SF2. Comprised of 15 non homologous bases and 30 homologous bases (starts with GCA). Contains 5′ *BamHI* restriction site (5′-GGATCC-3′) for cloning into pEFGP-N1 expression vector. Non-coding strand. 45 bases. 0.1mM stock.

5′-CGCGGATCCTCATTAGCAGTCTTTGTAGTACTCCGGATGCAGCTC-3′

WMK47: 3′ subcloning primer extracting HIV-1 Nef (ELI) coding region from pUC19-ELI. Comprised of 15 non homologous bases and 30 homologous bases (starts with GCA). Contains 5′ *BamHI* restriction site (5′-GGATCC-3′) for cloning into pEFGP-N1 expression vector. Non-coding strand. 45 bases. 0.1mM stock.

5′-CGCGGATCCTCATTAGTTTTTGTAGAACTCCGGATGCATCTCTCG-3′

WMK48: 3′ subcloning primer extracting HIV-1 Nef (LAI) coding region from pUC19-LAI. Comprised of 15 non homologous bases and 30 homologous bases (starts with GCA). Contains 5′ *BamHI* restriction site (5′-GGATCC-3′) for cloning into pEFGP-N1 expression vector. Non-coding strand. 45 bases. 0.1mM stock.

5′-CGCGGATCCTCATTAGTACTCCGGATGCAGCTCTCGGGCCACGTG-3′

WMK49: 3′ subcloning primer extracting HIV-1 Nef (NL4-3) coding region from pUC19-NL4-3. Comprised of 15 non homologous bases and 30 homologous bases (starts with GCA). Contains 5′ *BamHI* restriction site (5′-GGATCC-3′) for cloning into pEFGP-N1 expression vector. Non-coding strand. 45 bases. 0.1mM stock.

5′-CGCGGATCCTCATTAGCAGTTCTTGAAGTACTCCGGATGCAGCTC- 3′

WMK50: 5′ subcloning primer extracting the S4-S255 HIV-2 Nef (ST) coding region from pET32a-HL. Comprised of 18 non homologous bases and 26 homologous bases (starts with AGT; S4). Contains 5′ *EcoRI* restriction site (5′-GAATTC-3′) for cloning into pEFGP-N1. Contains M1-A3 N-terminal residues not present in the pET32a-HL expression vector. Coding strand. 44 bases. 0.1mM stock.

5′-CTGGAATTCATGGGCGCCAGTGGATCCAAGAAGCGTTCCGAGCC-3′

WMK51: 3′ subcloning primer extracting the S4-S255 HIV-2 Nef (ST) coding region from pET32a-HL. Comprised of 15 non homologous bases and 29 homologous bases (starts with GCA). Contains 5′ *BamHI* restriction site (5′-GGATCC-3′) for cloning into pEFGP-N1 expression vector. Non-coding strand. 44 bases. 0.1mM stock.

5′-CGCGGATCCTCATTAGCTAAACGGTATCCCTCTTGCTTTCAGTC- 3′

WMK52: 5′ subcloning primer extracting the A4-R263 SIV Nef (mac239) coding region from pET32a-SL. Comprised of 18 non homologous bases and 27 homologous bases (starts with GCT; A4). Contains 5′ *EcoRI* restriction site (5′-GAATTC-3′) for cloning into pEFGP-N1. Contains M1-G3 N-terminal residues not present in the pET32a-SL expression vector. Coding strand. 45 bases. 0.1mM stock.

5′-CTGGAATTCATGGGCGGCGCTATTTCCATGAGGCGGTCCAGGCCG-3′

WMK53: 3′ subcloning primer extracting the A4-R263 SIV Nef (mac239) coding region from pET32a-SL. Comprised of 9 non homologous bases and 36 homologous bases (starts with GCG). Contains 5′ *BamHI* restriction site (5′-GGATCC-3′) for cloning into pEFGP-N1 expression vector. Non-coding strand. 45 bases. 0.1mM stock.

5′-CGCGGATCCTCATTAGCGAGTTTCCTTCTTGTCAGCCATGTTAAG- 3′

WMK54: 5′ subcloning primer extracting the full-length HIV-1 Nef (consensus) coding region from pT7consnefhis6. Comprised of 9 non homologous bases and 35 homologous bases (starts with ATG; M1). Contains 5′ *EcoRI* restriction site (5′-GAATTC-3′) for cloning into pEFGP-N1 expression vector. Coding strand. 44 bases. 0.1mM stock. Tm = ^{o}C.

5′-CTGGAATTCATGGGTGGCAAGTGGTCAAAACGTAGTGTGAGTGG-3′

WMK55: 5′ sequencing primer for pEGFP-N1. Coding strand. Bases 561-580. 20 bases. 0.1mM stock.

5′-GCAGAGCTGGTTTAGTGAAC-3′

WMK56: 3′ sequencing primer for pEGFP-N1. Non-coding strand. Bases 724-705. 20 bases. 0.1mM stock.

5′-GGATGGGCACCACCCCGGTG-3′

WMK57: 5′ sequencing primer for pUC19. Provided by CFAR (UMass Medical School) as M13F(-40). Coding strand. 17 bases. 0.1mM stock.

5′-GTTTTCCCAGTCACGAC-3′

WMK58: 3′ sequencing primer for pUC19. Provided by CFAR (UMass Medical School) as M13R(-24). Non-Coding strand. 16 bases. 0.1mM stock.

5′-AACAGCTATGACCATG-3′

WMK59: 5′ sequencing primer for T7-based expression vector. Provided by CFAR (UMass Medical School) as T7. Coding strand. 19 bases. 0.1mM stock.

5′-TAATACGACTCACTATAGG-3′

WMK60: 5′ mutagenesis primer to delete stop codons (5′-TAATGAG-3′) from pEGFP-N1-SIV. SIVmac239 nef sequence ends with 5′-CGC-3′ and pEGFP-N1 sequence starts with 5′-GAT-3′. Comprised of 40 homologous bases. Coding strand. 40 bases. 0.1mM stock.

5′-GGCTGACAAGAAGGAAACTCGCGATCCACCGGTCGCCACC-3′

WMK61: 3′ mutagenesis primer to delete stop codons (5′-TAATGAG-3′) from pEGFP-
N1-SIV. Reverse complement of WMK60. Comprised of 40 homologous bases. Non-coding strand. 40 bases. 0.1mM stock.

5′-GGTGGCGACCGGTGGATCGCGAGTTTCCTTCTTGTCAGCC-3′

WMK62: 5′ mutagenesis primer to delete stop codons (5′-TAATGAG-3′) from pEGFP-N1-HIV-2. HIV-2 nef sequence ends with 5′-AGC-3′ and pEGFP-N1 sequence starts with 5′-GAT-3′. Comprised of 39 homologous bases. Coding strand. 39 bases. 0.1mM stock.

5′-GCAAGAGGGATACCGTTTAGCGATCCACCGGTCGCCACC-3′

WMK63: 3′ mutagenesis primer to delete stop codons (5′-TAATGAG-3′) from pEGFP-N1-HIV-2. Reverse complement of WMK62. Comprised of 39 homologous bases. Non-coding strand. 39 bases. 0.1mM stock.

5′-GGTGGCGACCGGTGGATCGCTAAACGGTATCCCTCTTGC-3′

WMK64: 5′ mutagenesis primer to delete stop codons (5′-TAATGA-3′) from pEGFP-N1-ARV2. ARV2 nef sequence ends with 5′-TGC-3′ and pEGFP-N1 sequence starts with 5′-GAT-3′. Comprised of 40 homologous bases. Coding strand. 39 bases. 0.1mM stock.

5′-CCGGAGTACTACAAAGACTGCGATCCACCGGTCGCCACC-3′

WMK65: 3′ mutagenesis primer to delete stop codons (5′-TAATGAG-3′) from pEGFP-N1-ARV2. Reverse complement of WMK64. Comprised of 39 homologous bases. Non-coding strand. 39 bases. 0.1mM stock.

5′-GGTGGCGACCGGTGGATCGCAGTCTTTGTAGTACTCCGG-3′

WMK66: 5′ mutagenesis primer to delete stop codons (5′-TAATGA-3′) from pEGFP-N1-LAI and pEGFP-N1-NL4-3. LAI/NL4-3 nef sequence ends with 5′-TGC-3′ and pEGFP-N1 sequence starts with 5′-GAT-3′. Comprised of 39 homologous bases. Coding strand. 39 bases. 0.1mM stock.

5′-CCGGAGTACTTCAAGAACTGCGATCCACCGGTCGCCACC-3′

WMK67: 3′ mutagenesis primer to delete stop codons (5′-TAATGAG-3′) from pEGFP-N1-LAI and pEGFP-N1-NL4-3. Reverse complement of WMK66. Comprised of 39 homologous bases. Non-coding strand. 39 bases. 0.1mM stock.

5′-GGTGGCGACCGGTGGATCGCAGTTCTTGAAGTACTCCGG-3′

WMK68: 5′ mutagenesis primer to delete stop codons (5′-TAATGA-3′) from pEGFP-N1-Cons. Consensus nef sequence ends with 5′-TGC-3′ and pEGFP-N1 sequence starts with 5′-GAT-3′. Comprised of 39 homologous bases. Coding strand. 39 bases. 0.1mM stock.

5′-CCGGAGTACTACAAAGACTGCGATCCACCGGTCGCCACC-3′

WMK69: 3′ mutagenesis primer to delete stop codons (5′-TAATGAG-3′) from pEGFP-N1-Cons. Reverse complement of WMK68. Comprised of 39 homologous bases. Non-coding strand. 39 bases. 0.1mM stock.

5′-GGTGGCGACCGGTGGATCGCAGTCTTTGTAGTACTCCGG-3′

WMK70: 5′ mutagenesis primer to delete stop codons (5′-TAATGA-3′) from pEGFP-N1-ELI. ELI nef sequence ends with 5′-AAC-3′ and pEGFP-N1 sequence starts with 5′-GAT-3′. Comprised of 43 homologous bases. Coding strand. 43 bases. 0.1mM stock.

5′-GATGCATCCGGAGTTCTACAAAAACGATCCACCGGTCGCCACC-3′

WMK71: 3′ mutagenesis primer to delete stop codons (5′-TAATGAG-3′) from pEGFP-N1-ELI. Reverse complement of WMK70. Comprised of 39 homologous bases. Non-coding strand. 39 bases. 0.1mM stock.

5′-GGTGGCGACCGGTGGATCGTTTTTGTAGAACTCCGGATGCATC-3′

WMK72: 5′ mutagenesis primer for pET32a-SS, pEGFP-N1-SIV to introduce D123G mutation. Substitution of residue 123 from D to G (D123G; GAT→GGC). Coding strand. 2 mismatched bases (AT→GC). 35 bases. 0.1mM stock. Tm =.

5′-GAAGGCATCATACCAG**GC**TGGCAGGATTACACCTC-3′

WMK73: 3′ mutagenesis primer for pET32a-SS, pEGFP-N1-SIV to introduce D123G mutation. Substitution of residue 123 from D to G (D123G; GAT→GGC). Non-coding strand. 2 mismatched bases (AT→GC). 35 bases. 0.1mM stock.

5′- GAGGTGTAATCCTGCCA**GC**CTGGTATGATGCCTTC-3′

WMK74: 5′ mutagenesis primer for pEGFP-ELI to introduce *BamHI* restriction digestion site (5′-GGATCC-3′) between N-terminal domain (M1-W57) and C-terminal domain (L58-N206). Coding strand. 37 bases. 5 mismatched bases (5′-GGATCC-3′). 0.1mM stock.

5′-GCTGACTGTGCCTGG**GGATCC**CTAGAAGCACAAGAAG-3′

WMK75: 3′ mutagenesis primer for pEGFP-ELI to introduce *BamHI* restriction digestion site (5′-GGATCC-3′) between N-terminal domain (M1-W57) and C-terminal domain (L58-N206). Non-coding strand. 37 bases. 5 mismatched bases (5′-GGATCC-3′). 0.1mM stock.

5′-CTTCTTGTGCTTCTAG**GGATCC**CCAGGCACAGTCAGC-3′

WMK76: 5′ mutagenesis primer for pEGFP-NL4-3 to introduce *BamHI* restriction digestion site (5′-GGATCC-3′) between N-terminal domain (M1-W57) and C-terminal domain (L58-C206). Coding strand. 37 bases. 5 mismatched bases (5′-GGATCC-3′). 0.1mM stock.

5′-GCTGCTTGTGCCTGG**GGATCC**CTAGAAGCACAAGAGG-3′

WMK77: 3′ mutagenesis primer for pEGFP-NL4-3 to introduce *BamHI* restriction digestion site (5′-GGATCC-3′) between N-terminal domain (M1-W57) and C-terminal domain (L58-C206). Non-coding strand. 37 bases. 5 mismatched bases (5′-GGATCC-3′). 0.1mM stock.

5′-CCTCTTGTGCTTCTAG**GGATCC**CCAGGCACAAGCAGC-3′

WMK78: 5′ mutagenesis primer for pEGFP-HIV-2 to introduce *BamHI* restriction digestion site (5′-GGATCC-3′) between N-terminal domain (M1-D88) and C-terminal domain (V89-S255). Coding strand. 41 bases. 5 mismatched bases (5′-GGATCC-3′). 0.1mM stock.

5′-GCAACAAAATATGGATGAT**GGATCC**GTAGATTCAGATGATG-3′

WMK79: 3′ mutagenesis primer for pEGFP-HIV-2 to introduce *BamHI* restriction digestion site (5′-GGATCC-3′) between N-terminal domain (M1-D88) and C-terminal domain (V89-S255). Non-coding strand. 41 bases. 5 mismatched bases (5′-GGATCC-3′). 0.1mM stock.

5′-CATCATCTGAATCTAC**GGATCC**ATCATCCATATTTTGTTGC-3′

WMK80: 5′ mutagenesis primer for pEGFP-SIV to introduce *BamHI* restriction digestion site (5′-GGATCC-3′) between N-terminal domain (M1-D89) and C-terminal domain (V90-S263). Coding strand. 47 bases. 5 mismatched bases (5′-GGATCC-3′). 0.1mM stock.

5′-CAGAAAACAAAATATGGATGAT**GGATCC**ATAGATGAGGAAGATGATG-3′

WMK81: 3′ mutagenesis primer for pEGFP-SIV to introduce *BamHI* restriction digestion site (5′-GGATCC-3′) between N-terminal domain

(M1-D89) and C-terminal domain (V90-S263). Coding strand. 47 bases. 5 mismatched bases (5′-GGATCC-3′). 0.1mM stock.

5′-CATCATCTTCCTCATCTAT**GGATCC**ATCATCCATATTTTGTTTTCTG-3′

WMK82: 5′ mutagenesis primer for pEGFP-ELI/NL4-3 to remove *BamHI* restriction digestion site (5′-GGATCC-3′) between ELI N-terminal domain (M1-W57) and NL4-3 C-terminal domain (L58-C206). Coding strand. 31 bases. 0.1mM stock.

5′-GCTGACTGTGCCTGGCTAGAAGCACAAGAGG-3′

WMK83: 3′ mutagenesis primer for pEGFP-ELI/NL4-3 to remove *BamHI* restriction digestion site (5′-GGATCC-3′) between ELI N-terminal domain (M1-W57) and NL4-3 C-terminal domain (L58-C206). Coding strand. 31 bases. 0.1mM stock.

5′-CCTCTTGTGCTTCTAGCCAGGCACAGTCAGC-3′

WMK84: 5′ mutagenesis primer for pEGFP-ELI/HIV-2 to remove *BamHI* restriction digestion site (5′-GGATCC-3′) between ELI N-terminal domain (M1-W57) and HIV-2 C-terminal domain (V89-S255). Coding strand. 31 bases. 0.1mM stock.

5′-GCTGACTGTGCCTGGGTAGATTCAGATGATG-3′

WMK85: 3′ mutagenesis primer for pEGFP-ELI/HIV-2 to remove *BamHI* restriction digestion site (5′-GGATCC-3′) between ELI N-terminal domain (M1-W57) and HIV-2 C-terminal domain (V89-S255). Coding strand. 31 bases. 0.1mM stock.

5′-CATCATCTGAATCTACCCAGGCACAGTCAGC-3′

WMK86: 5′ mutagenesis primer for pEGFP-ELI/SIV to remove *BamHI* restriction digestion site (5′-GGATCC-3′) between ELI N-terminal domain (M1-W57) and SIV C-terminal domain (V90-S263). Coding strand. 34 bases. 0.1mM stock.

5′-GCTGACTGTGCCTGGATAGATGAGGAAGATGATG-3′

WMK87: 3′ mutagenesis primer for pEGFP-ELI/SIV to remove *BamHI* restriction digestion site (5′-GGATCC-3′) between ELI N-terminal domain (M1-W57) and SIV C-terminal domain (V90-S263). Coding strand. 34 bases. 0.1mM stock.

5′-CATCATCTTCCTCATCTATCCAGGCACAGTCAGC-3′

WMK88: 5′ mutagenesis primer for pEGFP-NL4-3/ELI to remove *BamHI* restriction digestion site (5′-GGATCC-3′) between NL4-3 N-terminal domain (M1-W57) and ELI C-terminal domain (L58-N206). Coding strand. 34 bases. 0.1mM stock.

5′-GCTGCTTGTGCCTGGCTAGAAGCACAAGAAG-3′

WMK89: 3′ mutagenesis primer for pEGFP-NL4-3/ELI to remove *BamHI* restriction digestion site (5′-GGATCC-3′) between NL4-3 N-terminal domain (M1-W57) and ELI C-terminal domain (L58-N206). Coding strand. 34 bases. 0.1mM stock.

5′-CTTCTTGTGCTTCTAGCCAGGCACAAGCAGC-3′

WMK90: 5′ mutagenesis primer for pEGFP-NL4-3/HIV-2 to remove *BamHI* restriction digestion site (5′-GGATCC-3′) between NL4-3 N-terminal domain (M1-W57) and HIV-2 C-terminal domain (V89-S255). Coding strand. 31 bases. 0.1mM stock.

5′-GCTGCTTGTGCCTGGGTAGATTCAGATGATG-3′

WMK91: 3′ mutagenesis primer for pEGFP-NL4-3/HIV-2 to remove *BamHI* restriction digestion site (5′-GGATCC-3′) between NL4-3 N-terminal domain (M1-W57) and HIV-2 C-terminal domain (V89-S255). Coding strand. 31 bases. 0.1mM stock.

5′-CATCATCTGAATCTACCCAGGCACAAGCAGC-3′

WMK92: 5′ mutagenesis primer for pEGFP-NL4-3/SIV to remove *BamHI* restriction digestion site (5′-GGATCC-3′) between NL4-3 N-terminal domain (M1-W57) and SIV C-terminal domain (V90-S263). Coding strand. 34 bases. 0.1mM stock.

5′-GCTGCTTGTGCCTGGATAGATGAGGAAGATGATG-3′

WMK93: 3′ mutagenesis primer for pEGFP-NL4-3/SIV to remove *BamHI* restriction digestion site (5′-GGATCC-3′) between NL4-3 N-terminal domain (M1-W57) and SIV C-terminal domain (V90-S263). Coding strand. 34 bases. 0.1mM stock.

5′-CATCATCTTCCTCATCTATCCAGGCACAAGCAGC-3′

WMK94: 5′ mutagenesis primer for pEGFP-HIV-2/ELI to remove *BamHI* restriction digestion site (5′-GGATCC-3′) between HIV-2 N-terminal domain (M1-D88) and ELI C-terminal domain (L58-N206). Coding strand. 35 bases. 0.1mM stock.

5′-GCAACAAAATATGGATGATCTAGAAGCACAAGAAG-3′

WMK95: 3′ mutagenesis primer for pEGFP-HIV-2/ELI to remove *BamHI* restriction digestion site (5′-GGATCC-3′) between HIV-2 N-terminal domain (M1-D88) and ELI C-terminal domain (L58-N206). Coding strand. 35 bases. 0.1mM stock.

5′-CTTCTTGTGCTTCTAGATCATCCATATTTTGTTGC-3′

WMK96: 5′ mutagenesis primer for pEGFP-HIV-2/NL4-3 to remove *BamHI* restriction digestion site (5′-GGATCC-3′) between HIV-2 N-terminal

domain (M1-D88) and NL4-3 C-terminal domain (L58-C206). Coding strand. 35 bases. 0.1mM stock.

5′-GCAACAAAATATGGATGATCTAGAAGCACAAGAGG-3′

WMK97: 3′ mutagenesis primer for pEGFP-HIV-2/NL4-3 to remove *BamHI* restriction digestion site (5′-GGATCC-3′) between HIV-2 N-terminal domain (M1-D88) and NL4-3 C-terminal domain (L58-C206). Coding strand. 35 bases. 0.1mM stock.

5′-CCTCTTGTGCTTCTAGATCATCCATATTTTGTTGC-3′

WMK98: 5′ mutagenesis primer for pEGFP-HIV-2/SIV to remove *BamHI* restriction digestion site (5′-GGATCC-3′) between HIV-2 N-terminal domain (M1-D88) and SIV C-terminal domain (V90-S263). Coding strand. 38 bases. 0.1mM stock.

5′-GCAACAAAATATGGATGATATAGATGAGGAAGATGATG-3′

WMK99: 3′ mutagenesis primer for pEGFP-HIV-2/SIV to remove *BamHI* restriction digestion site (5′-GGATCC-3′) between HIV-2 N-terminal domain (M1-D88) and SIV C-terminal domain (V90-S263). Coding strand. 38 bases. 0.1mM stock.

5′-CATCATCTTCCTCATCTATATCATCCATATTTTGTTGC-3′

WMK100: 5′ mutagenesis primer for pEGFP-SIV/ELI to remove *BamHI* restriction digestion site (5′-GGATCC-3′) between SIV N-terminal domain (M1-D89) and ELI C-terminal domain (L58-N206). Coding strand. 38 bases. 0.1mM stock.

5′-CAGAAAACAAAATATGGATGATCTAGAAGCACAAGAAG-3′

WMK101: 3′ mutagenesis primer for pEGFP-SIV/ELI to remove *BamHI* restriction digestion site (5′-GGATCC-3′) between SIV N-terminal domain (M1-D89) and ELI C-terminal domain (L58-N206). Coding strand. 38 bases. 0.1mM stock.

5′-CTTCTTGTGCTTCTAGATCATCCATATTTTGTTTTCTG-3′

WMK102: 5′ mutagenesis primer for pEGFP-SIV/NL4-3 to remove *BamHI* restriction digestion site (5′-GGATCC-3′) between SIV N-terminal domain (M1-D89) and NL4-3 C-terminal domain (L58-C206). Coding strand. 38 bases. 0.1mM stock.

5′-CAGAAAACAAAATATGGATGATCTAGAAGCACAAGAGG-3′

WMK103: 3′ mutagenesis primer for pEGFP-SIV/NL4-3 to remove *BamHI* restriction digestion site (5′-GGATCC-3′) between SIV N-terminal domain (M1-D89) and NL4-3 C-terminal domain (L58-C206). Coding strand. 38 bases. 0.1mM stock.

5′-CCTCTTGTGCTTCTAGATCATCCATATTTTGTTTTCTG-3′

WMK104: 5′ mutagenesis primer for pEGFP-SIV/HIV-2 to remove *BamHI* restriction digestion site (5′-GGATCC-3′) between SIV N-terminal domain (M1-D89) and HIV-2 C-terminal domain (V89-S255). Coding strand. 38 bases. 0.1mM stock.

5′-CAGAAAACAAAATATGGATGATGTAGATTCAGATGATG-3′

WMK105: 3′ mutagenesis primer for pEGFP-SIV/HIV-2 to remove *BamHI* restriction digestion site (5′-GGATCC-3′) between SIV N-terminal domain (M1-D89) and HIV-2 C-terminal domain (V89-S255). Coding strand. 38 bases. 0.1mM stock.

5′-CATCATCTGAATCTACATCATCCATATTTTGTTTTCTG-3′

WMK106: 5′ mutagenesis primer for pET32a-HL to eliminate *BamHI* restriction digestion site (5′-GGATCC-3′) by silent mutation. Coding strand. 29 bases. 1 mismatched base (A→C). 0.1mM stock.

5′-GTGGCAGCAGTGG**C**TCCAAGAAGCGTTCC-3′

WMK107: 3′ mutagenesis primer for pET32a-HL to eliminate *BamHI* restriction digestion site (5′-GGATCC-3′) by silent mutation (5′-GG**C**TCC-3′). Coding strand. 29 bases. 1 mismatched base (A→C). 0.1mM stock.

5′-GGAACGCTTCTTGGA**G**CCACTGCTGCCAC-3′

WMK108: 5′ subcloning /mutatgenesis primer extracting the S4-S255 HIV-2 Nef (ST) coding region from pET32a-HL. Replaces WMK50. Comprised of 19 non homologous bases (including silent mutation A→C) and 26 homologous bases (starts with AGT; S4). Contains 5′ *EcoRI* restriction site (5′-GAATTC-3′) for cloning into pEFGP-N1. Contains M1-A3 N-terminal residues not present in the pET32a-HL expression vector. Coding strand. 44 bases. 0.1mM stock.

5′-CTGGAATTCATGGGCGCCAGTGG**C**TCCAAGAAGCGTTCCGAGCC-3′

WMK109: 5′ mutagenesis primer for pEGFP-ELI to introduce *BamHI* restriction digestion site (5′-GGATCC-3′) between N-terminal domain (M1-W57) and C-terminal domain (L58-N206). Repeat of WMK74, with extra bases on each end. Coding strand. 48 bases. 5 mismatched bases (5′-GGATCC-3′). 0.1mM stock.

5′-CTAATGCTGACTGTGCCTGG**GGATCC**CTAGAAGCACAAGAAGAGAGCG-3′

WMK110: 3′ mutagenesis primer for pEGFP-ELI to introduce *BamHI* restriction digestion site (5′-GGATCC-3′) between N-terminal domain (M1-W57) and C-terminal domain (L58-N206). Repeat of WMK75, with extra bases on each end. Non-coding strand. 48 bases. 5 mismatched bases (5′-GGATCC-3′). 0.1mM stock.

5′-CGCTCTCTTCTTGTGCTTCTAG**GGATCC**CCAGGCACAGTCAGCATTAG-3′

WMK111: 3′ sequencing primer for pEGFP-N1. Non-coding strand. In eGFP region. 22 bases. 0.1mM stock.

5′-GTTTACGTCGCCGTCCAGCTCG-3′

BIBLIOGRAPHY

Adams, P. D., Grosse-Kunstleve, R. W., Hung, L. W., Ioerger, T. R., McCoy, A. J., Moriarty, N. W., Read, R. J., Sacchettini, J. C., Sauter, N. K., and Terwilliger, T. C. (2002). PHENIX: building new software for automated crystallographic structure determination. Acta Crystallogr D Biol Crystallogr *58*, 1948-1954.

Aiken, C., Konner, J., Landau, N. R., Lenburg, M. E., and Trono, D. (1994). Nef induces CD4 endocytosis: requirement for a critical dileucine motif in the membrane-proximal CD4 cytoplasmic domain. Cell *76*, 853-864.

Aivazian, D., and Stern, L. J. (2000). Phosphorylation of T cell receptor zeta is regulated by a lipid dependent folding transition. Nat Struct Biol *7*, 1023-1026.

Anderson, S., Shugars, D. C., Swanstrom, R., and Garcia, J. V. (1993). Nef from primary isolates of human immunodeficiency virus type 1 suppresses surface CD4 expression in human and mouse T cells. J Virol *67*, 4923-4931.

Arien, K. K., and Verhasselt, B. (2008). HIV Nef: role in pathogenesis and viral fitness. Curr HIV Res *6*, 200-208.

Arold, S., Franken, P., Strub, M. P., Hoh, F., Benichou, S., Benarous, R., and Dumas, C. (1997). The crystal structure of HIV-1 Nef protein bound to the Fyn kinase SH3 domain suggests a role for this complex in altered T cell receptor signaling. Structure *5*, 1361-1372.

Bandres, J. C., and Ratner, L. (1994). Human immunodeficiency virus type 1 Nef protein down-regulates transcription factors NF-kappa B and AP-1 in human T cells in vitro after T-cell receptor stimulation. J Virol *68*, 3243-3249.

Barnham, K. J., Monks, S. A., Hinds, M. G., Azad, A. A., and Norton, R. S. (1997). Solution structure of a polypeptide from the N terminus of the HIV protein Nef. Biochemistry *36*, 5970-5980.

Barre-Sinoussi, F., Chermann, J. C., Rey, F., Nugeyre, M. T., Chamaret, S., Gruest, J., Dauguet, C., Axler-Blin, C., Vezinet-Brun, F., Rouzioux, C., *et al.* (1983). Isolation of a T-lymphotropic retrovirus from a patient at risk for acquired immune deficiency syndrome (AIDS). Science *220*, 868-871.

Baur, A. (2004). Functions of the HIV-1 Nef Protein. Curr Drug Targets Immune Endocr Metabol Disord *4*, 309-313.

Baur, A. S., Sawai, E. T., Dazin, P., Fantl, W. J., Cheng-Mayer, C., and Peterlin, B. M. (1994). HIV-1 Nef leads to inhibition or activation of T cells depending on its intracellular localization. Immunity *1*, 373-384.

Bell, I., Ashman, C., Maughan, J., Hooker, E., Cook, F., and Reinhart, T. A. (1998). Association of simian immunodeficiency virus Nef with the T-cell receptor (TCR) zeta chain leads to TCR down-modulation. J Gen Virol *79 (Pt 11)*, 2717-2727.

Bell, I., Schaefer, T. M., Trible, R. P., Amedee, A., and Reinhart, T. A. (2001). Down-modulation of the costimulatory molecule, CD28, is a conserved activity of multiple SIV Nefs and is dependent on histidine 196 of Nef. Virology *283*, 148-158.

Benson, R. E., Sanfridson, A., Ottinger, J. S., Doyle, C., and Cullen, B. R. (1993). Downregulation of cell-surface CD4 expression by simian immunodeficiency virus Nef prevents viral super infection. J Exp Med *177*, 1561-1566.

Brenchley, J. M., Schacker, T. W., Ruff, L. E., Price, D. A., Taylor, J. H., Beilman, G. J., Nguyen, P. L., Khoruts, A., Larson, M., Haase, A. T., and Douek, D. C. (2004). CD4+ T cell depletion during all stages of HIV disease occurs predominantly in the gastrointestinal tract. J Exp Med *200*, 749-759.

Bresnahan, P. A., Yonemoto, W., Ferrell, S., Williams-Herman, D., Geleziunas, R., and Greene, W. C. (1998). A dileucine motif in HIV-1 Nef acts as an internalization signal for CD4 downregulation and binds the AP-1 clathrin adaptor. Curr Biol *8*, 1235-1238.

Brooks, C. L., Blackler, R. J., Gerstenbruch, S., Kosma, P., Muller-Loennies, S., Brade, H., and Evans, S. V. (2008). Pseudo-symmetry and twinning in crystals of homologous antibody Fv fragments. Acta Crystallogr D Biol Crystallogr *64*, 1250-1258.

Carreer, R., Groux, H., Ameisen, J. C., and Capron, A. (1994). Role of HIV-1 Nef expression in activation pathways in CD4+ T cells. AIDS Res Hum Retroviruses *10*, 523-527.

Chaudhuri, R., Lindwasser, O. W., Smith, W. J., Hurley, J. H., and Bonifacino, J. S. (2007). Downregulation of CD4 by human immunodeficiency virus type 1 Nef is dependent on clathrin and involves direct interaction of Nef with the AP2 clathrin adaptor. J Virol *81*, 3877-3890.

Cheng, H., Hoxie, J. P., and Parks, W. P. (1999). The conserved core of human immunodeficiency virus type 1 Nef is essential for association with Lck and for enhanced viral replication in T-lymphocytes. Virology *264*, 5-15.

Coffin, J., Haase, A., Levy, J. A., Montagnier, L., Oroszlan, S., Teich, N., Temin, H., Toyoshima, K., Varmus, H., Vogt, P., and et al. (1986). Human immunodeficiency viruses. Science *232*, 697.

Collette, Y., Mawas, C., and Olive, D. (1996). Evidence for intact CD28 signaling in T cell hyporesponsiveness induced by the HIV-1 nef gene. Eur J Immunol *26*, 1788-1793.

Collins, K. L., Chen, B. K., Kalams, S. A., Walker, B. D., and Baltimore, D. (1998). HIV-1 Nef protein protects infected primary cells against killing by cytotoxic T lymphocytes. Nature *391*, 397-401.

Crump, C. M., Xiang, Y., Thomas, L., Gu, F., Austin, C., Tooze, S. A., and Thomas, G. (2001). PACS-1 binding to adaptors is required for acidic cluster motif-mediated protein traffic. Embo J *20*, 2191-2201.

Daniel, M. D., Letvin, N. L., King, N. W., Kannagi, M., Sehgal, P. K., Hunt, R. D., Kanki, P. J., Essex, M., and Desrosiers, R. C. (1985). Isolation of T-cell tropic HTLV-III-like retrovirus from macaques. Science *228*, 1201-1204.

Das, S. R., and Jameel, S. (2005). Biology of the HIV Nef protein. Indian J Med Res *121*, 315-332.

Deeks, S. G., Kitchen, C. M., Liu, L., Guo, H., Gascon, R., Narvaez, A. B., Hunt, P., Martin, J. N., Kahn, J. O., Levy, J., *et al.* (2004). Immune activation set point during early HIV infection predicts subsequent CD4+ T-cell changes independent of viral load. Blood *104*, 942-947.

DeGottardi, M. Q., Specht, A., Metcalf, B., Kaur, A., Kirchhoff, F., and Evans, D. T. (2008). Selective downregulation of rhesus macaque and sooty mangabey major histocompatibility complex class I molecules by Nef alleles of simian immunodeficiency virus and human immunodeficiency virus type 2. J Virol *82*, 3139-3146.

Dehghani, H., Brown, C. R., Plishka, R., Buckler-White, A., and Hirsch, V. M. (2002). The ITAM in Nef influences acute pathogenesis of AIDS-inducing simian immunodeficiency viruses SIVsm and SIVagm without altering kinetics or extent of viremia. J Virol *76*, 4379-4389.

Denny, M. F., Patai, B., and Straus, D. B. (2000). Differential T-cell antigen receptor signaling mediated by the Src family kinases Lck and Fyn. Mol Cell Biol *20*, 1426-1435.

Desrosiers, R. C. (1990). The simian immunodeficiency viruses. Annu Rev Immunol *8*, 557-578.

Desrosiers, R. C., Daniel, M. D., and Li, Y. (1989). HIV-related lentiviruses of nonhuman primates. AIDS Res Hum Retroviruses *5*, 465-473.

Djordjevic, J. T., Schibeci, S. D., Stewart, G. J., and Williamson, P. (2004). HIV type 1 Nef increases the association of T cell receptor (TCR)-signaling molecules with T cell rafts and promotes activation-induced raft fusion. AIDS Res Hum Retroviruses *20*, 547-555.

Douek, D. C., Roederer, M., and Koup, R. A. (2009). Emerging concepts in the immunopathogenesis of AIDS. Annu Rev Med *60*, 471-484.

Du, Z., Lang, S. M., Sasseville, V. G., Lackner, A. A., Ilyinskii, P. O., Daniel, M. D., Jung, J. U., and Desrosiers, R. C. (1995). Identification of a nef allele that causes lymphocyte activation and acute disease in macaque monkeys. Cell *82*, 665-674.

Duchardt, E., Sigalov, A. B., Aivazian, D., Stern, L. J., and Schwalbe, H. (2007). Structure induction of the T-cell receptor zeta-chain upon lipid binding investigated by NMR spectroscopy. Chembiochem *8*, 820-827.

Emsley, P., and Cowtan, K. (2004). Coot: model-building tools for molecular graphics. Acta Crystallogr D Biol Crystallogr *60*, 2126-2132.

Fackler, O. T., Lu, X., Frost, J. A., Geyer, M., Jiang, B., Luo, W., Abo, A., Alberts, A. S., and Peterlin, B. M. (2000). p21-activated kinase 1 plays a critical role in cellular activation by Nef. Mol Cell Biol *20*, 2619-2627.

Fackler, O. T., Wolf, D., Weber, H. O., Laffert, B., D'Aloja, P., Schuler-Thurner, B., Geffin, R., Saksela, K., Geyer, M., Peterlin, B. M., *et al.* (2001). A natural variability in the proline-rich motif of Nef modulates HIV-1 replication in primary T cells. Curr Biol *11*, 1294-1299.

Fenard, D., Yonemoto, W., de Noronha, C., Cavrois, M., Williams, S. A., and Greene, W. C. (2005). Nef is physically recruited into the immunological synapse and potentiates T cell activation early after TCR engagement. J Immunol *175*, 6050-6057.

Filipp, D., Leung, B. L., Zhang, J., Veillette, A., and Julius, M. (2004). Enrichment of lck in lipid rafts regulates colocalized fyn activation and the initiation of proximal signals through TCR alpha beta. J Immunol *172*, 4266-4274.

Filipp, D., Zhang, J., Leung, B. L., Shaw, A., Levin, S. D., Veillette, A., and Julius, M. (2003). Regulation of Fyn through translocation of activated Lck into lipid rafts. J Exp Med *197*, 1221-1227.

Foster, J. L., and Garcia, J. V. (2008). HIV-1 Nef: at the crossroads. Retrovirology *5*, 84.

Fultz, P. N. (1991). Replication of an acutely lethal simian immunodeficiency virus activates and induces proliferation of lymphocytes. J Virol *65*, 4902-4909.

Gallo, R. C., Sarin, P. S., Gelmann, E. P., Robert-Guroff, M., Richardson, E., Kalyanaraman, V. S., Mann, D., Sidhu, G. D., Stahl, R. E., Zolla-Pazner, S., *et al.* (1983). Isolation of human T-cell leukemia virus in acquired immune deficiency syndrome (AIDS). Science *220*, 865-867.

Garcia, J. V., and Miller, A. D. (1991). Serine phosphorylation-independent downregulation of cell-surface CD4 by nef. Nature *350*, 508-511.

Geyer, M., Fackler, O. T., and Peterlin, B. M. (2001). Structure--function relationships in HIV-1 Nef. EMBO Rep *2*, 580-585.

Geyer, M., Munte, C. E., Schorr, J., Kellner, R., and Kalbitzer, H. R. (1999). Structure of the anchor-domain of myristoylated and non-myristoylated HIV-1 Nef protein. J Mol Biol *289*, 123-138.

Giorgi, J. V., Hultin, L. E., McKeating, J. A., Johnson, T. D., Owens, B., Jacobson, L. P., Shih, R., Lewis, J., Wiley, D. J., Phair, J. P., *et al.* (1999). Shorter survival in advanced human immunodeficiency virus type 1 infection is more closely associated with T lymphocyte activation than with plasma virus burden or virus chemokine coreceptor usage. J Infect Dis *179*, 859-870.

Govindasamy, L., Reutzel, R., Agbandje-McKenna, M., and McKenna, R. (2004). Structural determination of a partially hemihedrally twinned actin crystal. Acta Crystallogr D Biol Crystallogr *60*, 1040-1047.

Granelli-Piperno, A., Finkel, V., Delgado, E., and Steinman, R. M. (1999). Virus replication begins in dendritic cells during the transmission of HIV-1 from mature dendritic cells to T cells. Curr Biol *9*, 21-29.

Greenway, A., Azad, A., Mills, J., and McPhee, D. (1996). Human immunodeficiency virus type 1 Nef binds directly to Lck and mitogen-activated protein kinase, inhibiting kinase activity. J Virol *70*, 6701-6708.

Grossman, Z., Meier-Schellersheim, M., Paul, W. E., and Picker, L. J. (2006). Pathogenesis of HIV infection: what the virus spares is as important as what it destroys. Nat Med *12*, 289-295.

Grzesiek, S., Bax, A., Clore, G. M., Gronenborn, A. M., Hu, J. S., Kaufman, J., Palmer, I., Stahl, S. J., and Wingfield, P. T. (1996a). The solution structure of HIV-1 Nef reveals an unexpected fold and permits delineation of the binding surface for the SH3 domain of Hck tyrosine protein kinase. Nat Struct Biol *3*, 340-345.

Grzesiek, S., Bax, A., Hu, J. S., Kaufman, J., Palmer, I., Stahl, S. J., Tjandra, N., and Wingfield, P. T. (1997). Refined solution structure and backbone dynamics of HIV-1 Nef. Protein Sci *6*, 1248-1263.

Grzesiek, S., Stahl, S. J., Wingfield, P. T., and Bax, A. (1996b). The CD4 determinant for downregulation by HIV-1 Nef directly binds to Nef. Mapping of the Nef binding surface by NMR. Biochemistry *35*, 10256-10261.

Guadalupe, M., Reay, E., Sankaran, S., Prindiville, T., Flamm, J., McNeil, A., and Dandekar, S. (2003). Severe CD4+ T-cell depletion in gut lymphoid tissue during primary human immunodeficiency virus type 1 infection and substantial delay in restoration following highly active antiretroviral therapy. J Virol *77*, 11708-11717.

Guy-Grand, D., and Vassalli, P. (1993). Gut intraepithelial T lymphocytes. Curr Opin Immunol *5*, 247-252.

Haase, A. T. (2005). Perils at mucosal front lines for HIV and SIV and their hosts. Nat Rev Immunol *5*, 783-792.

Hahn, B. H., Shaw, G. M., De Cock, K. M., and Sharp, P. M. (2000). AIDS as a zoonosis: scientific and public health implications. Science *287*, 607-614.

Hanna, Z., Kay, D. G., Cool, M., Jothy, S., Rebai, N., and Jolicoeur, P. (1998a). Transgenic mice expressing human immunodeficiency virus type 1 in immune cells develop a severe AIDS-like disease. J Virol *72*, 121-132.

Hanna, Z., Kay, D. G., Rebai, N., Guimond, A., Jothy, S., and Jolicoeur, P. (1998b). Nef harbors a major determinant of pathogenicity for an AIDS-like disease induced by HIV-1 in transgenic mice. Cell *95*, 163-175.

Hanna, Z., Priceputu, E., Chrobak, P., Hu, C., Dugas, V., Goupil, M., Marquis, M., de Repentigny, L., and Jolicoeur, P. (2009). Selective expression of HIV Nef in specific immune cell populations of transgenic mice is associated with distinct AIDS-like phenotypes. J Virol.

Hanna, Z., Priceputu, E., Hu, C., Vincent, P., and Jolicoeur, P. (2006). HIV-1 Nef mutations abrogating downregulation of CD4 affect other Nef functions and show reduced pathogenicity in transgenic mice. Virology *346*, 40-52.

Hatada, M. H., Lu, X., Laird, E. R., Green, J., Morgenstern, J. P., Lou, M., Marr, C. S., Phillips, T. B., Ram, M. K., Theriault, K., and et al. (1995). Molecular basis for interaction of the protein tyrosine kinase ZAP-70 with the T-cell receptor. Nature *377*, 32-38.

Helliwell, M., Collison, D., John, G. H., May, I., Sarsfield, M. J., Sharrad, C. A., and Sutton, A. D. (2006). Temperature-resolved study of three [M(M'O4)4(TBPO)4] complexes (MM' = URe, ThRe, ThTc). Acta Crystallogr B *62*, 68-85.

Hewitt, C. R., Lamb, J. R., Hayball, J., Hill, M., Owen, M. J., and O'Hehir, R. E. (1992). Major histocompatibility complex independent clonal T cell anergy by direct interaction of Staphylococcus aureus enterotoxin B with the T cell antigen receptor. J Exp Med *175*, 1493-1499.

Hirsch, V. M., Olmsted, R. A., Murphey-Corb, M., Purcell, R. H., and Johnson, P. R. (1989). An African primate lentivirus (SIVsm) closely related to HIV-2. Nature *339*, 389-392.

Hodge, S., Novembre, F. J., Whetter, L., Gelbard, H. A., and Dewhurst, S. (1998). Induction of fas ligand expression by an acutely lethal simian immunodeficiency virus, SIVsmmPBj14. Virology *252*, 354-363.

Howe, A. Y., Jung, J. U., and Desrosiers, R. C. (1998). Zeta chain of the T-cell receptor interacts with nef of simian immunodeficiency virus and human immunodeficiency virus type 2. J Virol *72*, 9827-9834.

Iafrate, A. J., Bronson, S., and Skowronski, J. (1997). Separable functions of Nef disrupt two aspects of T cell receptor machinery: CD4 expression and CD3 signaling. Embo J *16*, 673-684.

Jardetzky, T. S., Brown, J. H., Gorga, J. C., Stern, L. J., Urban, R. G., Strominger, J. L., and Wiley, D. C. (1996). Crystallographic analysis of endogenous peptides associated with HLA-DR1 suggests a common, polyproline II-like conformation for bound peptides. Proc Natl Acad Sci U S A *93*, 734-738.

Jerome, K. R. (2008). Viral modulation of T-cell receptor signaling. J Virol *82*, 4194-4204.

Kersh, E. N., Kersh, G. J., and Allen, P. M. (1999). Partially phosphorylated T cell receptor zeta molecules can inhibit T cell activation. J Exp Med *190*, 1627-1636.

Kestler, H. W., 3rd, Ringler, D. J., Mori, K., Panicali, D. L., Sehgal, P. K., Daniel, M. D., and Desrosiers, R. C. (1991). Importance of the nef gene for maintenance of high virus loads and for development of AIDS. Cell *65*, 651-662.

Kirchhoff, F., Greenough, T. C., Brettler, D. B., Sullivan, J. L., and Desrosiers, R. C. (1995). Brief report: absence of intact nef sequences in a long-term survivor with nonprogressive HIV-1 infection. N Engl J Med *332*, 228-232.

Kirchhoff, F., Schindler, M., Specht, A., Arhel, N., and Munch, J. (2008). Role of Nef in primate lentiviral immunopathogenesis. Cell Mol Life Sci *65*, 2621-2636.

Koblavi-Deme, S., Kestens, L., Hanson, D., Otten, R. A., Borget, M. Y., Bile, C., Wiktor, S. Z., Roels, T. H., Chorba, T., and Nkengasong, J. N. (2004). Differences in HIV-2 plasma viral load and immune activation in HIV-1 and HIV-2 dually infected persons and those infected with HIV-2 only in Abidjan, Cote D'Ivoire. Aids *18*, 413-419.

Krautkramer, E., Giese, S. I., Gasteier, J. E., Muranyi, W., and Fackler, O. T. (2004). Human immunodeficiency virus type 1 Nef activates p21-activated kinase via recruitment into lipid rafts. J Virol *78*, 4085-4097.

Laczko, I., Hollosi, M., Vass, E., Hegedus, Z., Monostori, E., and Toth, G. K. (1998). Conformational effect of phosphorylation on T cell receptor/CD3 zeta-chain sequences. Biochem Biophys Res Commun *242*, 474-479.

Lafont, B. A., Gloeckler, L., Beyer, C., Einius, S., Gut, J. P., and Aubertin, A. M. (2003). In vivo inactivation of Nef ITAM motif of chimeric simian/human immunodeficiency virus SHIVsbg-YE correlates with absence of increased virulence in Chinese rhesus macaques. Virology *313*, 322-334.

Landon (1977). Cleavage at aspartyl-prolyl bonds. Methods Enzymol *47*, 145-149.

Larsen, N. A., Heine, A., de Prada, P., Redwan el, R., Yeates, T. O., Landry, D. W., and Wilson, I. A. (2002). Structure determination of a cocaine hydrolytic antibody from a pseudomerohedrally twinned crystal. Acta Crystallogr D Biol Crystallogr *58*, 2055-2059.

Laskowski, R. A., Moss, D. S., and Thornton, J. M. (1993). Main-chain bond lengths and bond angles in protein structures. J Mol Biol *231*, 1049-1067.

Lawn, S. D., Butera, S. T., and Folks, T. M. (2001). Contribution of immune activation to the pathogenesis and transmission of human immunodeficiency virus type 1 infection. Clin Microbiol Rev *14*, 753-777, table of contents.

Le Gall, S., Heard, J. M., and Schwartz, O. (1997). Analysis of Nef-induced MHC-I endocytosis. Res Virol *148*, 43-47.

Lee, C. H., Leung, B., Lemmon, M. A., Zheng, J., Cowburn, D., Kuriyan, J., and Saksela, K. (1995). A single amino acid in the SH3 domain of Hck determines its high affinity and specificity in binding to HIV-1 Nef protein. Embo J *14*, 5006-5015.

Lee, C. H., Saksela, K., Mirza, U. A., Chait, B. T., and Kuriyan, J. (1996). Crystal structure of the conserved core of HIV-1 Nef complexed with a Src family SH3 domain. Cell *85*, 931-942.

Li, L., Li, H. S., Pauza, C. D., Bukrinsky, M., and Zhao, R. Y. (2005a). Roles of HIV-1 auxiliary proteins in viral pathogenesis and host-pathogen interactions. Cell Res *15*, 923-934.

Li, L., Promadej, N., McNicholl, J. M., and Bouvier, M. (2002). Crystallization and preliminary X-ray crystallographic studies of HLA-A*1101 complexed with an HIV-1 decapeptide. Acta Crystallogr D Biol Crystallogr *58*, 1195-1197.

Li, Q., Duan, L., Estes, J. D., Ma, Z. M., Rourke, T., Wang, Y., Reilly, C., Carlis, J., Miller, C. J., and Haase, A. T. (2005b). Peak SIV replication in resting memory CD4+ T cells depletes gut lamina propria CD4+ T cells. Nature *434*, 1148-1152.

Li, Q., Estes, J. D., Duan, L., Jessurun, J., Pambuccian, S., Forster, C., Wietgrefe, S., Zupancic, M., Schacker, T., Reilly, C., *et al.* (2008). Simian immunodeficiency virus-induced intestinal cell apoptosis is the underlying mechanism of the regenerative enteropathy of early infection. J Infect Dis *197*, 420-429.

Lindemann, D., Wilhelm, R., Renard, P., Althage, A., Zinkernagel, R., and Mous, J. (1994). Severe immunodeficiency associated with a human immunodeficiency virus 1 NEF/3'-long terminal repeat transgene. J Exp Med *179*, 797-807.

Lindwasser, O. W., Smith, W. J., Chaudhuri, R., Yang, P., Hurley, J. H., and Bonifacino, J. S. (2008). A diacidic motif in human immunodeficiency virus type 1 Nef is a novel determinant of binding to AP-2. J Virol *82*, 1166-1174.

Lubben, N. B., Sahlender, D. A., Motley, A. M., Lehner, P. J., Benaroch, P., and Robinson, M. S. (2007). HIV-1 Nef-induced down-regulation of MHC class I requires AP-1 and clathrin but not PACS-1 and is impeded by AP-2. Mol Biol Cell *18*, 3351-3365.

Luo, W., and Peterlin, B. M. (1997). Activation of the T-cell receptor signaling pathway by Nef from an aggressive strain of simian immunodeficiency virus. J Virol *71*, 9531-9537.

Luria, S., Chambers, I., and Berg, P. (1991). Expression of the type 1 human immunodeficiency virus Nef protein in T cells prevents antigen receptor-mediated induction of interleukin 2 mRNA. Proc Natl Acad Sci U S A *88*, 5326-5330.

Mangasarian, A., Foti, M., Aiken, C., Chin, D., Carpentier, J. L., and Trono, D. (1997). The HIV-1 Nef protein acts as a connector with sorting pathways in the Golgi and at the plasma membrane. Immunity *6*, 67-77.

Mariani, R., and Skowronski, J. (1993). CD4 down-regulation by nef alleles isolated from human immunodeficiency virus type 1-infected individuals. Proc Natl Acad Sci U S A *90*, 5549-5553.

Marsh, J. W. (1999). The numerous effector functions of Nef. Arch Biochem Biophys *365*, 192-198.

Matsuyama, T., Kobayashi, N., and Yamamoto, N. (1991). Cytokines and HIV infection: is AIDS a tumor necrosis factor disease? Aids *5*, 1405-1417.

Mattapallil, J. J., Douek, D. C., Hill, B., Nishimura, Y., Martin, M., and Roederer, M. (2005). Massive infection and loss of memory CD4+ T cells in multiple tissues during acute SIV infection. Nature *434*, 1093-1097.

Matthews, B. W. (1968). Solvent content of protein crystals. J Mol Biol *33*, 491-497.

Mehandru, S., Poles, M. A., Tenner-Racz, K., Horowitz, A., Hurley, A., Hogan, C., Boden, D., Racz, P., and Markowitz, M. (2004). Primary HIV-1 infection is associated with preferential depletion of CD4+ T lymphocytes from effector sites in the gastrointestinal tract. J Exp Med *200*, 761-770.

Moarefi, I., LaFevre-Bernt, M., Sicheri, F., Huse, M., Lee, C. H., Kuriyan, J., and Miller, W. T. (1997). Activation of the Src-family tyrosine kinase Hck by SH3 domain displacement. Nature *385*, 650-653.

Muesing, M. A., Smith, D. H., Cabradilla, C. D., Benton, C. V., Lasky, L. A., and Capon, D. J. (1985). Nucleic acid structure and expression of the human AIDS/lymphadenopathy retrovirus. Nature *313*, 450-458.

Munch, J., Janardhan, A., Stolte, N., Stahl-Hennig, C., Ten Haaft, P., Heeney, J. L., Swigut, T., Kirchhoff, F., and Skowronski, J. (2002). T-cell receptor:CD3 down-

regulation is a selected in vivo function of simian immunodeficiency virus Nef but is not sufficient for effective viral replication in rhesus macaques. J Virol *76*, 12360-12364.

Munch, J., Schindler, M., Wildum, S., Rucker, E., Bailer, N., Knoop, V., Novembre, F. J., and Kirchhoff, F. (2005). Primary sooty mangabey simian immunodeficiency virus and human immunodeficiency virus type 2 nef alleles modulate cell surface expression of various human receptors and enhance viral infectivity and replication. J Virol *79*, 10547-10560.

Nam, H. J., Poy, F., Saito, H., and Frederick, C. A. (2005). Structural basis for the function and regulation of the receptor protein tyrosine phosphatase CD45. J Exp Med *201*, 441-452.

Niederman, T. M., Garcia, J. V., Hastings, W. R., Luria, S., and Ratner, L. (1992). Human immunodeficiency virus type 1 Nef protein inhibits NF-kappa B induction in human T cells. J Virol *66*, 6213-6219.

Niederman, T. M., Hastings, W. R., Luria, S., Bandres, J. C., and Ratner, L. (1993). HIV-1 Nef protein inhibits the recruitment of AP-1 DNA-binding activity in human T-cells. Virology *194*, 338-344.

Padilla, J. E., and Yeates, T. O. (2003). A statistic for local intensity differences: robustness to anisotropy and pseudo-centering and utility for detecting twinning. Acta Crystallogr D Biol Crystallogr *59*, 1124-1130.

Page, K. A., van Schooten, W. C., and Feinberg, M. B. (1997). Human immunodeficiency virus type 1 Nef does not alter T-cell sensitivity to antigen-specific stimulation. J Virol *71*, 3776-3787.

Palacios, E. H., and Weiss, A. (2004). Function of the Src-family kinases, Lck and Fyn, in T-cell development and activation. Oncogene *23*, 7990-8000.

Pandrea, I. V., Gautam, R., Ribeiro, R. M., Brenchley, J. M., Butler, I. F., Pattison, M., Rasmussen, T., Marx, P. A., Silvestri, G., Lackner, A. A., *et al.* (2007). Acute loss of intestinal CD4+ T cells is not predictive of simian immunodeficiency virus virulence. J Immunol *179*, 3035-3046.

Parsons, S. (2003). Introduction to twinning. Acta Crystallogr D Biol Crystallogr *59*, 1995-2003.

Pekarsky, Y., Garrison, P. N., Palamarchuk, A., Zanesi, N., Aqeilan, R. I., Huebner, K., Barnes, L. D., and Croce, C. M. (2004). Fhit is a physiological target of the protein kinase Src. Proc Natl Acad Sci U S A *101*, 3775-3779.

Peter, F. (1998). HIV nef: the mother of all evil? Immunity *9*, 433-437.

Picker, L. J., Hagen, S. I., Lum, R., Reed-Inderbitzin, E. F., Daly, L. M., Sylwester, A. W., Walker, J. M., Siess, D. C., Piatak, M., Jr., Wang, C., *et al.* (2004). Insufficient production and tissue delivery of CD4+ memory T cells in rapidly progressive simian immunodeficiency virus infection. J Exp Med *200*, 1299-1314.

Picker, L. J., and Watkins, D. I. (2005). HIV pathogenesis: the first cut is the deepest. Nat Immunol *6*, 430-432.

Piguet, V., and Trono, D. (1999). The Nef protein of primate lentiviruses. Rev Med Virol *9*, 111-120.

Piguet, V., Wan, L., Borel, C., Mangasarian, A., Demaurex, N., Thomas, G., and Trono, D. (2000). HIV-1 Nef protein binds to the cellular protein PACS-1 to downregulate class I major histocompatibility complexes. Nat Cell Biol *2*, 163-167.

Preusser, A., Briese, L., and Willbold, D. (2002). Presence of a helix in human CD4 cytoplasmic domain promotes binding to HIV-1 Nef protein. Biochem Biophys Res Commun *292*, 734-740.

Resh, M. D. (1994). Myristylation and palmitylation of Src family members: the fats of the matter. Cell *76*, 411-413.

Resh, M. D. (1999). Fatty acylation of proteins: new insights into membrane targeting of myristoylated and palmitoylated proteins. Biochim Biophys Acta *1451*, 1-16.

Rey-Cuille, M. A., Berthier, J. L., Bomsel-Demontoy, M. C., Chaduc, Y., Montagnier, L., Hovanessian, A. G., and Chakrabarti, L. A. (1998). Simian immunodeficiency virus replicates to high levels in sooty mangabeys without inducing disease. J Virol *72*, 3872-3886.

Rhee, S. S., and Marsh, J. W. (1994). HIV-1 Nef activity in murine T cells. CD4 modulation and positive enhancement. J Immunol *152* 5128-5134.

Royce, R. A., Sena, A., Cates, W., Jr., and Cohen, M. S. (1997). Sexual transmission of HIV. N Engl J Med *336*, 1072-1078.

Rudolph, M. G., Wingren, C., Crowley, M. P., Chien, Y. H., and Wilson, I. A. (2004). Combined pseudo-merohedral twinning, non-crystallographic symmetry and pseudo-translation in a monoclinic crystal form of the gammadelta T-cell ligand T10. Acta Crystallogr D Biol Crystallogr *60*, 656-664.

Salmond, R. J., Filby, A., Qureshi, I., Caserta, S., and Zamoyska, R. (2009). T-cell receptor proximal signaling via the Src-family kinases, Lck and Fyn, influences T-cell activation, differentiation, and tolerance. Immunol Rev *228*, 9-22.

Salvi, R., Garbuglia, A. R., Di Caro, A., Pulciani, S., Montella, F., and Benedetto, A. (1998). Grossly defective nef gene sequences in a human immunodeficiency virus type 1-seropositive long-term nonprogressor. J Virol *72*, 3646-3657.

Sawai, E. T., Baur, A. S., Peterlin, B. M., Levy, J. A., and Cheng-Mayer, C. (1995). A conserved domain and membrane targeting of Nef from HIV and SIV are required for association with a cellular serine kinase activity. J Biol Chem *270*, 15307-15314.

Schacker, T., Collier, A. C., Hughes, J., Shea, T., and Corey, L. (1996). Clinical and epidemiologic features of primary HIV infection. Ann Intern Med *125*, 257-264.

Schaefer, T. M., Bell, I., Fallert, B. A., and Reinhart, T. A. (2000). The T-cell receptor zeta chain contains two homologous domains with which simian immunodeficiency virus Nef interacts and mediates down-modulation. J Virol *74*, 3273-3283.

Schaefer, T. M., Bell, I., Pfeifer, M. E., Ghosh, M., Trible, R. P., Fuller, C. L., Ashman, C., and Reinhart, T. A. (2002). The conserved process of TCR/CD3 complex down-modulation by SIV Nef is mediated by the central core, not endocytic motifs. Virology *302*, 106-122.

Schindler, M., Munch, J., Kutsch, O., Li, H., Santiago, M. L., Bibollet-Ruche, F., Muller-Trutwin, M. C., Novembre, F. J., Peeters, M., Courgnaud, V., *et al.* (2006). Nef-mediated suppression of T cell activation was lost in a lentiviral lineage that gave rise to HIV-1. Cell *125*, 1055-1067.

Schrager, J. A., and Marsh, J. W. (1999). HIV-1 Nef increases T cell activation in a stimulus-dependent manner. Proc Natl Acad Sci U S A *96*, 8167-8172.

Schwartz, D. H., Viscidi, R., Laeyendecker, O., Song, H., Ray, S. C., and Michael, N. (1996). Predominance of defective proviral sequences in an HIV + long-term non-progressor. Immunol Lett *51*, 3-6.

Schwartz, O., Arenzana-Seisdedos, F., Heard, J. M., and Danos, O. (1992). Activation pathways and human immunodeficiency virus type 1 replication are not altered in CD4+ T cells expressing the nef protein. AIDS Res Hum Retroviruses *8*, 545-551.

Sigalov, A., Aivazian, D., and Stern, L. (2004). Homooligomerization of the cytoplasmic domain of the T cell receptor zeta chain and of other proteins containing the immunoreceptor tyrosine-based activation motif. Biochemistry *43*, 2049-2061.

Sigalov, A. B., Kim, W. M., Saline, M., and Stern, L. J. (2008). The Intrinsically Disordered Cytoplasmic Domain of the T Cell Receptor zeta Chain Binds to the Nef Protein of Simian Immunodeficiency Virus without a Disorder-to-Order Transition. Biochemistry.

Silvestri, G., Sodora, D. L., Koup, R. A., Paiardini, M., O'Neil, S. P., McClure, H. M., Staprans, S. I., and Feinberg, M. B. (2003). Nonpathogenic SIV infection of sooty mangabeys is characterized by limited bystander immunopathology despite chronic high-level viremia. Immunity *18*, 441-452.

Simard, M. C., Chrobak, P., Kay, D. G., Hanna, Z., Jothy, S., and Jolicoeur, P. (2002). Expression of simian immunodeficiency virus nef in immune cells of transgenic mice leads to a severe AIDS-like disease. J Virol *76*, 3981-3995.

Simmons, A., Aluvihare, V., and McMichael, A. (2001). Nef triggers a transcriptional program in T cells imitating single-signal T cell activation and inducing HIV virulence mediators. Immunity *14*, 763-777.

Skowronski, J., Parks, D., and Mariani, R. (1993). Altered T cell activation and development in transgenic mice expressing the HIV-1 nef gene. Embo J *12*, 703-713.

Smith-Garvin, J. E., Koretzky, G. A., and Jordan, M. S. (2009). T cell activation. Annu Rev Immunol *27*, 591-619.

Sousa, A. E., Carneiro, J., Meier-Schellersheim, M., Grossman, Z., and Victorino, R. M. (2002). CD4 T cell depletion is linked directly to immune activation in the pathogenesis of HIV-1 and HIV-2 but only indirectly to the viral load. J Immunol *169*, 3400-3406.

Specht, A., DeGottardi, M. Q., Schindler, M., Hahn, B., Evans, D. T., and Kirchhoff, F. (2008). Selective downmodulation of HLA-A and -B by Nef alleles from different groups of primate lentiviruses. Virology *373*, 229-237.

Storoni, L. C., McCoy, A. J., and Read, R. J. (2004). Likelihood-enhanced fast rotation functions. Acta Crystallogr D Biol Crystallogr *60*, 432-438.

Swigut, T., Greenberg, M., and Skowronski, J. (2003). Cooperative interactions of simian immunodeficiency virus Nef, AP-2, and CD3-zeta mediate the selective induction of T-cell receptor-CD3 endocytosis. J Virol *77*, 8116-8126.

Swigut, T., Iafrate, A. J., Muench, J., Kirchhoff, F., and Skowronski, J. (2000). Simian and human immunodeficiency virus Nef proteins use different surfaces to downregulate class I major histocompatibility complex antigen expression. J Virol *74*, 5691-5701.

Swigut, T., Shohdy, N., and Skowronski, J. (2001). Mechanism for down-regulation of CD28 by Nef. Embo J *20*, 1593-1604.

Thoulouze, M. I., Sol-Foulon, N., Blanchet, F., Dautry-Varsat, A., Schwartz, O., and Alcover, A. (2006). Human immunodeficiency virus type-1 infection impairs the formation of the immunological synapse. Immunity *24*, 547-561.

Veazey, R. S., DeMaria, M., Chalifoux, L. V., Shvetz, D. E., Pauley, D. R., Knight, H. L., Rosenzweig, M., Johnson, R. P., Desrosiers, R. C., and Lackner, A. A. (1998). Gastrointestinal tract as a major site of CD4+ T cell depletion and viral replication in SIV infection. Science *280*, 427-431.

Veazey, R. S., and Lackner, A. A. (2005). HIV swiftly guts the immune system. Nat Med *11*, 469-470.

Veazey, R. S., Mansfield, K. G., Tham, I. C., Carville, A. C., Shvetz, D. E., Forand, A. E., and Lackner, A. A. (2000a). Dynamics of CCR5 expression by CD4(+) T cells in lymphoid tissues during simian immunodeficiency virus infection. J Virol *74*, 11001-11007.

Veazey, R. S., Tham, I. C., Mansfield, K. G., DeMaria, M., Forand, A. E., Shvetz, D. E., Chalifoux, L. V., Sehgal, P. K., and Lackner, A. A. (2000b). Identifying the target cell in primary simian immunodeficiency virus (SIV) infection: highly activated memory CD4(+) T cells are rapidly eliminated in early SIV infection in vivo. J Virol *74*, 57-64.

Villinger, F., Folks, T. M., Lauro, S., Powell, J. D., Sundstrom, J. B., Mayne, A., and Ansari, A. A. (1996). Immunological and virological studies of natural SIV infection of disease-resistant nonhuman primates. Immunol Lett *51*, 59-68.

Wan, L., Molloy, S. S., Thomas, L., Liu, G., Xiang, Y., Rybak, S. L., and Thomas, G. (1998). PACS-1 defines a novel gene family of cytosolic sorting proteins required for trans-Golgi network localization. Cell *94*, 205-216.

Wang, J. K., Kiyokawa, E., Verdin, E., and Trono, D. (2000). The Nef protein of HIV-1 associates with rafts and primes T cells for activation. Proc Natl Acad Sci U S A *97*, 394-399.

Weissenhorn, W., Eck, M. J., Harrison, S. C., and Wiley, D. C. (1996). Phosphorylated T cell receptor zeta-chain and ZAP70 tandem SH2 domains form a 1:3 complex in vitro. Eur J Biochem *238*, 440-445.

Willard-Gallo, K. E., Furtado, M., Burny, A., and Wolinsky, S. M. (2001). Down-modulation of TCR/CD3 surface complexes after HIV-1 infection is associated with differential expression of the viral regulatory genes. Eur J Immunol *31*, 969-979.

Xu, X. N., Laffert, B., Screaton, G. R., Kraft, M., Wolf, D., Kolanus, W., Mongkolsapay, J., McMichael, A. J., and Baur, A. S. (1999). Induction of Fas ligand expression by HIV involves the interaction of Nef with the T cell receptor zeta chain. J Exp Med *189*, 1489-1496.

Yeates, T. O. (1988). Simple statistics for intensity data from twinned specimens. Acta Crystallogr A *44 (Pt 2)*, 142-144.

Yeates, T. O. (1997). Detecting and overcoming crystal twinning. Methods Enzymol *276*, 344-358.

Yoon, K., and Kim, S. (1999). Lack of negative influence on the cellular transcription factors NF-kappaB and AP-1 by the nef protein of human immunodeficiency virus type 1. J Gen Virol *80 (Pt 11)*, 2951-2956.